

N O T I C E

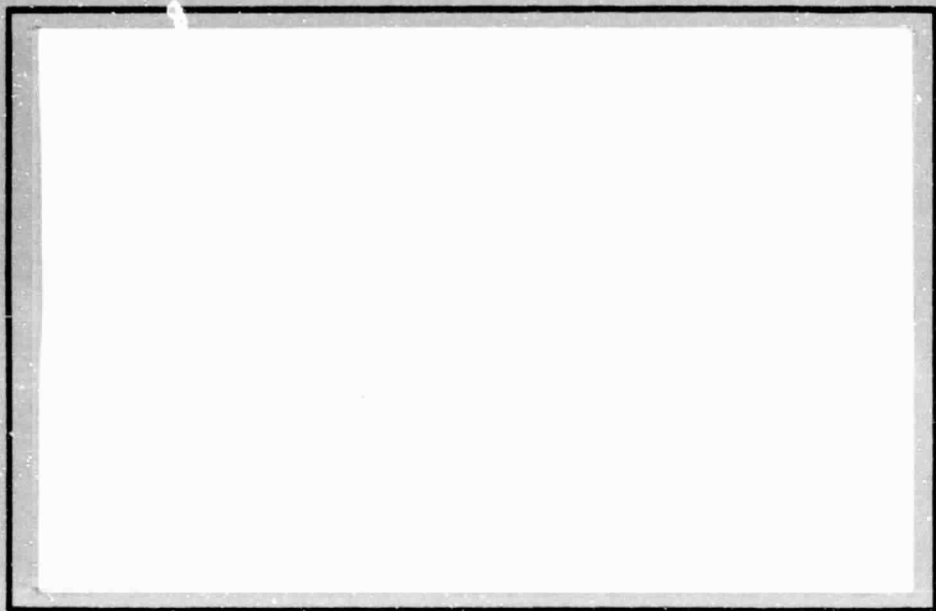
THIS DOCUMENT HAS BEEN REPRODUCED FROM
MICROFICHE. ALTHOUGH IT IS RECOGNIZED THAT
CERTAIN PORTIONS ARE ILLEGIBLE, IT IS BEING RELEASED
IN THE INTEREST OF MAKING AVAILABLE AS MUCH
INFORMATION AS POSSIBLE

(NASA-TM-80788) THERMAL EXPANSION OF
COMPOSITES USING MOIRE INTERFEROMETRY (NASA)
149 p HC A07/MF A01 CSCL 11D

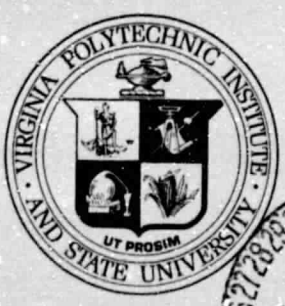
N80-29429

G3/24 Unclas
28328

**COLLEGE
OF
ENGINEERING**



**VIRGINIA
POLYTECHNIC
INSTITUTE
AND
STATE
UNIVERSITY**



**BLACKSBURG,
VIRGINIA**

College of Engineering
Virginia Polytechnic Institute and State University
Blacksburg, Virginia 24061

VPI-E-80-19

August, 1980

THERMAL EXPANSION OF COMPOSITES
USING MOIRE INTERFEROMETRY

David E. Bowles¹

Daniel Post²

Carl T. Herakovich²

Darrel R. Tenney³

Department of Engineering Science and Mechanics

Interim Report No. 20
The NASA-Virginia Tech Composites Program

NASA Grant NGR 47-004-129 and NASA Cooperative Agreement NCCI-15

¹ Graduate Student (presently with NASA-LaRC)

² Professor of Engineering Science and Mechanics

³ Materials Engineer - NASA-LaRC

REPORT DOCUMENTATION PAGE		READ INSTRUCTIONS BEFORE COMPLETING FORM
1. REPORT NUMBER VPI-E-80-19	2. GOVT ACCESSION NO.	3. RECIPIENT'S CATALOG NUMBER
4. TITLE (and Subtitle) THERMAL EXPANSION OF COMPOSITES USING MOIRE INTERFEROMETRY		5. TYPE OF REPORT & PERIOD COVERED
		6. PERFORMING ORG. REPORT NUMBER VPI-E-80-19
7. AUTHOR(s) David E. Bowles, Daniel Post, Carl T. Herakovich, and Darrel R. Tenny		8. CONTRACT OR GRANT NUMBER(s)
9. PERFORMING ORGANIZATION NAME AND ADDRESS Virginia Polytechnic Institute & State University Engineering Science & Mechanics Blacksburg, Virginia 24061		10. PROGRAM ELEMENT, PROJECT, TASK AREA & WORK UNIT NUMBERS NASA Grant NCCI-15 NGR 47-004-129
11. CONTROLLING OFFICE NAME AND ADDRESS National Aeronautics & Space Administration Langley Research Center Hampton, Virginia 23665		12. REPORT DATE August 1980
		13. NUMBER OF PAGES
14. MONITORING AGENCY NAME & ADDRESS (if different from Controlling Office) Virginia Polytechnic Institute & State University Engineering Science & Mechanics Blacksburg, Virginia 24061		15. SECURITY CLASS. (of this report) unclassified
		15a. DECLASSIFICATION/DOWNGRADING SCHEDULE
16. DISTRIBUTION STATEMENT (of this Report) Approved for public release, distribution unlimited		
17. DISTRIBUTION STATEMENT (of the abstract entered in Block 20, if different from Report) Approved for public release, distribution unlimited		
18. SUPPLEMENTARY NOTES		
19. KEY WORDS (Continue on reverse side if necessary and identify by block number) composites, thermal expansion, moire interferometry, graphite-epoxy, strain gages, temperature dependence		
20. ABSTRACT (Continue on reverse side if necessary and identify by block number) see page iv		

ACKNOWLEDGMENTS

The authors wish to acknowledge that this research was supported by the NASA-Virginia Tech Composites Program (NASA Grant NGR 47-004-129 and NASA Cooperative Agreement NCCI-15). In addition, the authors wish to acknowledge Dr. M. W. Hyer for assistance concerning certain technical aspects of this reserach, and to Mrs. Frances Hale for her excellent typing of the manuscript.

THERMAL EXPANSION OF COMPOSITES USING MOIRE INTERFEROMETRY

(ABSTRACT)

A new experimental technique for precise measurement of the thermal response of fiber-reinforced composite materials is presented. The technique uses moire interferometry with fringe multiplication which yields a sensitivity of 833 nm (32.8 μ in.) per fringe. Results from the technique are compared with those obtained from electrical resistance strain gages, and also those predicted from classical lamination theory.

The investigation has shown that moire interferometry is an effective and accurate technique for the determination of temperature dependent coefficients of thermal expansion for composite materials subjected to thermal cycling in the temperature range of 297 K (75°F) to 422 K (300°F). Coefficients of thermal expansion were determined for four laminate configurations ($[0]$, $[90]$, $[0/\pm 45/90]_S$ and $[0/90/\pm 45]_S$) of T300/5208 graphite epoxy, and ranged from $-0.107 \mu\epsilon K^{-1}$ ($-0.059 \mu\epsilon ^\circ F^{-1}$) for the $[0]$ laminate to $32.16 \mu\epsilon K^{-1}$ ($17.88 \mu\epsilon ^\circ F^{-1}$) for the $[90]$ laminate. Moisture was found to greatly influence the thermal response of a quasi-isotropic laminate, resulting in hysteresis and residual compressive strain as the moisture content was reduced.

Comparisons between moire and strain gage measurements were inconclusive with both techniques giving consistent but systematically different results. Differences of as much as 29% were observed. Lamination theory predictions compared reasonably well with experimental results, but were sensitive to changes in elastic property data.

TABLE OF CONTENTS

	<u>Page</u>
ACKNOWLEDGMENTS	iii
ABSTRACTS	iv
LIST OF TABLES	viii
LIST OF FIGURES	ix
 <u>CHAPTER</u>	
1 INTRODUCTION	1
1.1 Background	1
1.2 Purpose of Investigation	2
1.2.1 Experimental	2
1.2.2 Analytical	4
2 SURVEY OF METHODS FOR MEASUREMENT OF THERMAL EXPANSION	5
2.1 Electro-Mechanical Techniques	6
2.2 Optical Non-interferometric Techniques	8
2.3 Optical Interferometric Techniques	9
3 LITERATURE REVIEW	15
3.1 Thermal Expansion of Fiber-Reinforced Composites.	15
3.2 Moire Strain Analysis of Composites	19
4 THEORETICAL CONSIDERATIONS	24
4.1 Micromechanics	24
4.2 Laminate Analysis	29
4.2.1 Thermoelastic Formulation	29
4.2.2 Moisture Effects	33
5 EXPERIMENTAL PROCEDURE	35
5.1 Method of Measurement	35
5.1.1 Optical Consideration	35
5.1.2 Experimental Apparatus	40
5.1.3 Formation and Replication of Specimen Gratings	46

Table of Contents (continued)

<u>Chapter</u>		<u>Page</u>
5	5.2 Data Collection and Reduction	51
	5.2.1 Alignment Procedures	51
	5.2.2 Temperature Measurement	52
	5.2.3 Fringe Interpretation	53
	5.2.4 Correction for Expansion of Reference Grating	58
	5.3 Calibration	60
	5.3.1 Determination of ULE Behavior	61
	5.3.2 Calibration of Reference Grating	64
	5.4 Specimen Description	64
	5.4.1 Materials	64
	5.4.2 Surface Preparation and Environmental Conditioning	65
	5.4.3 Strain Gage Techniques	67
6	RESULTS AND DISCUSSION	70
	6.1 Reference Grating Calibration	70
	6.1.1 ULE Expansion	70
	6.1.2 Thermal Expansion of Reference Grating	73
	6.2 Apparent Strain for Strain Gages Subjected to Thermal Loading	75
	6.3 Thermal Expansion of Composites	79
	6.3.1 Unidirectional Laminates	79
	6.3.1.1 [0] Laminate	79
	6.3.1.2 [90] Laminate	84
	6.3.2 Quasi-Isotropic Laminates	90
	6.3.2.1 [0/±45/90] _s and [0/90/±45] _s Laminates (Dry)	90
	6.3.2.2 Comparison with Lamination Theory.	96
	6.3.2.3 [0/±45/90] _s Laminate (Moist)	101
7	CONCLUSIONS	115

Table of Contents (continued)

	<u>Page</u>
REFERENCES	118
<u>APPENDIX</u>	
A Error Analysis of Moire Measurements	122
B Strain Gage Results for the [0] Laminate	129

LIST OF TABLES

<u>Table</u>		<u>Page</u>
1	Specimen Information	66
2	Polynomial Coefficients for Thermal Strain as a Function of Temperature	72
3	Temperature Dependent Coefficients of Thermal Expansion for T300/5208 Laminates	89
4	Elastic Properties for T300/5208	98
5	Sensitivity Analysis for Quasi-Isotropic Laminate	100
6	Thermal Cycles for the Quasi-Isotropic Laminates with Moisture	104
7	CTE Values for Thermal Cycling of a Quasi-Isotropic Laminate with Moisture	107
A.1	Limits on CTE Values for a One Standard Deviation Error Band	128

LIST OF FIGURES

<u>Figure</u>		<u>Page</u>
1	Lamina Coordinate System	26
2	Laminate Geometry	31
3	Ray Diagram for Moiré Interferometry	36
4	Schematic Diagram of Moiré Interferometry Experimental Apparatus	41
5	Moiré Interferometry Experimental Apparatus	44
6	Schematic Diagram of Specimen and Reference Grating Fixture	45
7	Specimen and Reference Grating Fixture	47
8	Formation of Master Grating used as a Mold for Specimen Grating	48
9	Scanning Election Photomicrograph of 600 lpm (15240 lpi) Master Grating used to Replicate on Specimen	50
10	Composite Specimen Geometry	55
11	Typical Moiré Fringe Pattern Showing Position of Gage Marks	57
12	Schematic Diagram of Fizeau Interferometry Setup for Determination of ULE Behavior	62
13	Thermal Expansion of ULE	71
14	Thermal Expansion of Reference Grating	74
15	Apparent Strain Curves for Strain Gages on ULE	77
16	Moiré Fringe Pattern for [0] Laminate	80
17	Moiré Thermal Expansion of [0] Laminate	82
18	Thermal Expansion of [90] Laminate	85
19	Moiré Fringe Pattern for [90] Laminate	86

<u>Figure</u>		<u>Page</u>
20	Thermal Expansion of $[0/\pm 45/90]_s$ Laminate	91
21	Thermal Expansion of $[0/90/\pm 45]_s$ Laminate	92
22	Moire Fringe Pattern for Quasi-Isotropic Laminate	94
23	Comparison of Temperature Dependent Analysis with Experimental Results for Quasi-Isotropic Laminates ...	102
24	Moire Thermal Expansion for Heating of $[0/\pm 45/90]_s$ Laminate with Moisture	105
25	Moire Thermal Expansion for Heating and Cooling of $[0/\pm 45/90]_s$ Laminate with Moisture	106
26	Moire Thermal Expansion After Drying of $[0/\pm 45/90]_s$ Laminate	110
27	Thermal Response of Quasi-Isotropic Laminates with and without Moisture	113
A.1	Typical Error Band for Strain versus Temperature Response	126
A.2	Typical Error Band with Limiting Values of Strain versus Temperature Response	127
B.1	Comparison of Moire and Strain Gage Data for $[0]$ Laminate	131

Chapter 1

INTRODUCTION

1.1 Background

One of the most important reasons for the use of fiber-reinforced composites is the capability to tailor the material properties to achieve the desired structural performance. This material design capability, combined with the high specific strength and stiffness properties of composites, has led to widespread use of these materials in aerospace applications as well as increasing usage in the commercial aviation and automotive industries. Recently, there has been an increased use of composites in applications where the thermal response is an important consideration. Composites have the advantage that their thermal expansion properties, as well as their strength and stiffness, can be designed to meet specific applications. Trade-offs between these properties must often be made in order to obtain the optimum design. However, composites provide a much wider range of options than conventional materials.

One example where the need to control the thermal expansion properties of a structure is an important design consideration is space erectable antennas. For this particular application, the dimensional stability of the supporting structure is critical to the performance of the antenna. By utilizing fiber-reinforced composites, structures may be designed to have "near zero" thermal expansion in a specified direction over a fairly large temperature range. This produces a

dimensionally stable structure during the cyclic thermal loading of the structure in its space environment.

A second example of the importance of thermal properties is the large scale orbiting space structure, an application of composites that NASA is currently pursuing. While in its orbit, this large space structure will be subjected to thermal cycling, and in many instances, large thermal gradients will be present over the structure. This is because portions of the structure are being subjected to direct sunlight while other portions are shaded. Small thermal strains which have not been accounted for in the design may cause very large deformations and stresses when amplified over a large structure.

The thermal behavior of fiber-reinforced composites subjected to thermal loading must be well understood if composites are to be successfully applied to applications where dimensional stability is critical. Therefore, reliable experimental methods for determining the thermal behavior of these materials are needed. Analytical methods and models to predict composite thermal behavior and to extrapolate this information to predict the response of the entire structure are also essential.

1.2 Purpose of Investigation

1.2.1 Experimental

Because of the nature of the current applications of composite materials, it is clear that an experimental method for determining their thermal response must have the capability of measuring both very small

and quite large thermal strains with a high degree of accuracy and reliability. It is also desirable that the method be capable of measurement while the material is subjected to various types of loading, including cyclic and static thermal loading, and combined thermal and mechanical loading. In addition, the method should be inexpensive and easy to maintain and operate. Of the presently available techniques, no single one meets all of these criteria. Techniques that are capable of handling various loading conditions while being easy to use, such as strain gages, may not provide the needed accuracy for some applications. Likewise, currently existing techniques employed for their high degree of accuracy rely on measuring the displacements of the ends of the given specimen. This can introduce error due to contact and other end effects. In addition, these techniques are often limited in the specimen geometries which can be analyzed, and are frequently sensitive to their surroundings. All of the existing methods will be described in detail in the following chapter.

After studying the available methods, an optical technique based on the moiré method was selected. The particular method used has increased sensitivity over the classical moire technique. It is a full-field technique, which allows the examination of a finite region of the specimen, and is independent of end effects. It is also applicable for a variety of loading conditions and specimen geometries, and the experimental set-up is relatively insensitive to its surroundings. The rationale behind the selection of this experimental technique over other methods, the details of the experimental

procedure, and the experimental results will be presented in later chapters.

1.2.2 Analytical

In addition to the need for accurate experimental data for composite thermal response, reliable analytical methods to predict the thermal response of laminated composites are also needed. This is because there is an infinite number of possible composite laminate configurations, and it is therefore impossible to experimentally test them all. The analytical method used in this investigation is based on classical laminated plate theory, taking into consideration the temperature-dependent nature of the thermoelastic properties of a lamina. Included in this analysis is the effect of small variations in the ply orientations for various laminates. This not only affects the laminate coefficient of thermal expansion values (hereafter referred to as CTE values), but may also cause the laminate to become unsymmetrical, thus giving rise to coupling between extensional and bending behavior upon heating. The formulation of this analytical method considering the above-mentioned effects will be presented in some detail, and the predicted and experimental results will be compared.

Chapter 2

SURVEY OF METHODS FOR MEASUREMENT OF THERMAL EXPANSION

There is a wide variety of existing techniques for measuring thermally induced strains in materials. Resolution capabilities of these techniques range from 10^{-6} meters to fractions of a wavelength of light ($< 10^{-8}$ meters). Their usage usually depends upon the specific requirements of the measurement to be made. The desired requirements for measurement of thermal strains in fiber-reinforced composites may be summarized as follows:

1. the method should have the capability to measure very small as well as intermediate strains with a high degree of accuracy;
2. it should be capable of measuring strains under static and cyclic thermal loading, as well as combined thermal and mechanical loading;
3. it should be easy to maintain and operate without the need of complicated experimental equipment and procedures.

The available techniques can be divided into three general categories: electro-mechanical, optical non-interferometric, and optical interferometric techniques. Wolff [1] presented a comprehensive discussion of the available methods, listing such parameters as resolution, range, and accuracy of each, as well as discussing their

advantages and disadvantages. A brief summary based on Wolff's paper follows.

2.1 Electro-Mechanical Techniques

The two methods of primary importance which fall in this category employ the resistance strain gage and an LVDT (linear variable differential transformer) used as the sensing device on a quartz tube dilatometer. These two methods differ greatly, the first being essentially a point measurement technique, and the second employing the entire specimen length.

The fundamentals of the operation of a resistance strain gage will not be discussed here, but rather, some of the advantages and limitations of their use for measuring thermal strains will be given. A detailed description of resistance strain gages is given in reference [2]. Briefly, when the test temperature changes during a test (which is obviously the case for a thermal expansion test), the most important factor that must be considered is the apparent strain induced in the gage by this temperature change. To obtain the true thermal strain of the specimen, this apparent strain must be known in order to correct for it. (A detailed description of apparent strain is given in reference [3] and an outline of the equations and procedures used to correct for it in thermal expansion tests are given in Chapter 5). The basic procedure is to bond an identical gage on a material whose thermal expansion is well known. When this material undergoes some temperature change, the apparent strain in the gage may be computed,

since the true thermal response of the material is known. Assuming identical gage and bonding on the test specimen, this method assumes that the apparent strain of the gage is identical to that already determined, and thus the true thermal response of the sample can be determined.

The assumption of identical gages on the specimen and on the material of known thermal expansion behavior is one of the limitations to this method. No two gages are exactly identical, and in addition, no two gages are bonded to a specimen in exactly the same manner with the same amount of adhesive. This can lead to significant errors in the calculation of the thermal response of the specimen, especially when the strain levels of interest are small, as in the case of unidirectional and selected laminate orientations of graphite-epoxy composites. Other errors associated with resistance strain gages are caused by cyclic effects on the gage adhesive and reinforcement effects from the gage. The main advantages of resistance strain gages are their ease of use and the fact that they are applicable to a wide variety of specimen geometries and loading conditions.

Semiconductor strain gages also fall into the category of electro-mechanical techniques. They have a higher sensitivity than resistance strain gages, making them capable of measuring smaller strains. However, they are also much more sensitive to temperature changes [1], making the correction factors less reliable.

LVDT's as the sensing device on a dilatometer is a common procedure used to conduct thermal expansion measurements. The basic

theory of operation of an LVDT is described in reference [2]. In practice, a voltage is induced in the secondary winding by the axial core position of the transducer, after which a D.C. output, proportional to the position of the core, is monitored [1]. The basic construction and operation of the dilatometer to which the LVDT is used as a sensing device is given in the ASTM E228 standard test method [4]. It consists primarily of a pushrod resting on one end of the specimen. The other end of the specimen rests on a base. This apparatus is placed in a furnace, and the movement of the pushrod corresponds to the expansion of the specimen. Since corrections must be made for the expansion of the apparatus itself, both the pushrod and the base are generally made of quartz, because quartz has a low and well known coefficient of thermal expansion. The LVDT is then positioned such that the motion of the pushrod produces a motion of the LVDT core. An advantage of this technique is that the resolution is limited only by the accuracy with which one is able to measure a D.C. voltage. Some of the disadvantages of this method include a limit on the specimen size and shape, limited loading conditions, heating effects on the LVDT, and contact errors between the specimen and pushrod, as well as between the pushrod and LVDT.

2.2 Optical Non-interferometric Techniques

The technique in this category that is most often employed for the measurement of thermal strains in fiber-reinforced composites is an optical-mechanical lever-type device used in conjunction with a

standard dilatometer. This technique is described in detail by Freeman and Campbell [5]. Its basic operation consists of a rotatable prism through which the movement of the pushrod is transmitted and magnified. Light is passed through the prism and a lens system which further magnifies the displacement. As in the case of the LVDT, the main disadvantages to this technique are the limited size and shape of the specimen, limited loading conditions, and contact errors between the pushrod and specimen ends. The accuracy of this method is stated as $\pm 5 \mu\text{e}$ for a two inch long specimen [5].

2.3 Optical Interferometric Techniques

The four main types of interferometric measurements that are applicable for thermal expansion measurements are the techniques of conventional interferometry (two-beam and multiple reflection), holographic interferometry, speckle interferometry, and moiré interferometry. The basic operation for any interferometer is the recombination of two light beams (derived from a split beam) into a third beam whose intensity varies cyclically as the optical path length of one beam changes relative to the other; one cycle of intensity change corresponds to one wavelength change of optical path length. In practice, an interferometric technique yields a fringe pattern, seen as alternating dark and light bands, which changes its spacing and orientation as the specimen being studied expands or contracts. By using fringe interpolation techniques to detect small fractional fringe movements, the sensitivity of these methods becomes a small fraction of a wavelength.

The experimental setup for both two-beam and multiple reflection interferometers are similar. Both employ two reflecting surfaces connected to the specimen such that one of them is displaced relative to the other as the specimen expands or contracts. Wolff [1] describes three different interferometers that can be used for thermal expansion measurements, these being the Michelson, Fabry-Perot, and Fizeau interferometers. ASTM standard test method E289 [6] also describes the experimental procedure for a Fizeau interferometer for measuring the thermal expansion of rigid solids. The basic sensitivity of both two-beam and multiple reflection interferometers is $\lambda/2$ per interference fringe, where λ is the wavelength of the light being used as the source. There is a difference in the resolution that can be achieved with the two methods. In the two-beam interferometer, interference between the two beams give rise to a third beam whose intensity varies sinusoidally, producing fringes of equal widths (i.e. the width of the dark and light bands are the same). Interferometers using multiple reflections produce a beam whose intensity varies in a spiked fashion. In this case, the fringes are not of equal thickness, but rather, are very narrow bands of interference. This increases the degree of accuracy to which the center of these bands may be determined, thus increasing the accuracy with which fractional fringe shifts may be observed. This results directly in an increase of resolution obtainable by the technique.

In both types of interferometers, some type of reflecting surface is attached to the ends of the specimen. Thus, the measurement will

include any contact errors that result from this attachment. Wolff and Eselun [7] describe a "contactless" double Michelson interferometer for thermal expansion measurements. This is a very elaborate test setup, and the use of signal processing yields sensitivities in the range of $\lambda/1000$ per fringe. To minimize these contact errors, specimen dimensions are very critical. This places severe restrictions on the types of specimen geometries that can be studied. This is demonstrated in ASTM E289 [6] which suggests several specimen geometries. It would be quite difficult to fabricate any of these from fiber-reinforced composites. Another limitation to these techniques is the elaborate test setups needed in order to perform the measurement. However, these interferometers have a major advantage in that they offer the highest resolution of any of the measurement techniques used at this time.

A brief description of holographic and speckle interferometry is given by Wolff [1]. Neither of these two methods have the sensitivity of the conventional interferometers described above, and in both cases, the test setup is relatively elaborate. For these reasons, no further discussion of these methods will be given here.

Moiré interferometry, in the conventional sense, is accomplished by placing two gratings of nearly equal pitch (distance between grating lines) in series. In practice, one of these gratings is rigidly attached to the specimen (specimen grating) such that its deformation is the same as that of the surface of the specimen, while the other grating (reference grating) remains undeformed. When this system is illuminated and the specimen is deformed in some manner, a fringe

pattern results in which the displacements of the specimen surface are given by

$$d = Ng_r \quad (2.1)$$

where d is the displacement component of a point on the surface of the specimen normal to the reference grating lines, N is the change in moiré fringe order at that point, and g_r is the pitch of the reference grating. Chiang [8] gives a very thorough description of the theory, application, and interpretation of this type of moiré interferometry. The sensitivity of this method, as shown in equation 2.1, is governed by the pitch of the reference grating, which in this case is the same as the specimen grating pitch. Therefore, the sensitivity of this method is limited by the pitch of the grating that is attached or replicated on the surface of the composite. There is a practical limit to the pitch of a grating that can be replicated on the specimen. This limit yields sensitivities in the range of $25.4 \mu\text{m}$ ($1000 \mu \text{ in.}$) per fringe to $2.54 \mu\text{m}$ ($100 \mu \text{ in.}$) per fringe [9-14]. A discussion of all of the previous uses of moiré strain analysis as applied to composites will be given in Chapter 3.

Post [15-18] has developed a fringe multiplication technique that can be used to greatly increase the sensitivity from that of the conventional moiré method. By using a specimen grating whose pitch is β_g times that of the reference grating, and by isolating and analyzing specific diffraction orders, the sensitivity is increased β_g times that of the conventional moiré method. This shows that the

sensitivity depends only on the pitch of the reference grating and is independent of the pitch of the specimen grating. β_g is called the fringe multiplication factor, and is a whole integer. It follows that relatively coarse (large pitch) gratings may be used as the specimen grating, while a much finer (small pitch) commercially available grating may be used as the reference grating. Reference gratings are available commercially that will yield sensitivities of the same order of magnitude as λ , and therefore approach the sensitivity of conventional two-beam interferometry. This corresponds to a sensitivity in the range of 635 nm (25 μ in.) per fringe. Fringe interpolation techniques may then be used for increased resolution to yield more precise measurements.

The advantages of the moiré method utilizing the fringe multiplication technique of Post may be summarized as follows:

1. it is a purely geometrical measurement technique;
2. resolutions in the range of 5 μ e may be obtained;
3. unknown specimen end effects can be eliminated;
4. the technique yields full field observation permitting measurement of end and edge effects;
5. it is applicable to various specimen geometries and loading conditions;
6. the technique is easy to implement and inexpensive.

For these reasons, it was decided to pursue this basic technique in developing a practical method for measuring the thermal response of

fiber-reinforced composites. Details of the theory and implementation will be presented in Chapter 5.

Chapter 3

LITERATURE REVIEW

Considerable research has been conducted on the thermal expansion behavior of fiber-reinforced composites, including both experimental and analytical investigations. The first section in this chapter provides a brief summary of the more relevant research in this area. The second section briefly describes research that has been conducted concerning the application of moiré methods of strain analysis to composite materials. Although none of the research in the area of moiré strain techniques is directly concerned with measuring thermally induced strains, it is felt that a discussion of the technique applied to composites should be included. Many of the procedures and advantages that are discussed apply directly to the measurement of thermal strains in composites.

3.1 Thermal Expansion of Fiber-Reinforced Composites

The majority of the early research [19-23] (which took place in the 1960's and early 1970's) dealt primarily with predicting the thermal response of an individual lamina from the thermoelastic properties of its constituents (i.e. fiber and matrix). These predictions are based on analytical models derived by making certain assumptions concerning the behavior of the fiber and matrix, and their interactions when exposed to a temperature change. This method of analysis is most commonly referred to as micromechanics; a description of several micromechanics models will be discussed in Section 4.1.

Considerable experimental work has also been conducted in the above-mentioned area in order to assess the validity of these analytical models. Numerous researchers [23-29] have conducted experiments in which CTE's of unidirectional composites, both parallel and transverse to the fiber direction, have been measured. In most instances these measurements were made using either conventional interferometric techniques, or quartz dilatometers with sensing devices capable of detecting small length changes, giving the dilatometer the capability of measuring the very small strains which are usually encountered in the fiber direction of unidirectional composites. Both techniques are described in Chapter 2. The results of some of these experiments will be presented in conjunction with the theoretical predictions in Section 4.1. Experimental research [24,25,27-30] has also been conducted on off-axis unidirectional panels to show that the lamina CTE's, α_1 and α_2 , obey a standard second order tensor transformation law.

Experiments have also been conducted on multilayer composite laminates. Work in this area ranges from comparing the results on angle-ply laminates with predictions from lamination theory [25,28,30], to fabricating and testing laminates designed to exhibit isotropic expansion [26,31,32]. Freeman and Campbell [5] conducted a rather extensive experimental program on various graphite-epoxy systems fabricated into unidirectional and various laminate configurations. Measurements made using a dilatometer with an optical-mechanical lever sensing device were compared to those taken by resistance

strain gages. Such variables as the effect of moisture and thermal cycling, and the applicability of strain gages for measuring thermal strains on composites were also discussed.

Hyer and Hagaman [33] conducted an extensive series of tests to study thermal cycling effects on graphite-polyimide composites. Bending and axial strains were measured with resistance strain gages on curved unsymmetric laminates when subjected to repeated thermal cycles. Strain gage measurements were also made on flat unidirectional specimens and on titanium silicate (used as a reference to correct for thermal effects of the gage) which were subjected to repeated thermal cycles. This study gave not only insight into the thermal expansion of graphite-polyimide, but also served as a valuable source of data on the applicability of strain gages to measure thermal strains in composites. Results, when applicable to the present work, will be discussed in Chapter 6.

Eselun et al [34] investigated the effects of matrix microcracking on the thermal expansion of graphite-epoxy tubes. Thermal expansion measurements were made with a modified Michelson interferometer and microcracking was detected by both optical and acoustical techniques.

Analytical investigations have been conducted for the purpose of designing laminates for near-zero thermal expansion [35]. For various graphite-epoxy systems, it has been shown that by selecting the appropriate ply angle (by means of classical lamination theory) in a $[0_i/\pm\theta]_s$ symmetric laminate, a zero CTE may be obtained in one direction. However, the resulting CTE in a perpendicular direction may be

quite large. Sensitivities of this near-zero CTE to small variations in ply orientation have also been shown in reference [35]. A factor that was not discussed is that variations in ply orientation may cause the laminate to become unsymmetrical, thus causing a coupling between bending and extension upon heating. This may cause significant problems when the measurement technique relies on the relative displacement of the specimen ends. Reference [35] also discussed the sensitivities of these laminates to changes in elastic properties, as well as methods of obtaining near-zero CTE laminates by replacing a percentage of the graphite fibers with a fiber of a different CTE but equal stiffness, to maintain structural efficiency.

Reference [36] describes the development of an analytical model to predict combined laminate thermal and mechanical response. This is a non-linear analysis in which the total strain cannot be separated into the mechanical strain and free thermal strain. Thus, a laminate coefficient of expansion as described in Chapter 4 may not be correct for laminates which are both mechanically and thermally loaded. Experimental tests were conducted on a graphite-polyimide $[\pm 45]_s$ laminate with thermal and mechanical strains measured with resistance strain gages. The authors state that numerical agreement between experimental and analytical results is only fair.

The above cited literature indicates that an accurate, reliable, and easily employed test method for measuring thermal strains in composites is needed. Test methods that provide accuracy and reliability often limit the specimen geometry and loading conditions

that can be examined. In particular, methods such as classical interferometry or dilatometry with accurate sensing devices which rely on measuring the relative displacement of the specimen ends, are subject to inaccuracies due to the edge effects that exist in composites. They are also incapable of separating bending and extension behavior which may exist in supposedly symmetric laminates with ply misorientations. Resistance strain gages do not suffer from these limitations, but their accuracy and reliability for measuring small thermal strains is questionable. The moiré method that has been pursued in this work does not suffer from these limitations, and does provide the needed accuracy and reliability.

3.2 Moiré Strain Analysis of Composites

Although the moire technique has been widely used for strain measurements, no information could be found in the literature on using the moiré technique to measure the thermal expansion properties of composites. Because many of the same procedures apply to thermal expansion measurements, a brief description of this research will be given.

Pipes and Daniel [9] applied moiré strain analysis techniques to study interlaminar edge effects in composites. A graphite-epoxy composite was used in the study, with the laminate configuration chosen so as to maximize the edge effect. A thin layer of aluminum was first vacuum deposited on the surface of the specimen. A 39 line per mm (1pmm) (1000 line per inch (1pi)) grating was then photo-printed on the surface by a photoresist process. The specimens were

loaded mechanically, and fringe patterns were photographed in a conventional moiré setup, thus yielding a sensitivity of $25.4 \mu\text{m}$ ($1000 \mu\text{in.}$) per fringe. Experimental results agreed well with elasticity solutions in predicting the edge effect phenomenon. Because the moiré technique provided a full-field observation, the extent to which the edge effect extended into the center of the specimen could be easily observed.

Daniel and Rowlands [10] used moiré techniques for the determination of strain concentrations of composite plates with holes. A thin film with a 39 lpmm (1000 lpi) grating etched in it was bonded onto the surface of a glass epoxy composite. These films were bonded in two perpendicular directions to produce a crossed grating, thus allowing for the determination of two orthogonal in-plane displacement components. The specimens were loaded and fringe patterns were photographed in a conventional moiré technique. The results were then used to determine stress concentration factors. Again, the main advantage of the moiré technique for this application was that it yielded full-field displacement information.

Chaing [11] used the moiré technique to study crack growth in composites. Twelve 1pmm (300 lpi) crossed gratings were applied to notched double cantilever fracture specimens of unidirectional fiberglass. Cracks that initiated at the notch tip were studied by using the moiré fringe patterns to determine the crack length and the strain distribution around the crack tip. Again, moiré was chosen because it yields full-field displacement information, but the

sensitivity (approximately $83.8 \mu\text{m}$ ($3300 \mu\text{in.}$) per fringe) limited the experiment to more qualitative than quantitative information.

Oplinger, Parker, and Chiang [12] have also applied moiré methods to the study of edge effects in composite laminates. Gratings on thin films were bonded to both the face and to the edge of boron-epoxy and graphite-epoxy angle-ply laminates. Thirty-nine 1pmm (1000 lpi) gratings were bonded on the surface, while 100 lpm (2540 lpi) gratings were bonded on the edge. The specimens were mechanically loaded and surface displacements were computed from the moiré fringe patterns. These experimentally determined surface displacements were compared to theoretical predictions of displacements incorporating the edge-effect phenomenon. A moiré technique was chosen for this application because it allowed the full-field determination of displacements along the narrow edge (2.16 mm ($.085 \text{ in.}$)) of the composite. Again, the degree of quantitative information that could be obtained was somewhat limited by the sensitivity of the method, in this case, $25.4 \mu\text{m}$ ($1000 \mu\text{in.}$) per fringe on the surface and $10 \mu\text{m}$ ($400 \mu\text{in.}$) per fringe on the edge.

Marchant and Bishop [13] developed and used a moiré technique on graphite-epoxy specimens. The specimen was coated with a photoresist and then exposed to two superimposed coherent collimated beams of laser light. Exposure to these two superimposed beams produces an interference pattern which results in a grating being formed on the photoresist-coated specimen. Gratings of almost any pitch, as well as crossed gratings can be easily formed. The

specimen, while under load, is then viewed in the same optical system used to produce the grating, thus having the effect of two gratings in series. When the specimen is loaded and its pitch changes, moiré fringes are formed. For this particular study, a unidirectional graphite-epoxy plate with a transverse notch cut in the center was used. A crossed grating with a pitch of approximately 350 lpmm (9000 lpi) was formed on the surface of the specimen. The specimen was loaded perpendicular to the notch, and the moiré fringe pattern was used to determine the displacement field around the notch. This technique was unique in the way in which gratings were formed on the specimen and in the manner in which the specimen was illuminated to form the moiré fringes. The sensitivity of this particular application, approximately $2.8 \mu\text{m}$ (110 $\mu\text{in.}$) per fringe, was much better than that obtained with the previously-mentioned research.

Daniel, Rowlands and Post [14] have applied both conventional and fringe multiplication moiré techniques to strain analysis in composites. In the conventional technique, gratings of 39 lpmm (1000 lpi) were photoprinted on glass-epoxy and boron-epoxy laminates by a photoresist process. In the case of the boron-epoxy, a smooth surface first had to be cast on the composite. A thin layer of aluminum was then vacuum deposited to increase the reflectivity before the photoresist process could be used. These specimens were viewed in series with a 39 lpmm (1000 lpi) reference grating to produce moiré fringe patterns when the specimen was loaded. This technique was used to study strain distributions around composites plates with holes in them.

The authors used the same specimen preparation for the fringe multiplication technique. A 20 dot per mm (500 dot per inch) grating was then applied to the specimen by the same photoresist method. The specimen was then placed in the test machine and loaded. Replicas of the deformed specimen grating were made by photographing the specimen with a special distortion-free camera. The magnification was adjusted so as to produce a 20 lpmm grating on the photographic plate from the 20 dot per mm grating of the specimen. These replicas of the specimen grating were then analyzed in an optical setup with a 200 lpmm (5080 lpi) reference grating to produce fringe multiplication by a factor of 10. This resulted in a measurement sensitivity of approximately 5 μm (200 $\mu\text{in.}$) per fringe. The fringe multiplication technique was developed by Post [15-18], and the details of its operation will be discussed later.

In all of the above instances, the moiré technique was chosen because it provided full-field displacement information, which is essential in studying non-homogeneous strain fields. This is of particular interest in the field of composites, where non-homogeneous strains exist at free boundaries. The main drawback in the use of moiré techniques is the limited sensitivity, but this can be greatly increased by fringe multiplication methods.

Chapter 4

THEORETICAL CONSIDERATIONS

The fundamental building block of any fiber-reinforced material is the composite lamina which is composed of parallel fibers embedded in a matrix material. Individual lamina are then stacked together with the direction of the fibers in each lamina varying from layer to layer. This forms the composite laminate which may then be used for the desired structural application. The process of forming the composite laminate from individual laminae is known as curing, a description of which may be found in reference [37]. Two different analytical approaches are required in the analysis of these laminates. First, the behavior of the lamina must be related to the behavior of its constituent properties, i.e. the fiber and matrix. Secondly, the behavior of the laminate must be related to the behavior of the individual lamina and the geometry of their assemblage. The first analytical approach is commonly referred to as micromechanics while the second is referred to as macromechanics.

4.1 Micromechanics

Because the main thrust of this investigation is concerned with the thermal response of composite laminates, only those relations describing the CTE of the lamina in terms of the thermoelastic properties of the fiber and matrix will be discussed. Similar relationships have been derived for the elastic properties of the lamina in terms of constituent properties and may be found in the literature.

There are several basic assumptions concerning the behavior of the

fiber and matrix which are used in the development of these micro-mechanics relations. They may be stated as follows:

1. the fibers are homogeneous, linearly elastic, and isotropic or transversely isotropic, depending on the fiber being studied;
2. the matrix is homogeneous, linearly elastic, and isotropic;
3. there is a perfect bond between the fiber and matrix.

The fiber and lamina coordinate system that will be used is shown in Fig. 1.

Numerous researchers [19-23], using different methods of analysis, have all derived essentially the same relationship between the longitudinal CTE of the lamina and the constituent properties. The relationship may be written as follows:

$$\alpha_l = \frac{\alpha_{FL} E_{FL} V_F + \alpha_m E_m V_m}{E_{FL} V_F + E_m V_m} \quad (4.1)$$

where α_{FL} and E_{FL} are the CTE and elastic modulus, respectively, of the fiber in the longitudinal direction. The terms α_m and E_m are the CTE and elastic modulus of the matrix, respectively. Volume fractions of the fiber and matrix are denoted by V_F and V_m , respectively. It is basically a rule of mixtures relationship with elastic modulus included in each term.

There are several relationships given in the literature [12-26] for the transverse CTE. Many of these make the assumption that the fiber is isotropic, which is valid for fibers such as glass. This assumption, however, becomes invalid when the fiber reinforcement is a

1, 2, 3 LAMINA COORDINATES
x, y, z LAMINATE COORDINATES

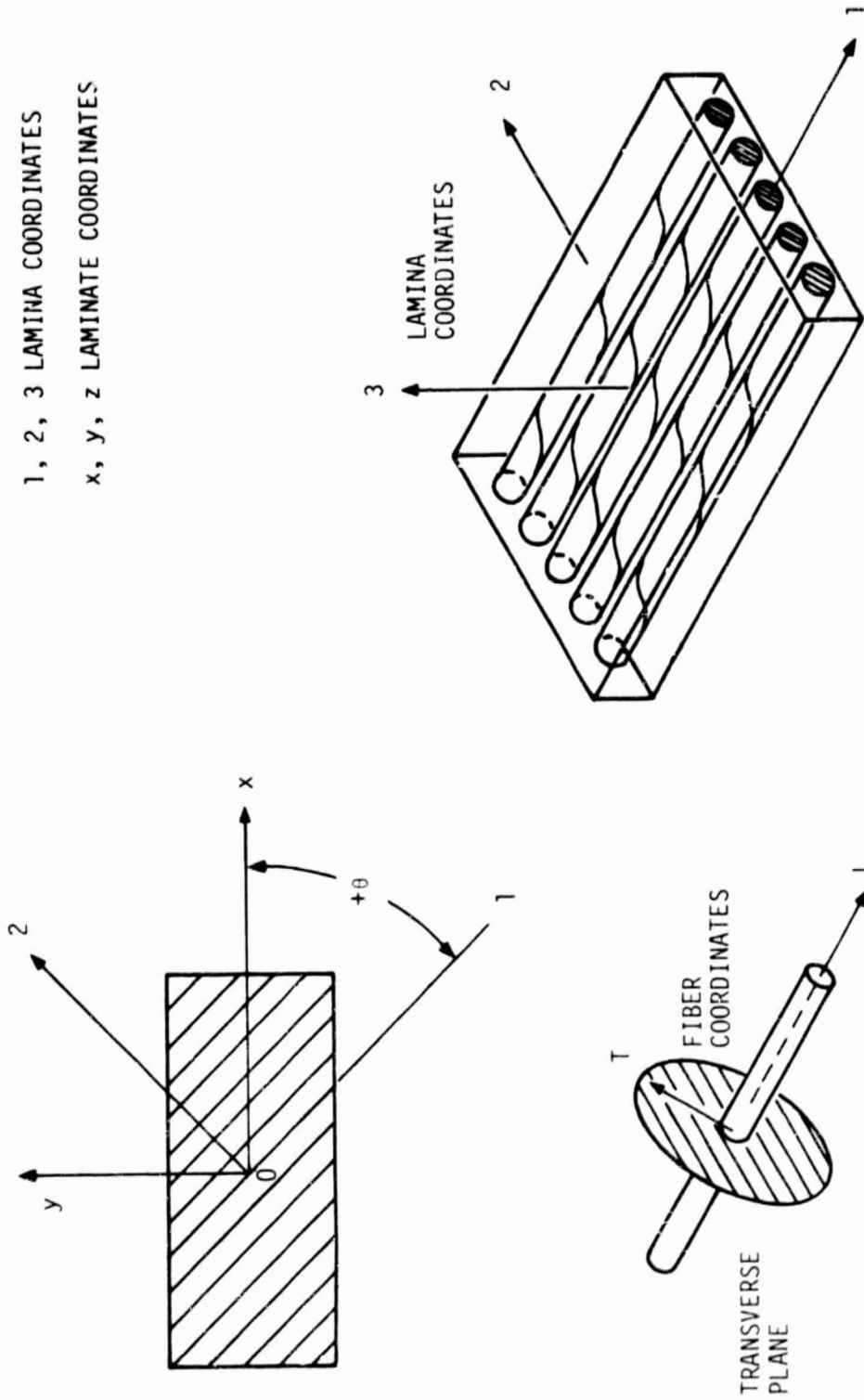


FIGURE 1. LAMINA COORDINATE SYSTEM

ORIGINAL PAGE IS
OF POOR QUALITY

high modulus graphite fiber where the CTE of the fiber is highly anisotropic. Knibbs et al [23] derived a formula for the transverse CTE taking into account the fiber anisotropy, which may be written as

$$\alpha_2 = \alpha_{FT}V_F + \alpha_m V_m (1 + \nu_m) \quad (4.2)$$

where α_{FT} is the CTE of the fiber in the transverse direction, and ν_m is Poisson's ratio of the matrix. They stated that the above relationship does not hold for small fiber volume fractions or for fibers with high longitudinal expansion. Fiber properties were approximated from graphite single crystals and used in Equ. (4.2) to compute α_2 . Their results were compared with experimentally determined values, showing reasonable agreement.

Schneider [21] gave a rather complicated form of an expression for the transverse CTE, and Kalnin [26] modified this expression for the case of anisotropic high modulus graphite fibers. Kalnin used this expression in conjunction with experimentally determined values of α_1 , α_2 , and α_m for a high modulus graphite epoxy to compute α_{FL} and α_{FT} . His results compared reasonably well with the values approximated from a single graphite fiber by Knibbs [23] for α_{FL} . However, there was approximately 30% difference between the approximated value and the computed value for α_{FT} .

Chamberlain [22] derived the following expression for α_2 assuming transversely isotropic fibers,

$$\alpha_2 = \frac{\alpha_m + 2(\alpha_{FT} - \alpha_m)V_F}{2\nu_m(F-1+V_m) + (F+V_F) + E_m(1-\nu_{FLT})(F-1+V_m)/E_{FL}} \quad (4.3)$$

where ν_{FLT} is Poisson's ratio of the fiber in the L-T plane, and F is the packing factor, equal to 0.9096 for hexagonal packing and 0.7854 for square packing. Rogers et al [24] used the above equation in conjunction with an experimentally determined value of α_m and approximated values of α_{FT} and α_{FL} (obtained from single graphite crystals) to compare predicted and experimental values of α_1 and α_2 . The results agreed reasonably well.

Stife and Prewo [25] used Equ. (4.3) to compare experimental and predicted results for Kevlar/epoxy. They also compared results obtained from a modified version of an expression for the transverse CTE given by Schapery [19]. The modification consisted of replacing α_f with α_{FT} , thus making the expression applicable to transversely isotropic fibers. The modified expression was given as

$$\alpha_2 = (1+\nu_m)\alpha_m V_m + (1+\nu_{FLT})\alpha_{FLT} - \alpha_1 \nu_{12} \quad (4.4)$$

where α_1 is given by Equ. (4.1) and ν_{12} is equal to $\nu_{FLT}V_F + \nu_m V_m$. Predicted results using Equ's. (4.1), (4.3) and (4.4) were compared with experimentally obtained results of α_1 and α_2 for Kevlar/epoxy composite. The results showed poor agreement with equation (4.1), but more reasonable agreement with Equ's. (4.3) and (4.4) (approximately 15% difference from measured values).

The purpose of this section is not to discuss the derivations of the above relationship or their merits, but rather, to give a brief description of the current research in this area. It is clear from the above that in order to assess the validity of any of the relation-

ships, it would be necessary to collect a large amount of data on the thermal expansion of numerous composite laminae. To accomplish this, one needs a reliable, accurate, and inexpensive test method, which is the main thrust of this research effort.

4.2 Laminate Analysis

4.2.1 Thermoelastic Formulation

A macromechanics approach will be used to predict the thermoelastic response of the composite laminate. This method is based upon classical laminated plate theory, and uses the thermoelastic behavior of the individual laminae in conjunction with the orientation and thickness of each lamina to predict the thermoelastic behavior of the composite laminate. A brief summary of the thermoelastic formulation will be given here. It follows the approach used by Hahn and Pagano [38]. A more complete derivation of lamination theory is given by Jones [37].

The basic assumptions of classical laminated plate theory may be listed as follows:

1. the laminate is composed of macroscopically homogeneous, transversely isotropic laminae, each in a state of plane stress, and perfectly bonded together (i.e. no slip between laminae);
2. the Kirchoff assumptions for plates applies, i.e. normals to the midplane remain straight and normal to the deformed midplane, and do not change in length.

In this thermoelastic formulation, all lamina material properties are

assumed to be functions of temperature. Appropriate simplifications will be pointed out for the case of temperature independent properties.

Referring to the laminate coordinate system as shown in Fig. 2, the total strain in the k^{th} layer is written as the sum of the mechanical strain and free thermal strain,

$$\{\epsilon(T)\}^k = \{\epsilon^\sigma(T)\}^k + \{\epsilon^T(T)\}^k \quad (4.5)$$

where the free thermal strain is defined as

$$\{\epsilon^T(T)\}^k = \int_{T_1}^{T_2} \{\alpha(\zeta)\}^k d\zeta \quad (4.6)$$

for a temperature change T_1 to T_2 with T_1 being the strain free temperature. It should be noted that α is the temperature dependent CTE of the k^{th} layer. If the lamina CTE is independent of temperature, then Equ. (4.6) simplifies to

$$\{\epsilon^T\}^k = \{\alpha\}^k (T_2 - T_1) \quad (4.7)$$

The total strain in the k^{th} layer may be written in terms of the midplane strains and curvatures, thus the mechanical strain may be written as

$$\{\epsilon^\sigma(T)\}^k = \{\epsilon^o(T)\} + z\{\kappa(T)\} - \{\epsilon^T(T)\}^k \quad (4.8)$$

and, the stress-strain relation for the k^{th} layer becomes

$$\{\sigma(T)\}^k = [Q(T)]^k \{\epsilon^\sigma(T)\}^k \quad (4.9)$$

where $[Q(T)]^k$ are the transformed stiffnesses of the k^{th} layer, which may be functions of temperature.

ORIGINAL PAGE IS
OF POOR QUALITY

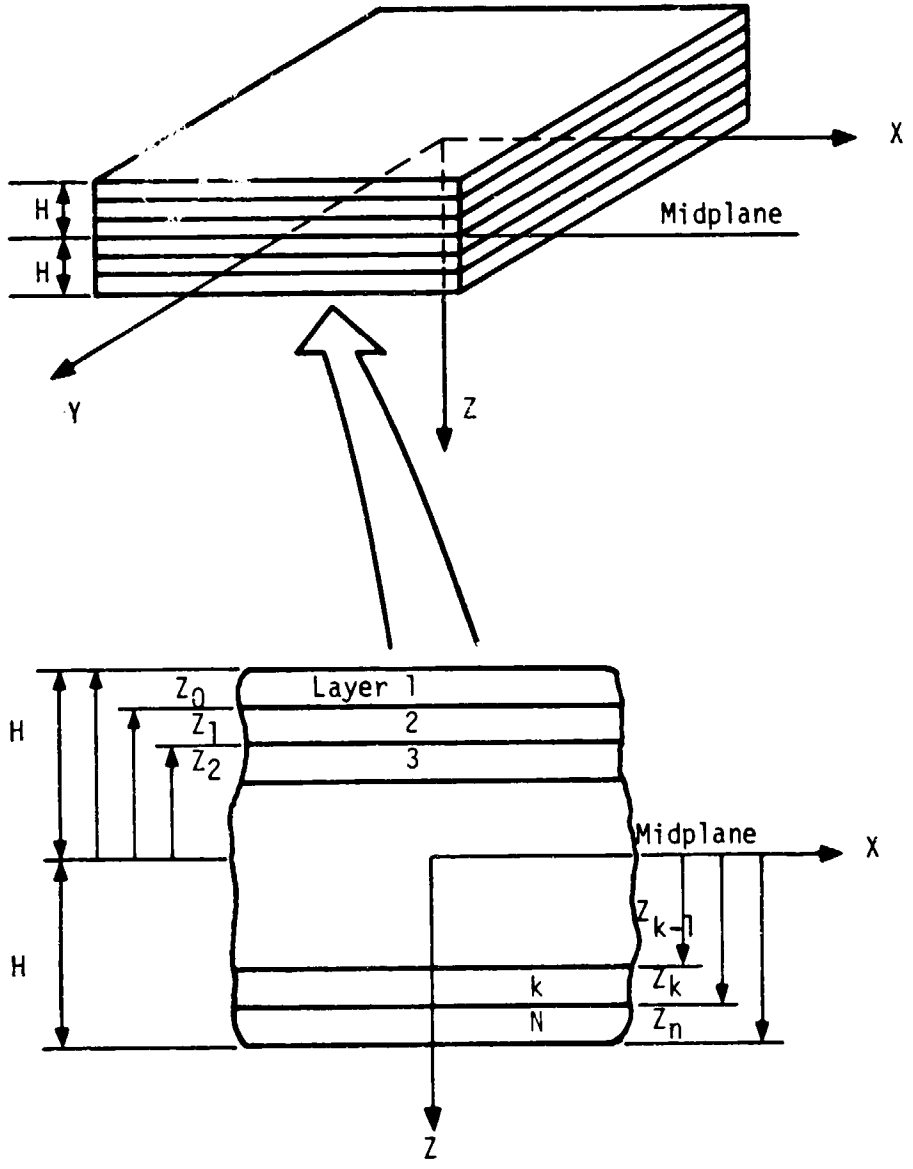


FIGURE 2. LAMINATE GEOMETRY

Integrating the stresses through the thickness of the laminate the constitutive equations may be written in terms of the force and moment resultants as

$$\begin{Bmatrix} N^\sigma(T) + N^T(T) \\ M^\sigma(T) + M^T(T) \end{Bmatrix} = \begin{bmatrix} A(T) & B(T) \\ B(T) & D(T) \end{bmatrix} \begin{Bmatrix} \epsilon^\circ(T) \\ \kappa(T) \end{Bmatrix} \quad (4.10)$$

where $\{N^\sigma(T)\}$ and $\{M^\sigma(T)\}$ are the mechanical force and moment resultants and $[A(T)]$, $[B(T)]$, and $[D(T)]$ are the extensional, coupling, and bending stiffness matrices respectively. These quantities are defined in the same manner as they are in lamination theory, except that they now may be functions of temperature. $\{N^T(T)\}$ and $\{M^T(T)\}$ are the thermal force and moment resultants, and are defined by

$$\begin{aligned} \{N^T(T)\} &= \int_{-H}^H [Q(T)]^k \{\epsilon^T(T)\}^k dz \\ \{M^T(T)\} &= \int_{-H}^H [Q(T)]^k \{\epsilon^T(T)\}^k z dz \end{aligned} \quad (4.11)$$

For thermal loading only ($\{N^\sigma(T)\} = \{M^\sigma(T)\} = 0$), the laminate constitutive equations in inverted form become

$$\begin{Bmatrix} \epsilon^\circ(T) \\ \kappa(T) \end{Bmatrix} = \begin{bmatrix} A'(T) & B'(T) \\ B'(T) & D'(T) \end{bmatrix} \begin{Bmatrix} N^T(T) \\ M^T(T) \end{Bmatrix} \quad (4.12)$$

$[A'(T)]$, $[B'(T)]$, and $[D'(T)]$ are obtained from inversion of Equ. (4.10). Laminate coefficients of free thermal expansion and curvature may now be defined as

$$\{\bar{\alpha}\} = \frac{d\epsilon^0(T)}{dT} = \frac{d([A'(T)]\{N^T(T)\} + [B'(T)]\{M^T(T)\})}{dT} \quad (4.13)$$

$$\{\bar{\lambda}\} = \frac{d\kappa(T)}{dT} = \frac{d([B'(T)]\{N^T(T)\} + [D'(T)]\{M^T(T)\})}{dT}$$

If none of the lamina material properties are functions of temperature, then several simplifications may be made. The thermal force and moment resultants may be written as

$$\{N^T\} = \int_{-H}^H [\bar{Q}]^k \{\alpha\}^k (T_2 - T_1) dz \quad (4.14)$$

$$\{M^T\} = \int_{-H}^H [\bar{Q}]^k \{\alpha\}^k (T_2 - T_1) dz$$

Since [A], [B], and [D] are no longer functions of temperature, expressions for $\{\bar{\alpha}\}$ and $\{\bar{\lambda}\}$ become

$$\{\bar{\alpha}\} = ([A']\{N_{(T_2)}^T\} + [B']\{M_{(T_2)}^T\}) / (T_2 - T_1) \quad (4.15)$$

$$\{\bar{\lambda}\} = ([B']\{N_{(T_2)}^T\} + [D']\{M_{(T_2)}^T\}) / (T_2 - T_1)$$

4.2.2 Moisture Effects

Changes in the moisture content also produce dimensional changes in composite materials. The problem of moisture induced dimensional changes should be considered in the thermoelastic formulation, because when the composite undergoes a change in temperature the moisture content will change, giving rise to moisture induced strains as well as to thermally induced strains.

Assuming that the total strain in the k^{th} layer may be written

as the sum of the mechanical, free thermal, and free moisture strains of that layer, gives

$$\{\epsilon\}^k = (\{\epsilon^\sigma\}^k + \{\epsilon^T\}^k + \{\epsilon^M\}^k) \quad (4.16)$$

Now if $\{\beta\}^k$ is the coefficient of moisture expansion (CME) for the k^{th} layer, then laminate coefficients of free moisture expansion and curvature may be derived in an exactly analogous manner to that of laminate coefficients of free thermal expansion and curvature.

For a change in moisture content only, from m_1 to m_2 , then

$$\{\bar{\beta}\} = ([A']\{N_{(m_2)}^M\} + [B']\{M_{(m_2)}^M\}) / (m_2 - m_1) \quad (4.17)$$

$$\{\bar{\phi}\} = ([B']\{N_{(m_2)}^M\} + [D']\{M_{(m_2)}^M\}) / (m_2 - m_1)$$

where m_1 is the strain free moisture content.

Chapter 5

EXPERIMENTAL PROCEDURE

5.1 Method of Measurement

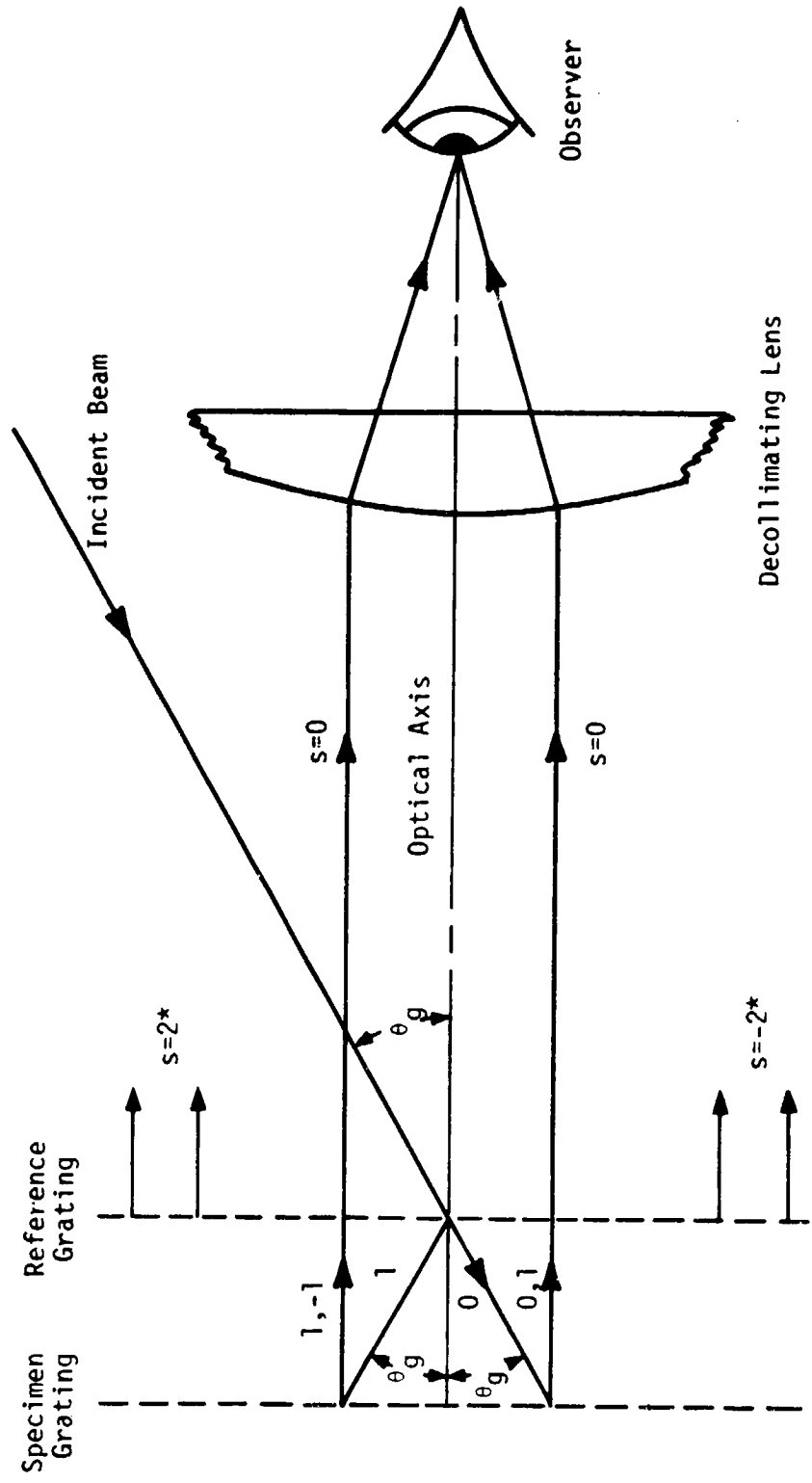
5.1.1 Optical Consideration

Moiré interferometry using fringe multiplication was chosen as the measurement technique to study the thermal expansion of composites. Reasons for its selection were stated in Chapter 2. Post [15-18] has described several methods to obtain this fringe multiplication phenomenon, and the particular method used for this research will now be described.

In reference [17], Post described an optimum configuration for obtaining fringe multiplication with specimen and reference gratings of unequal pitch. In this method, the pitch of the specimen grating is approximately β_g times the pitch of the reference grating, where β_g is the fringe multiplication factor.

Consider the optical configuration of Fig. 3. A reference grating is chosen such that dominant diffraction occurs in the zeroth and first orders. The system is illuminated by a beam of collimated light whose plane of incidence is perpendicular to the rulings of the grating. The angle of incidence is arranged such that the normal to the reference grating bisects the angle between the dominant diffraction orders. This angle of incidence, θ_g , is given by

$$\sin\theta_g = \frac{\lambda}{2g_r} \quad (5.1)$$



*After diffraction back through reference grating

FIGURE 3. RAY DIAGRAM FOR MOIRÉ INTERFEROMETRY

where λ is the wavelength of the light used for illumination and g_r is the pitch of the reference grating.

The specimen should have a pitch, g_s , of approximately β_g times that of the reference grating. For the present application β_g equals 2. The specimen grating also should exhibit symmetrical diffraction intensities with respect to its zeroth order. In the method described by Post the specimen grating was used in transmission, and observations were made on the side of the grating opposite from that of the illumination. In the present research the specimen grating is used in reflection and observation takes place on the same side as the illumination.

Diffraction rays are shown in Fig. 3. Numbers attached to the rays indicate the diffraction order, and a pair of numbers separated by commas indicate diffraction orders experienced at the reference and specimen gratings, respectively. Assume that the pitch of the specimen grating is exactly equal to β_g times that of the reference grating, i.e.

$$g_s = \beta_g g_r \quad (5.2)$$

For this case (Fig. 3), pairs of parallel rays emerge from the specimen grating. Post gave relations for determining the direction of these rays and classified each pair of rays as an s group. Since in his system the specimen grating was used in transmission, these pairs of rays emerged from the grating on the side opposite from the illumination, passed through a decollimating lens and converged to a point in the focal plane of a lens. Each s group converges to a different point in the focal

plane. The s groups are numbered such that the $s=0$ group consists of rays which are parallel to the optical axis (a line normal to the gratings). s is a whole number, either positive or negative, and s groups of increasing positive or negative number consist of rays with increasing angle to the optical axis.

In the current research effort the reference grating pitch is 833 nm (32.8 $\mu\text{in.}$) and the specimen grating pitch is approximately 1.67 μm (65.6 $\mu\text{in.}$). For this particular configuration rays of diffraction orders 0,1 and 1,-1 constitute the $s=0$ group, as can be seen in Fig. 3.

Because the specimen grating is used in reflection, rays in the various s groups must pass back through the reference grating, and be diffracted, before they may be observed. Zeroth order diffraction does not change the direction of a ray and, therefore, rays in the $s=0$ group, (1,-1 and 0,1) remain parallel to the optical axis. Likewise, zeroth order diffraction does not change the direction of rays in any of the other s groups. In this particular application, because of the pitch of the reference and specimen gratings and consequent large angle between s -groups, and the size and position of the decollimating lens, only rays in the $s=0$ group will be available for observation. It is the two rays in this s group that constitute the interference pattern and result in the formation of moiré fringes. This process will be described shortly.

A complication arises from the fact that the various s groups must pass back through the reference grating before observation.

Some s groups which experience other than zeroth order diffraction as they pass back through the reference grating will be approximately parallel to the $s=0$ group. This means that when these s groups pass through the decollimating lens they will all converge very close to the same point, forming overlapping interference patterns. In particular, s groups 2 and -2, which experience diffraction orders -1 and 1, respectively, will emerge in approximately the same direction as the $s=0$ group as they pass back through the reference grating. This is shown in Fig. 3.

Even though the energy of these s groups will be considerably less than the energy of the $s=0$ group, they will still conflict with the viewing of the $s=0$ group if allowed to converge to the same point. To overcome this problem, these s groups must be made to converge to a point distinct from where the $s=0$ group converges, so that an aperture plate may be used in the focal plane to stop the extraneous light and allow only light from the $s=0$ group to be viewed. In the present application, this was accomplished by introducing a wedge-shaped air gap between the reference and specimen gratings. The apex of the wedge-shaped gap is parallel to the grating rulings.

What has been described above for a single ray applies to every ray in the incident beam. The diffracted rays emerging from the specimen grating may be considered as normal to the emerging wavefronts. The moiré pattern that results from this method is a consequence of the optical interference between the two wavefronts in any particular s group. If g_s is exactly equal to $\beta_g g_r$, and if the rulings of the two

gratings are parallel, then the two wavefronts in an s group are parallel, and the resulting moiré pattern is a null field (i.e. no fringes). If g_s does not exactly equal $\beta_g g_r$, as will be the case as the specimen undergoes deformation, then the two wavefronts in an s group will be inclined planes that intersect along a line parallel to the grating rulings, and moiré fringes of extension will appear. If the rulings of the two gratings are not exactly parallel, then the two wavefronts will be inclined planes intersecting along a line perpendicular to the bisector of the grating rulings, and moiré fringes of rotation will appear.

Post has shown that the displacement, d , of the specimen are related to changes in the fringe pattern by Equ. (2.1), that is

$$d = Ng_r$$

This indicates that the sensitivity of the method (displacement per fringe) depends only on the pitch of the reference grating, and is independent of the pitch of the specimen grating.

5.1.2 Experimental Apparatus

A schematic diagram of the experimental apparatus used in this investigation is shown in Fig. 4. The setup is in the vertical plane. A 5 mW helium-neon laser was used as a light source. The collimated beam that illuminates the reference and specimen gratings was produced by the use of a 40X microscope objective, (serving as a beam expander) and a high quality collimating lens. By placing the node of the beam emerging from the microscope objective at the focal point of the

ORIGINAL PAGE IS
OF POOR QUALITY

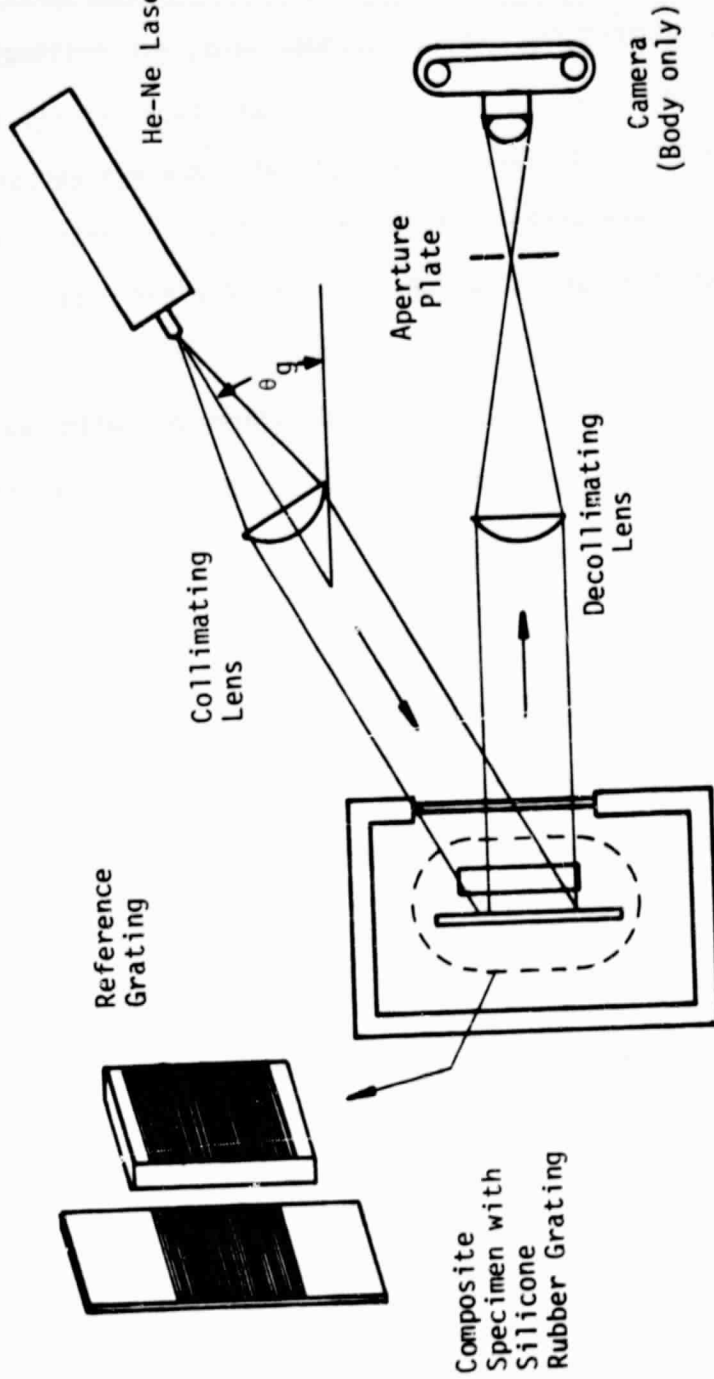


FIGURE 4. SCHEMATIC DIAGRAM OF MOIRÉ INTERFEROMETRY EXPERIMENTAL APPARATUS

collimating lens, a well-collimated beam approximately 76 mm (3 in.) in diameter was produced. An optical track was built from steel angle and plate stock to support the laser, expander lens, and collimating lens. It was designed so as to provide adjustment capabilities in both the horizontal and vertical planes. The optical track was supported at approximately the correct angle of incidence by four supports connected to a thick aluminum plate which served as a base for the entire experimental setup.

The fixture which held the specimen and reference grating was supported by a pedestal arrangement attached to the base. The fixture was enclosed in a laboratory oven (ATS Series 2911) capable of maintaining temperatures in the range 88 to 700 K (-300 to 800°F). The steel pedestal that extended up through the bottom of the oven was insulated with fiberglass, and a block of pyrex glass separated the fixture from the pedestal. The block of glass was inserted to serve as a heat barrier, so as not to provide a continuous metal path through which heat could flow. The oven had a viewing window in the door, and a pyrex window was installed in the side to provide for illumination and observation of the moiré fringes. The oven was also equipped with a dry nitrogen supply. This could be used to create a predominately nitrogen atmosphere inside the oven, greatly reducing the amount of moisture present.

A decollimating lens, aperture plate, and 35 mm camera were also attached to the base to provide a means of viewing and permanently recording the fringe patterns. The positions of these components were

adjustable so as to allow for correct positioning and magnification after the specimen was installed. Only the body of the 35 mm camera was needed since the decollimating lens also served as the camera lens. A photograph of the actual experimental apparatus is shown in Fig. 5.

The fixture used to support the specimen and reference grating, as shown in Fig. 6, consisted of two parts, an L-shaped bracket and a plate with a groove machined into it. The reference grating (52 mm by 52 mm Bausch and Lomb grating, catalog No. 35-54-06-540, on a fused silica blank) was attached to the bracket by means of a silicone rubber adhesive in such a manner as to produce the correct wedge-shaped gap when the specimen was put in place. This also connected to the pedestal extending from the base to support the entire fixture. The specimen was attached to the plate through the use of a small solid cylinder glued to the specimen with an epoxy adhesive. The cylinder fit into a hole in the groove, and was held in place by a set screw. The groove was sized so that the surface of the specimen was slightly lower than the surface of the plate, and the width of the specimen was slightly smaller than the width of the groove. This allowed for unrestricted expansion of the specimen. Care was taken in drilling the hole in the plate and finishing the top of the cylinder to assure that when the specimen was installed, the surface would be parallel to the plate surface. This plate was then attached to the back of the bracket, with the design allowing for rotational adjustments in the plane of the specimen to be made before the specimen was locked into

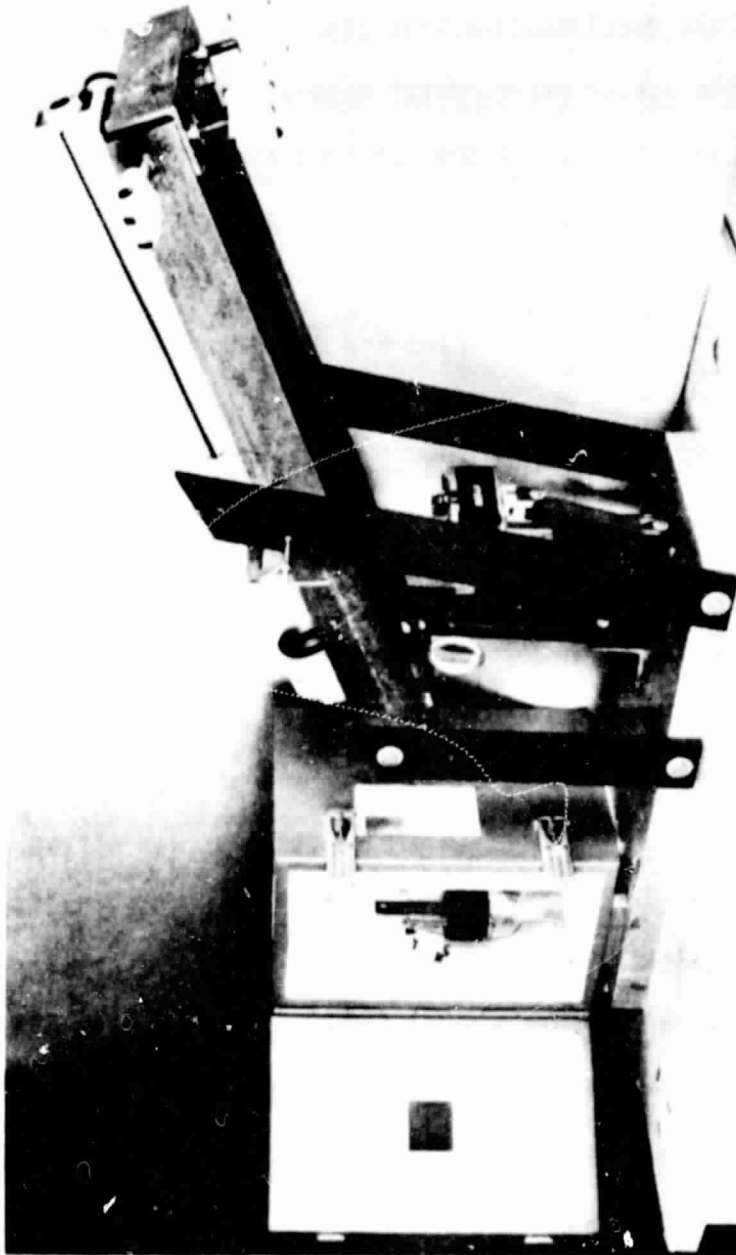
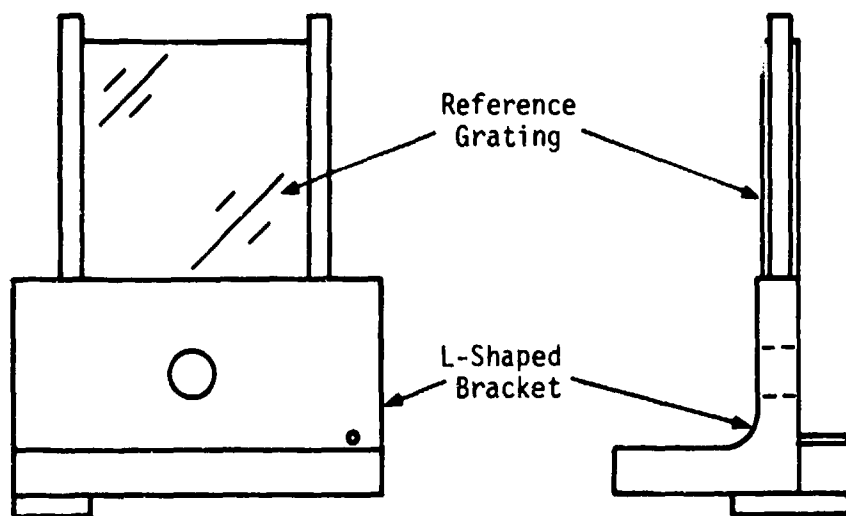
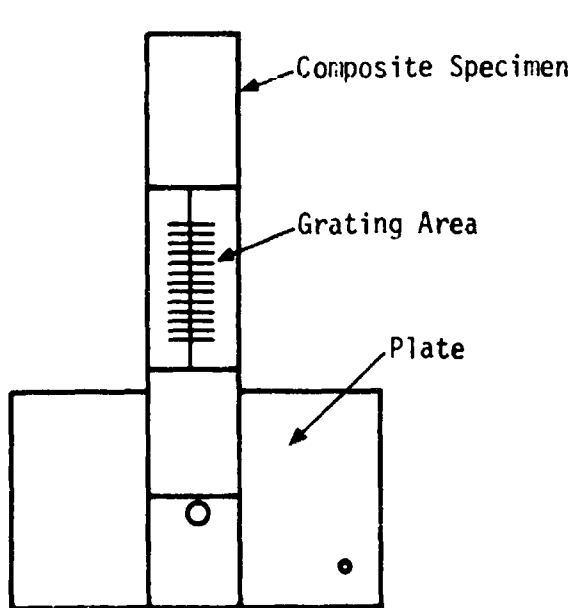


FIGURE 5. MOIRÉ INTERFEROMETRY EXPERIMENTAL APPARATUS

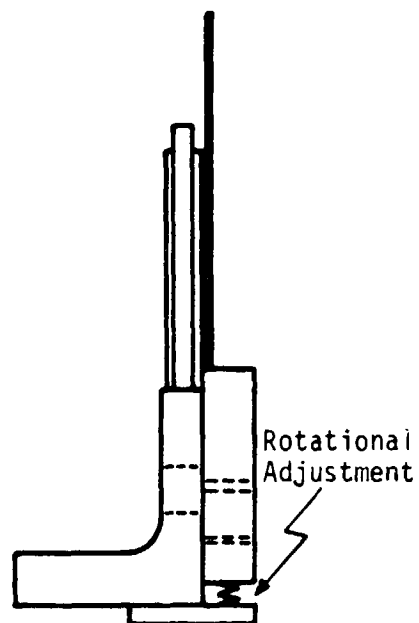
ORIGINAL PAGE IS
OF POOR QUALITY



(a) Reference Grating Support



(b) Specimen Support



(c) Assembled Fixture

FIGURE 6. SCHEMATIC DIAGRAM OF SPECIMEN AND REFERENCE GRATING FIXTURE

place. A photograph of this fixture with a composite specimen in place is shown in Fig. 7.

5.1.3 Formation and Replication of Specimen Gratings

This particular method requires that a grating be attached to the surface of the specimen, and that deformations of the specimen produce simultaneous and equal displacements of the grating. In meeting these requirements, the grating must not impose any reinforcement effect on the specimen, thus altering the true strain response of the specimen. A technique of casting a phase grating in RTV (room temperature vulcanizing) silicone rubber between the specimen and a master phase grating was developed. Silicone rubber was selected because of its low modulus (10^{-3} to 10^{-4} times that of the specimen) so as not to produce any reinforcement effect; its easy curing process without the need for a release agent on the master grating; and its wide range of operating temperatures. The particular silicone rubber chosen was a G.E. type RTV 615 with an operating temperature of 116 to 450 K (-250 to 350°F).

A phase grating that would produce symmetrical diffraction intensities with respect to its zeroth order was needed for use as the master grating in the replication process. It was produced in the laboratory by exposing a photographic plate to a steady-state interference pattern. Two coherent beams of light strike the photographic plate at angles $\pm\theta_m$ to the normal of the plate (Fig. 8), and superposition of light waves in this zone create the interference pattern in which destructive interference occurs as straight parallel lines. The angle, θ_m , is determined from

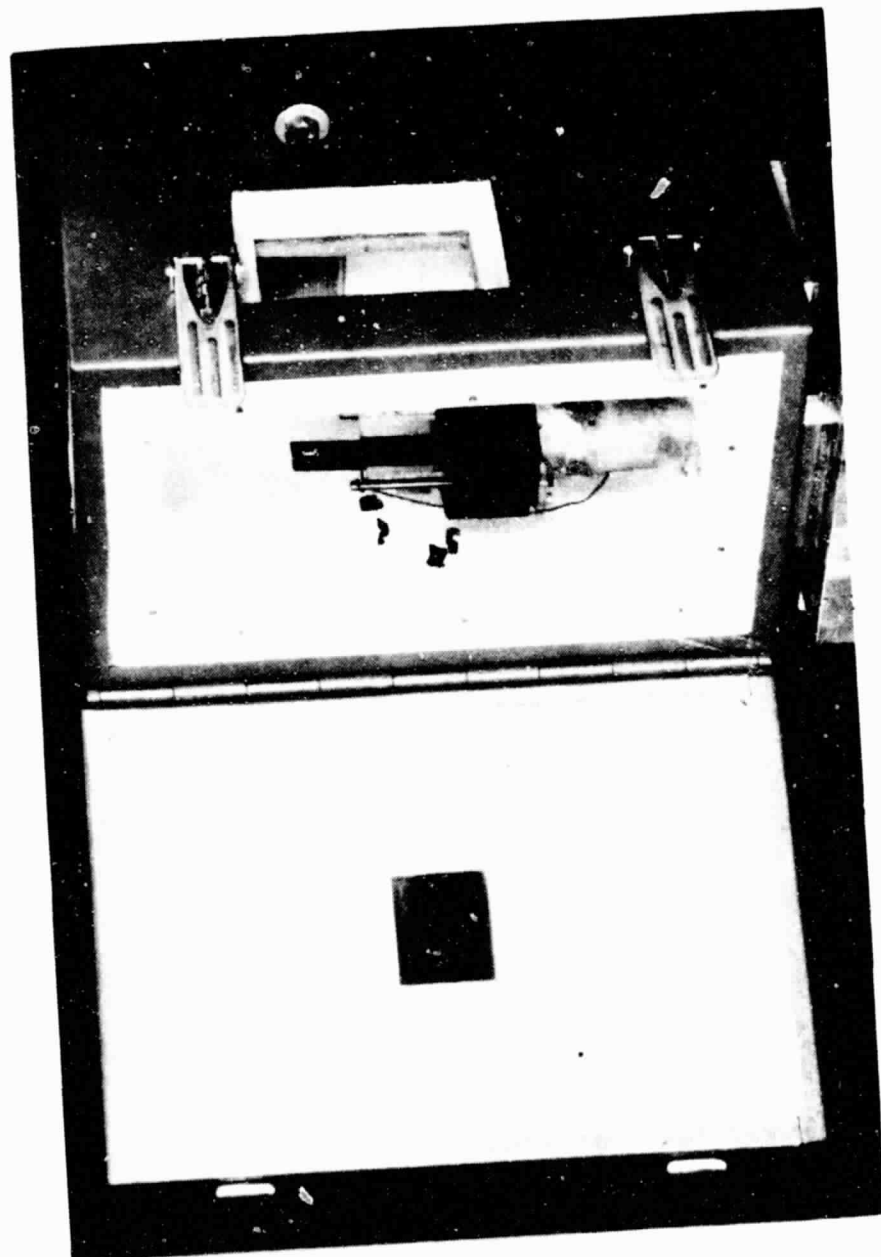


FIGURE 7. SPECIMEN AND REFERENCE GRATING FIXTURE

ORIGINAL PAGE IS
OF POOR QUALITY

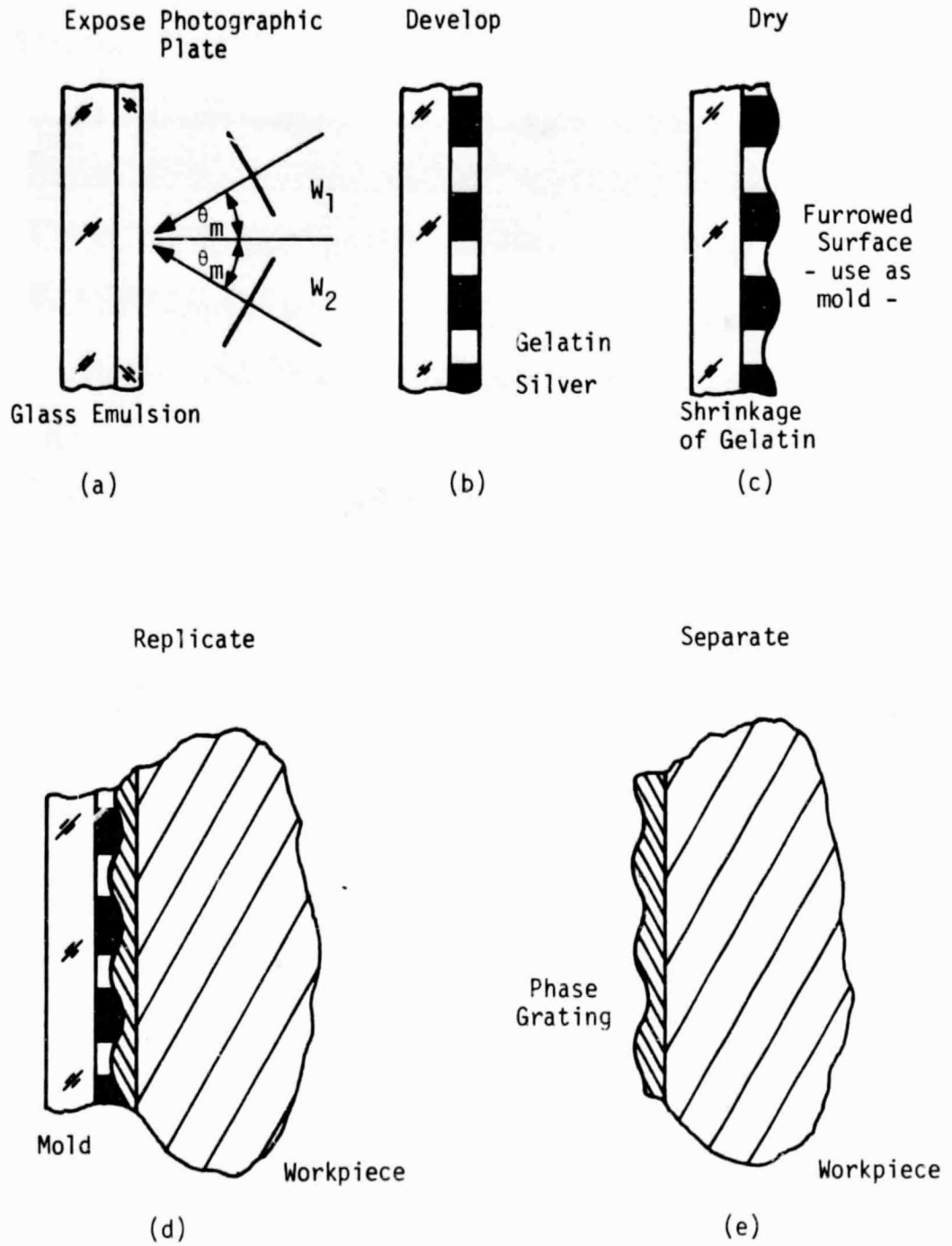


FIGURE 8. FORMATION OF MASTER GRATING USED AS A MOLD FOR SPECIMEN GRATING.

$$\sin\theta_m = \frac{\lambda}{2g_m} \quad (5.3)$$

where g_m is the desired pitch of the grating to be formed and λ is the wavelength of light used to illuminate it. In the current research, gratings of pitch $1.67 \mu\text{m}$ ($65.6 \mu\text{in.}$) were formed. A helium-neon laser ($\lambda = 632.8 \text{ nm}$ ($25 \mu\text{in.}$)) was used for the exposure in conjunction with Kodak Spectrographic Plates 649-F. Formation of the master grating is illustrated in Fig. 8 a, b and c. After exposure and development (in Kodak D-19) the emulsion consists of gelatin with bands of silver crystals imbedded in the zones of constructive interference. The gelatin shrinks upon drying, but shrinkage is restrained by the silver, resulting in unequal shrinkage and a regularly furrowed surface of the emulsion. This surface is used later as a mold to produce a phase grating on the specimen. A SEM (scanning electron microscope) photograph of one of these gratings is shown in Fig. 9. Formation of these gratings, and control of furrow depth to increase diffraction efficiency is a topic of current research being conducted under the guidance of Professor D. Post at VPI & SU.

The first step in replicating these gratings onto the specimen was mixing the silicone rubber. The G.E. RTV 615 consisted of two liquid components which were thoroughly mixed together, and in doing so, a large number of air bubbles were formed. The mixture was then placed in a vacuum chamber to destroy these bubbles. The second step was to clean and prime the surface of the specimen to provide for adhesion by the silicone rubber. A G.E. type SS4120 silicone primer was used.

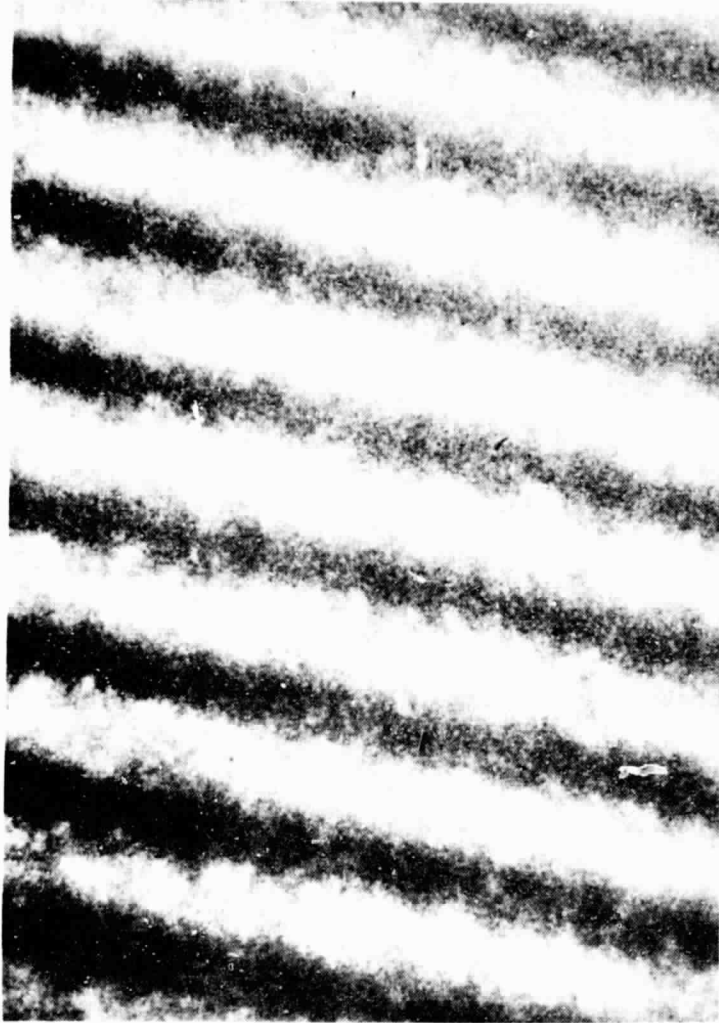


FIGURE 9. SCANNING ELECTRON PHOTOMICROGRAPH OF 600 μm
(15240 lp/in) MASTER GRATING USED TO REPLICATE
ON SPECIMEN

ORIGINAL PAGE IS
OF POOR QUALITY

Care was taken to assure that a thin, even layer of the primer was applied. A small amount of silicone rubber was poured on the surface of the specimen. The master grating was placed on top (grating side down) with care taken not to form any air bubbles, and a piece of tape was used to hold the grating in position. Then, a small weight (approximately 0.1 kg. (0.22 lbs.)) was placed on top, and the assembly was allowed to cure for approximately 48 hours. After curing the grating was easily removed by slightly flexing the specimen, since the silicone rubber is self-releasing from the grating. The above process resulted in a grating of uniform thickness of approximately 25 μm (0.001 in.).

5.2 Data Collection and Reduction

5.2.1 Alignment Procedures

Before thermal expansion measurements can be made on a specimen, adjustments must be performed to ensure proper alignment of the optical elements. The optical track must be positioned such that the plane of incidence of the collimated beam is perpendicular to the rulings of the reference grating, and illumination is at the proper angle of incidence as given by Equ. (5.1). This may be accomplished before the specimen is installed by adjusting the optical track so that the light from the reference grating, reflected in its first diffraction order, passes back through the collimating lens and into the source, or in this case, into the microscope objective.

After the specimen was installed, rotational adjustments in the

plane of the specimen were performed until the desired initial fringe pattern was observed. In the case of this research, this initial fringe pattern was a few fringes of extension, with no fringes of rotation present. A perfectly null field was not obtainable due to the fact that the pitch of the specimen grating was not exactly equal to β_g times the pitch of the reference grating. The absence of a null field at room temperature does not detract from the accuracy of the measurement.

After the specimen was properly adjusted, the aperture plate was positioned such that only the desired light ($s=0$) entered the camera. The decollimating lens and camera were then positioned to provide a properly focused image of the desired magnification. (Magnification for the current research was adjusted so as to provide viewing of a 33 mm (1.3 in.) gage length on the specimen.) Fringe pattern information was then permanently recorded with the 35 mm camera on black and white film (Kodak Plus X). It was found that for gratings used in this research, an exposure time of one second provided the optimum density in the photograph.

5.2.2 Temperature Measurement

Temperature was monitored by means of type J, iron-constantan thermocouples, and recorded on a strip chart recorder capable of monitoring up to six thermocouples with an accuracy of ± 1 K ($\pm 1.8^\circ\text{F}$). Thermocouples were attached to the specimens by means of a high temperature adhesive tape.

An initial study was performed to determine temperature distribu-

tions inside the oven. Thermocouples were attached to the top and both sides of the reference grating, as well as to various locations on the specimen (front and back of a composite specimen and top and both sides of the calibration specimen). Temperature readings were taken at five different temperatures between room temperature 297 K (75°F), and 422 K (300°F). By allowing approximately one half hour for temperatures to stabilize between readings, the maximum difference between any two thermocouples was no more than 1.7 K (3°F). This maximum difference occurred across the width of the reference grating, and thus the temperature of the reference grating for future tests was taken to be the temperature as given by a thermocouple attached to the top center of the grating. The readings from this location agreed to within less than 1 K (1.8°F) to those on the specimen. In addition, heating for all future tests was conducted in a step-wise fashion allowing one half hour between readings, rather than in a continuous heating manner.

5.2.3 Fringe Interpretation

For a given test, photographs of the fringe patterns were taken at each temperature. Displacements were related to the fringe pattern through Equ. (2.1), and the displacements arising from a change in temperature were related to the change in fringe order across the gage length, not the absolute fringe order at a particular temperature.

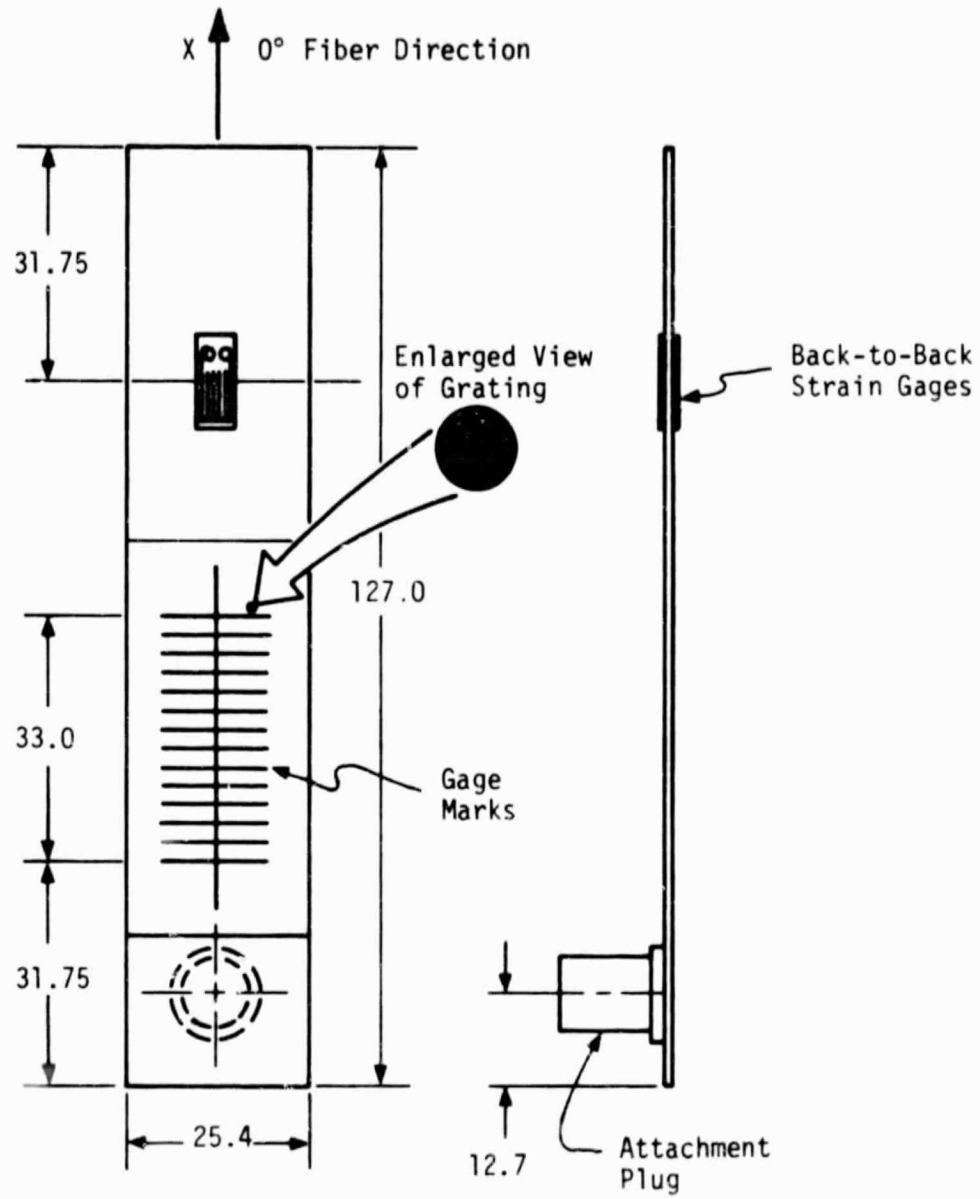
The thermal strain incurred during heating was determined from the change in fringe order for a temperature change from a reference temperature to the temperature of interest. Room temperature was

chosen as the reference temperature in this research. The strain at any other temperature was found by differentiating Equ. (2.1) to obtain

$$\epsilon_x = \left(\frac{dN}{dx}\right)g_r \quad (5.4)$$

In this equation, N is the change in fringe order, at a particular location X , for a particular temperature. The algebraic sign of N is determined from the first temperature increment upon heating. If in this first increment the fringe density increases, then N is taken to be positive. All future increases in density are then positive, and any decreases in fringe density are taken to be negative. Conversely, if the fringe density decreases in the first increment, N is again taken to be positive, with all future decreases also producing positive N values. Any increases in fringe density would then be taken as negative. The X direction is measured normal to the rulings of the reference grating (Fig. 10), and g_r is the pitch of the reference grating.

Equ. (5.4) gives the strain in a direction normal to the grating rulings as a function of position, thus providing full field strain information. Chiang [8] discussed several methods for determining these strain distributions depending upon the particular problem (geometry and loading conditions). Subjecting a specimen to a uniform change in temperature results, in most instances, in a homogeneous strain field. Exceptions to this arise from edge effects in certain composite laminates, which result in nonhomogeneous strains near free boundaries. In an area of homogenous strains the term dN/dx in Equ. (5.4) is a constant. The method used to determine this value



(Dimensions given in mm)

FIGURE 10. COMPOSITE SPECIMEN GEOMETRY

for specimens studied in the present research is described below.

A line was inscribed normal to the rulings of the master grating used for replicating the grating on the specimen, with small gage marks inscribed perpendicular to this line at approximately 2.5 mm (0.1 in.) intervals (Fig. 10). The exact distance between these gage marks was determined to the nearest 2.5 μm (0.0001 in.). During the replication process these marks were copied into the silicone rubber, and thus onto the surface of the specimen, and were clearly visible when analyzing the photographs of the fringe patterns (Fig. 11). The master grating was positioned such that the line normal to the grating rulings was in the center of the specimen and parallel to the longitudinal axis, as shown in Fig. 10.

The change in fringe order, N , due to a temperature change was determined at each gage mark. This information was then used to construct a plot of N versus position, X , for each temperature. For a homogeneous strain field, as is the case along the center of the composite specimen, N versus position is linear with slope dN/dx . A numerical value of this slope was determined by a least squares curve fitting procedure. Once dN/dx was determined for each temperature, it was used in Equ. (5.4) to compute the strain at each temperature.

In constructing the plots of N versus position, photographs of the fringe patterns were analyzed by observing the 35 mm negatives with a standard microfiche reader. This provided the necessary clarity and magnification to estimate the fringe order at each gage mark to the nearest tenth of a fringe with the aid of a pair of dividers and

ORIGINAL PAGE IS
OF POOR QUALITY

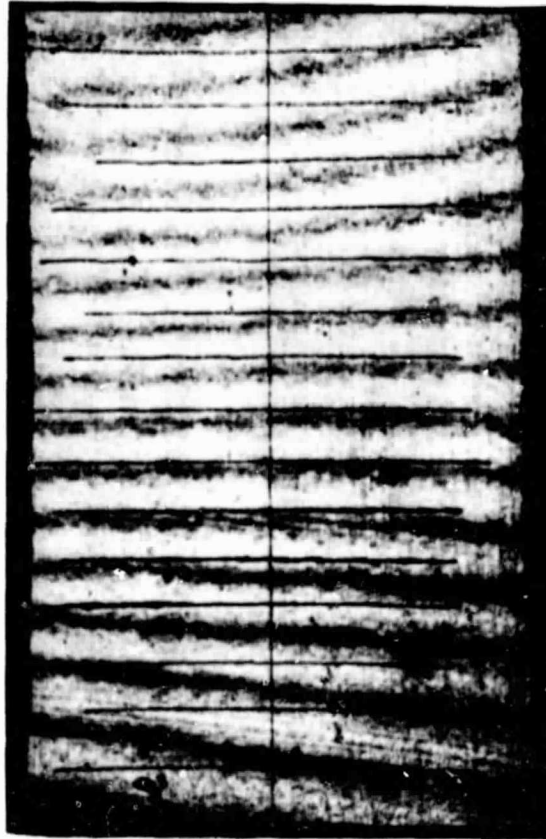


FIGURE 11. TYPICAL MOIRÉ FRINGE PATTERN SHOWING POSITION OF
GAGE MARKS

a scale. A photograph of a typical fringe pattern showing the gage marks is given in Fig. 11. In the present application, the use of a reference grating with a pitch of 833 nm (32.8 μ in.) provided a basic sensitivity of approximately 833 nm (32.8 μ in.) per fringe. Thus, estimating fringe orders to the nearest tenth provided a resolution of 83 nm (3.3 μ in.). However, resolution will be quoted as 167 nm (6.6 μ in.), assuming that fringe orders can only be accurately estimated to the nearest fifth of a fringe using the above method. This is a conservative assumption because the least-squares fit of the N versus position, X , data improves the accuracy relative to that of any single data point. The total gage length used in constructing the N versus position plots was approximately 33 mm (1.3 in.), thus providing a strain resolution capability of 5 $\mu\epsilon$. By using sophisticated techniques for fringe interpolation, which require additional equipment, resolution capabilities may be increased by as much as an order of magnitude. However, it was decided that the present procedure provided the best compromise between cost, ease of implementation, and resolution capabilities.

5.2.4 Correction for Expansion of Reference Grating

Equ. (5.4) cannot be used alone to determine the thermal expansion of a specimen. This is due to the fact that, unlike most conventional moiré techniques in which the reference grating is not exposed to any load, both the specimen and reference grating were exposed to the same change in temperature. This implies that the strain as calculated from Equ. (5.4) is not the absolute strain in the

specimen, but rather, the relative strain between the specimen and reference grating. To account for this, correction factors must be applied.

As stated previously, a perfectly null field does not exist when the rulings of the two gratings are parallel due to the fact that g_s does not exactly equal β_g times g_r . This means that the initial fringe pattern represents a few fringes of extension. It must first be determined which of the following cases exist:

$$\text{case 1) } g_s > \beta_g g_r$$

$$\text{case 2) } g_s < \beta_g g_r$$

This may be determined either by applying a small extensional strain to the specimen and observing whether the number of fringes increases or decreases, or by applying a small in-plane rotation to the specimen and observing the direction of fringe rotation [8]. For the composite specimens the first technique was used. From the above it was determined that case 2) existed for all of the specimens in the present research. Because the reference grating had a positive coefficient of thermal expansion, α_r , the pitch of the grating increased upon heating. An increase in the fringe density upon heating implies a further departure from the condition

$$g_s = \beta_g g_r$$

in the same direction as given in case 2). For an increase in fringe density, the reference grating expands more than the specimen. This implies that for a given change in temperature, the strain of the

specimen, ϵ_s , is equal to the strain of the reference grating ϵ_r minus the apparent strain, ϵ_{app} , calculated from Equ. (5.4)

$$\epsilon_s = \epsilon_r - \epsilon_{app}$$

The above may be summarized as follows:

For a positive α_r : if $g_s < \beta_g g_r$, and

a) the fringe density increases upon heating, then

$$\epsilon_s = \epsilon_r - \epsilon_{app} \quad (5.5)$$

b) the fringe density decreases upon heating, then

$$\epsilon_s = \epsilon_r + \epsilon_{app} \quad (5.6)$$

If $g_s > \beta_g g_r$, then the converse of the above holds true. In computing the apparent strain from Equ. (5.4), g_r was assumed to be constant which at first seems contradictory to what is stated above. However, because of the low thermal expansion of the reference grating the change in g_r upon heating had a negligible effect on the numerical results of Equ. (5.4).

5.3 Calibration

As stated in Section 5.2.4, corrections must be made to account for the thermal expansion of the reference grating. Therefore the thermal expansion characteristics of the grating must be known. The reference grating was on a fused silica blank, and ideally, should have exhibited the same thermal expansion as the fused silica. In this research the blank material was Corning fused silica code 7940, and plots of strain

versus temperature are available. This information is also obtainable by applying the present experimental technique of moiré interferometry, using as the specimen some material whose thermal expansion is known a priori. This calibration procedure provides first-hand information, rather than relying on the manufacturer's information.

5.3.1 Determination of ULE Behavior

Corning ULE (Ultra Low Expansion)TM titanium silicate code 7971 was selected as the specimen material in the calibration experiment. Although information on the thermal expansion of this material is available from the manufacturer, it was decided to experimentally determine it by means of conventional Fizeau interferometry. The basic theory involved in this type of interferometry is described in Section 2.3, and will not be discussed here. One of the main disadvantages of this method is that contact errors may be induced due to the fact that the method relies on the attachment of a reflecting surface to the ends of the specimen. For this particular application, the problem of contact errors is eliminated.

A schematic diagram of the specimen configuration and experimental setup is shown in Fig. 12. As can be seen, both reflecting surfaces and the specimen were blocks of ULE. These three components were assembled by means of an optical contact, in which the joining surfaces were so highly polished (flat to within 1/10 of a wavelength of green light) that they were held together by molecular forces. ULE is fabricated in such a manner as to form a very homogeneous and isotropic material, and therefore, when this configuration is subjected to a

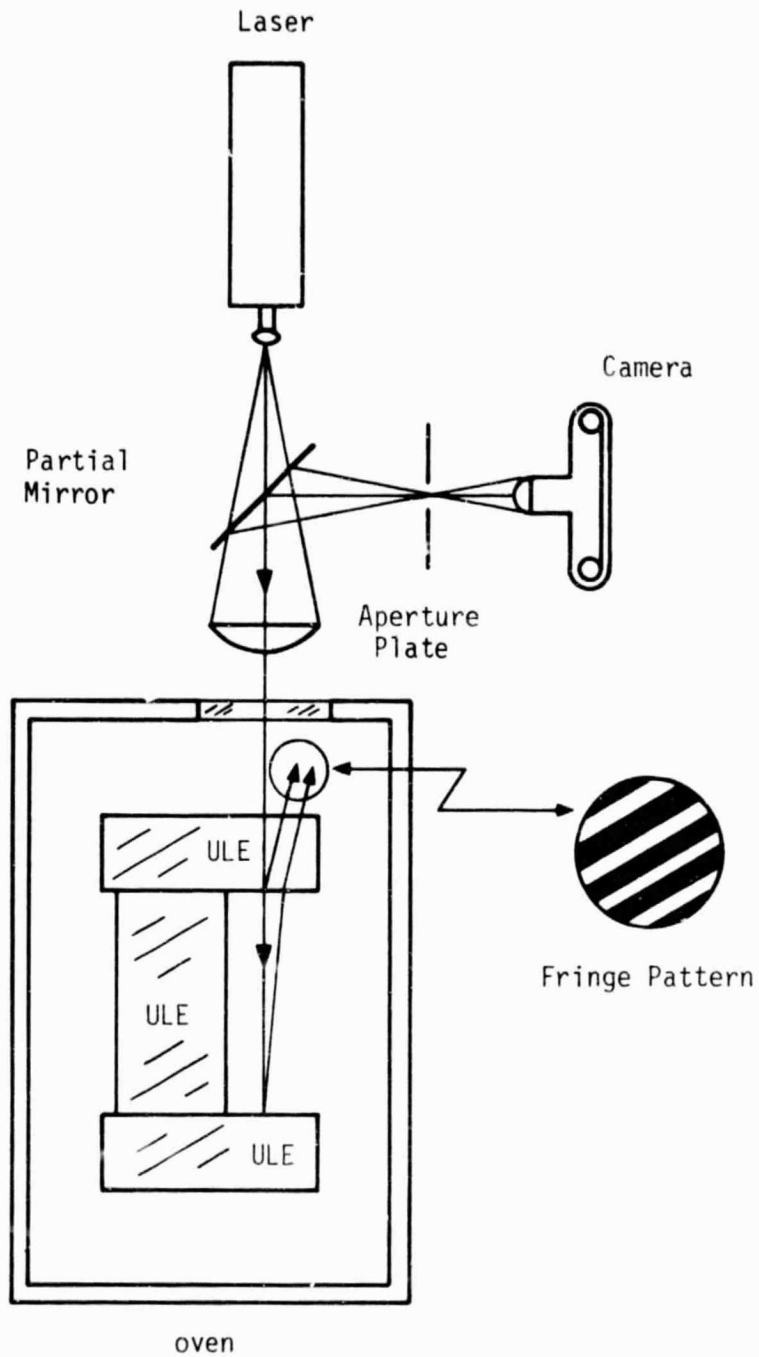


FIGURE 12. SCHEMATIC DIAGRAM OF FIZEAU INTERFEROMETRY SETUP FOR DETERMINATION OF ULE BEHAVIOR

ORIGINAL PAGE IS
OF POOR QUALITY

uniform temperature change, the upper and lower optical flats maintain their initial orientation with respect to each other. Heating and cooling rates were kept small (approximately 1/2 K (0.9°F) per minute) in order to avoid any large temperature gradients through the specimen configuration which might have broken the optical contact. In addition, the specimen was allowed to soak at each temperature for one half hour so as to assure temperature equilibrium throughout the specimen.

In this type of interferometry, the fringe density does not change as the specimen undergoes a deformation. Rather, the fringes shift across the field of view, and it is therefore impossible to distinguish anything but fractional fringe shifts, unless a continuous record of fringe movement is kept. This is in contrast to moiré interferometry, in which the fringe density does change, and hence only discrete observations are needed to determine changes in fringe order. Since fringe information was being recorded on a 35 mm camera, continuous observations were not feasible. To overcome this problem, measurements were taken at temperature intervals at which deformations were small enough to cause only fractional fringe shifts.

The basic sensitivity of this type of interferometry is $\lambda/2$ per fringe, where λ is the wavelength of the light used for illumination, and in this case was 316.4 nm (12.5 μ in.) per fringe. The gage length used in this experiment was approximately 76.2 mm (3.0 in.), resulting in a strain sensitivity of 4.15 $\mu\epsilon$ per fringe. Assuming fringe shifts can be accurately determined only to a fifth of a fringe (using the same procedure as described in Section 5.2.3), a resolution of 0.83

μe was obtained. Results of this experiment are given in Section 6.1.

5.3.2 Calibration of Reference Grating

Once the thermal expansion of the ULE was determined, it was used to determine the expansion of the reference grating. A grating was applied to a block of ULE by the methods described in Section 5.1.3. The block was then used as a specimen in the moiré interferometry setup. Minor modifications in the specimen fixture had to be made in order to accommodate the ULE specimen, due to its size. However, the same alignment procedures as described earlier were used.

The specimen was heated from 297 K (75°F) to 450 K (350°F) and then cooled back to 297 K (75°F) with measurements taken at 40 K (72°F) intervals. Photographs of the fringe pattern were taken at each temperature step. Results from this experiment are presented in Section 6.2.

5.4 Specimen Description

5.4.1 Materials

Graphite-epoxy was selected as the material system for use as specimens in this research. The specific composite system was T300/5208, and specimens were cut from the same composite panels as used in the experimental program described in reference [39].

Four laminate configurations, $[0]$, $[90]$, $[0/\pm 45/90]_s$, and $[0/90/\pm 45]_s$ were selected for the initial experimental program to determine the applicability of moiré interferometry for measuring thermal strains in composites. The specimens were machined to the

dimensions shown in Fig. 10. A summary of all pertinent specimen information is given in Table 1.

5.4.2 Surface Preparation and Environmental Conditioning

In preliminary tests it was found that gratings could not be successively applied to composites so that fringe patterns could be viewed without some prior surface preparation. This surface preparation consisted of removing the weave pattern that exists in the surface of most composites as a result of fabrication. This weave consists mainly of the resin material, and may be removed by lightly sanding with 280 grit silicon carbide paper. When this weave pattern was not removed, it tended to be visible through the grating, masking the fringe pattern. Sanding away approximately 1/4 of a ply thickness was sufficient to remove the weave. Because mainly resin material is being removed by this sanding, it should not appreciably affect the thermal response of the laminate. Specimen 43-4B was inadvertently sanded more than needed (approximately 1/2 of a ply thickness removed), and in doing so, both fibers and resin were removed. Consequences of this will be discussed in Chapter 6. For both the [0] and [90] specimens, no sanding was performed since these specimens came from panels that were fabricated with one side possessing no weave pattern.

All specimens, except 43-4B, were dried prior to testing to remove all moisture. The specimens were dried at 340 K (152°F) in an oven equipped with a dry nitrogen purge. Specimens were kept in the oven prior to application of the grating or strain gages for approximately

TABLE 1
SPECIMEN INFORMATION

Specimen Identification	Laminate Configuration	No. of Plys	Length ¹ mm (in.)	Width ¹ mm (in.)	Thickness ² mm (in.)	
					Before	After
38-15A	[0]	8	127 (5.0)	25.4 (1.0)	1.0414 (0.0410)	1.0414 (0.0410)
39-11B	[90]	8	127 (5.0)	25.4 (1.0)	1.0414 (0.0410)	1.0414 (0.0410)
43-4B	[0/±45/90] _s	8	127 (5.0)	25.4 (1.0)	1.1278 (0.0444)	1.0744 (0.0423)
43-1A	[0/±45/90] _s	8	127 (5.0)	25.4 (1.0)	1.1608 (0.0457)	1.1354 (0.0447)
44-1B	[0/90/±45] _s	8	127 (5.0)	25.4 (1.0)	1.1278 (0.0444)	1.0947 (0.0431)

¹Nominal Size

²Refers to thickness under grating before and after sanding

1 month. Specimens were then removed and equipped with gratings and strain gages, a process which usually took approximately one week. Specimens were then returned to the oven for an additional week to remove any moisture absorbed during the application of gratings and strain gages. Total weight loss during conditioning was on the average about 0.7%. After drying, specimens were stored in a desiccator until tested. Specimen 43-4B was tested without being dried to examine the effects of moisture on the thermal expansion behavior.

5.4.3 Strain Gage Techniques

For purposes of comparing thermal expansion measurements made with moiré interferometry and electrical resistance strain gages, all specimens were equipped with strain gages as well as with gratings. Back to back gages were placed on each specimen in the positions shown in Fig. 10. The type of gages used for this research were Micro-Measurements WK series 350 ohm single gages. Due to availability, two different gage lengths were used, 6.35 mm (0.25 in.) and 3.175 mm (0.125 in.). Strain gage measurements were recorded with the aid of a Vishay portable strain indicator. The bonding techniques used were those recommended by Micro-Measurements.

As discussed in Section 2.1, anytime a strain gage is used in a test in which the temperature changes during the test, corrections must be made to account for the apparent strain induced in the gage by this change in temperature. As described in reference [3], the total temperature induced strain for a change in temperature ΔT may be written as follows

$$\epsilon_{app} = (\gamma_G/F)\Delta T + \alpha_s\Delta T - \alpha_G\Delta T \quad (5.7)$$

where ϵ_{app} is the thermal strain as given directly by the strain gage output, γ_G is the thermal coefficient of resistance of the gage conductor, F is the gage factor, α_s is the CTE of the specimen, and α_G is the CTE of the gage material. The above equation may be rearranged to solve for those factors that are influenced by the gage alone, giving

$$\epsilon_{gage} = \epsilon_{app} - \epsilon_s \quad (5.8)$$

Note that ϵ_s is equal to $\alpha_s\Delta T$ and ϵ_{gage} is $(\gamma_G/F - \alpha_G)\Delta T$. If the thermal strain of the specimen is known, then ϵ_{gage} may be computed. It is important to note that ϵ_{gage} is a constant for a particular type of gage. If the same type of gage is placed on a specimen of unknown thermal expansion, Equ. (5.8) may be rewritten as

$$\epsilon_s = \epsilon_{app} - \epsilon_{gage} \quad (5.9)$$

ϵ_s is now the true thermal strain of the specimen, ϵ_{app} is the strain taken directly from the strain gage, and ϵ_{gage} is the strain determined previously.

Whenever a strain gage is used in other than a uniaxial stress field, and on a material with Poisson's ratio different from the one used to determine its gage factor, a correction factor must be applied. This is commonly referred to as a transverse sensitivity correction, and for a single element gage the corrected strain $\hat{\epsilon}_s$, is given in reference [2] as

$$\hat{\epsilon}_s = \epsilon_s \left(\frac{1 - \nu_0 k_t}{1 + \epsilon_t / \epsilon_a k_t} \right) \quad (5.10)$$

where ϵ_s is the strain as determined from Equ. (5.9), ν_0 is Poisson's ratio of the material used by the manufacturer to determine the gage factor (0.285 in this case), k_t is the transverse sensitivity of the gage as quoted by the manufacturer, and ϵ_t/ϵ_a is the ratio of the transverse to axial strain of the test specimen.

To correct for the strain induced in the gage by heating, gages were bonded to a block of ULE whose thermal expansion had been previously determined (Section 5.3.1). Apparent strain versus temperature curves were generated for both gage sizes and for repeated thermal cycling. Gage variability was also examined by placing back to back gages on the ULE and comparing the output. Results of these tests are presented in Section 6.2.

Chapter 6

RESULTS AND DISCUSSION

6.1 Reference Grating Calibration

6.1.1 ULE Expansion

Results for the experimentally determined thermal expansion of the ULE are shown in Fig. 13. Also shown in the Figure are the upper and lower bounds on the thermal expansion of ULE as given by the manufacturer. Materials with thermal expansion outside these bounds are, by their definition, not ULE. The coefficients for a third order least-squares polynomial fit to the data are given in Table 2.

A limited amount of experimental scatter was present in the data, the origin of which is not fully understood. The magnitude of this scatter was small, with the maximum deviation of an experimental data point from the least-squares curve being no more than $1.3 \mu\epsilon$. The resolution capability of this method, as stated in section 5.3.1, was $0.83 \mu\epsilon$. The above scatter therefore could not be totally explained by random errors in computing fringe shifts. The temperature of the specimen was monitored by one thermocouple attached to the specimen surface. A possible source of the experimental scatter could be the surface temperature not being truly representative of the specimen temperature. However, the slow heating and cooling rates and the temperature soak of one-half hour before each measurement makes this highly unlikely.

In this type of interferometry, when data is taken only at a discrete number of points, it is impossible to determine the absolute

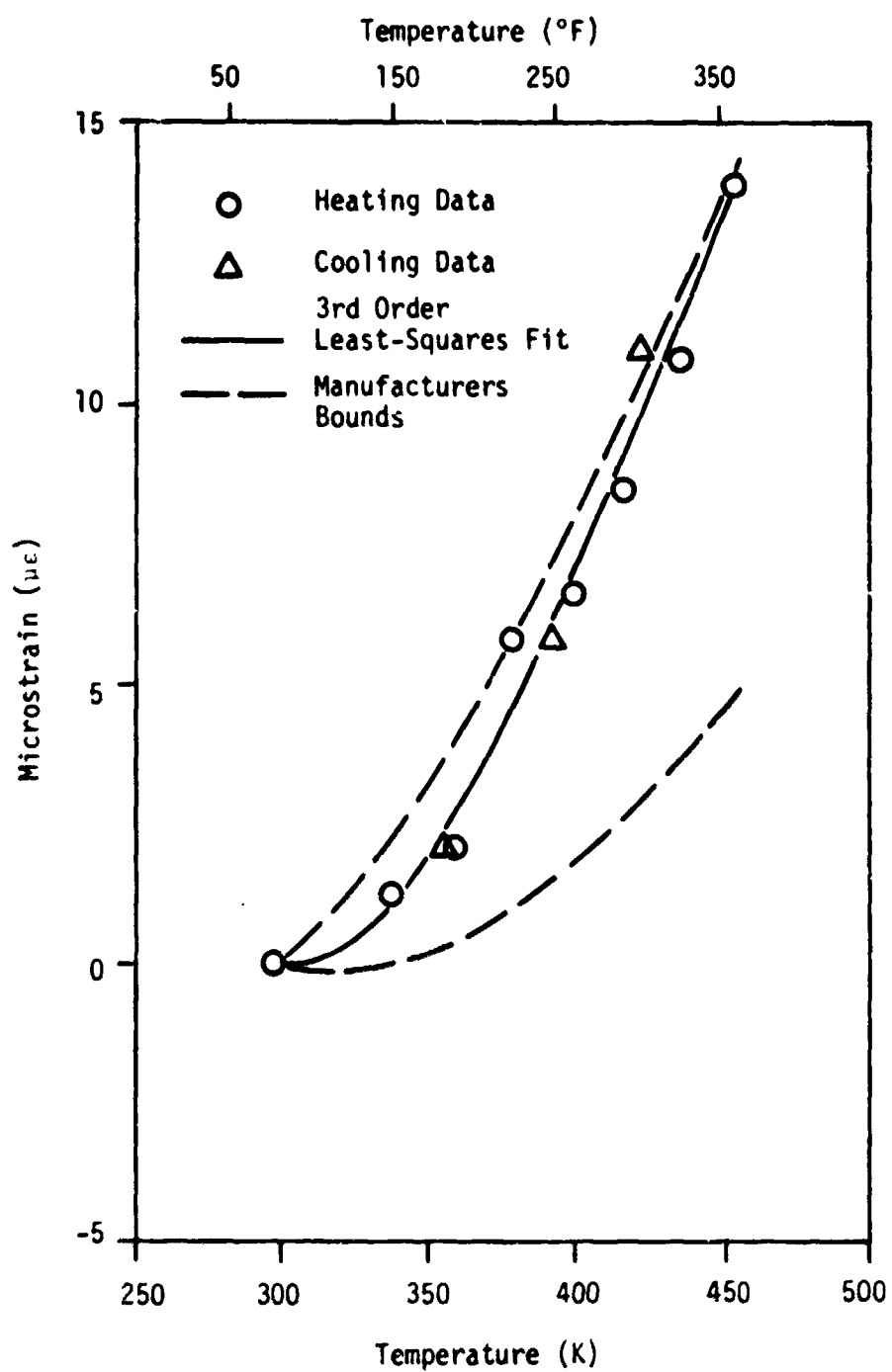


FIGURE 13. THERMAL EXPANSION OF ULE

TABLE 2
POLYNOMIAL COEFFICIENTS FOR THERMAL STRAIN AS A FUNCTION OF TEMPERATURE

ϵ $\mu\epsilon$	A_0 $\mu\epsilon$ ($\mu\epsilon$)	A_1^{-1} $\mu\epsilon K^{-1}$ ($\mu\epsilon^\circ F^{-1}$)	A_2^{-2} $\mu\epsilon K^{-2}$ ($\mu\epsilon^\circ F^{-2}$)	A_3^{-3} $\mu\epsilon K^{-3}$ ($\mu\epsilon^\circ F^{-3}$)
ϵ_{ULE}	1.71424×10^2 (2.20232×10^0)	-1.38536×10^0 (-5.684408×10^{-2})	3.54245×10^{-3} (3.93171×10^{-4})	-2.76556×10^{-6} (-4.00045×10^{-7})
ϵ_r (Reference Grating)	6.88818×10^1 (-1.63891×10^1)	-1.23475×10^0 (1.83035×10^{-1})	4.45746×10^{-3} (5.14743×10^{-4})	-3.64134×10^{-6} (-6.24372×10^{-7})
ϵ_{app}^I (Strain Gage Type I)	-4.09454×10^3 (-1.48786×10^2)	2.92264×10^1 (2.63786×10^0)	-6.59742×10^{-2} (-9.22191×10^{-3})	4.71145×10^{-5} (8.07862×10^{-6})
ϵ_{app}^{II} (Strain Gage Type II)	-3.67325×10^3 (-1.23608×10^2)	2.65198×10^1 (2.23710×10^0)	-6.01740×10^{-2} (-8.61275×10^{-3})	4.21198×10^{-5} (7.22219×10^{-6})

$$\epsilon = A_0 + A_1 T + A_2 T^2 + A_3 T^3$$

shift. Rather, only the fractional shift can be ascertained. (For example, the difference between an absolute fringe shift of 0.2, 1.2, 2.2 etc. cannot be distinguished.) In this experiment, scatter could have been reduced by assuming certain fringe shifts are one plus the fraction, rather than the fractional shift. However, the resulting thermal strain would have approximately doubled in magnitude, falling well outside the bounds given by the manufacturer. Data were taken at intervals which, according to the manufacturer, should have corresponded to only fractional fringe shifts. The fractional fringe shift computations resulted in the expansion shown in Fig. 13. It was felt that the experimentally determined expansion shown in Fig. 13 is a valid representation of the ULE's thermal expansion.

6.1.2 Thermal Expansion of Reference Grating

The thermal expansion of the reference grating is shown in Fig. 14. This expansion was obtained by using ULE as the specimen and applying the appropriate correction factors as outlined in Section 5.2.4. The thermal strain of the reference grating, ϵ_r , was computed by rearranging Equ. (5.5) to give

$$\epsilon_r = \epsilon_s + \epsilon_{app}$$

where ϵ_s is the thermal strain of the ULE, and ϵ_{app} is the strain as computed from Equ. (5.4). It should be noted that different blanks of ULE were used for verification of the ULE properties and determination of reference grating properties. However, the specimens were cut out of the same slab of material, which in turn was taken from a large ULE

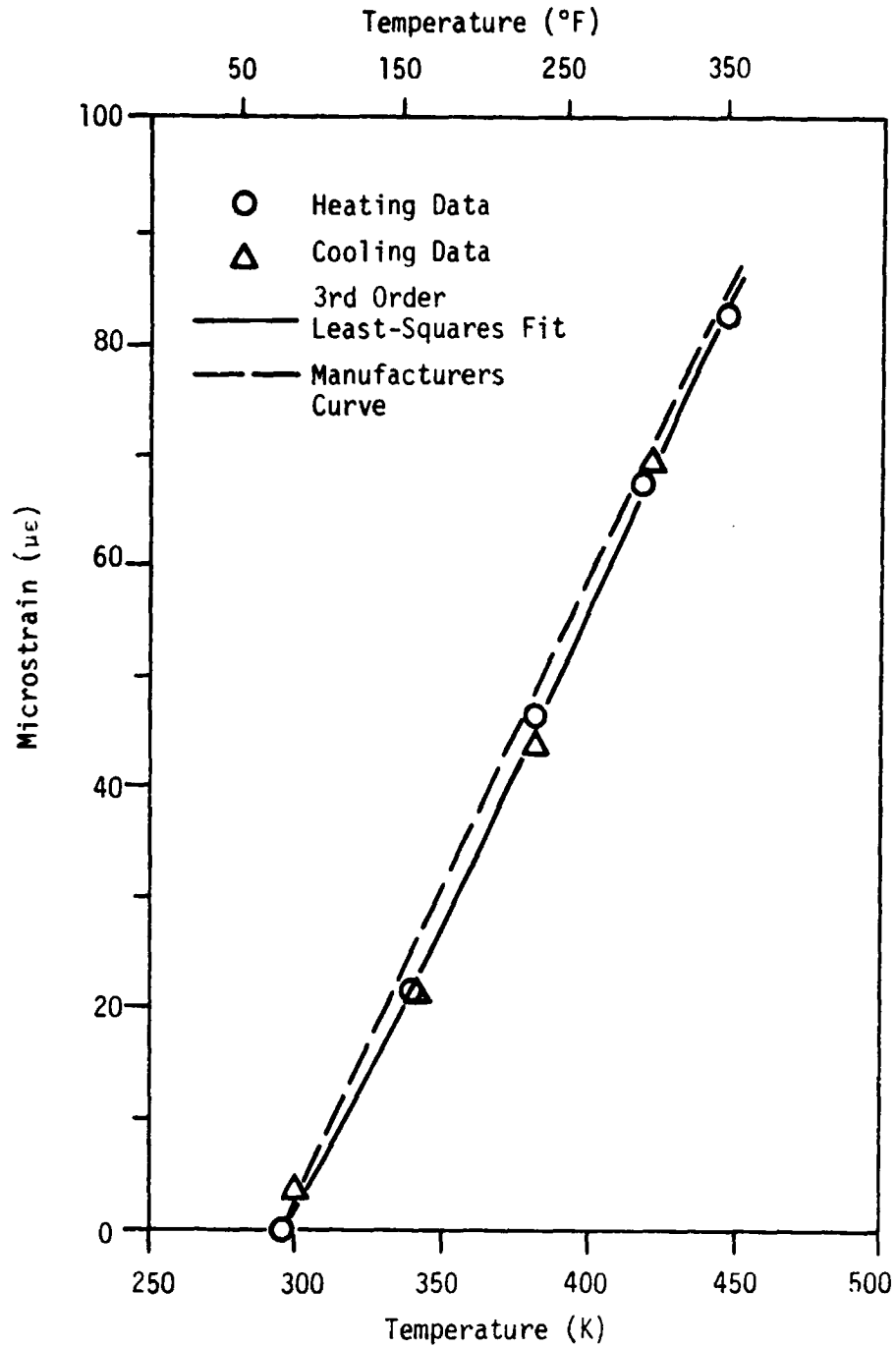


FIGURE 14. THERMAL EXPANSION OF REFERENCE GRATING

ingot. The assumption was therefore made that the measured expansion of the ULE was representative of both pieces.

A third order polynomial was fit to the data obtained from Equ. (5.4) for ϵ_{app} by a least-squares method. This polynomial was then added to the polynomial obtained for the thermal expansion of the ULE to obtain an expression for ϵ_r . The coefficients for the polynomial representation of ϵ_r are given in Table 2. The experimental results are compared to the manufacturers curve for fused silica in Fig. 14.

As indicated in the Figure, there is good agreement between the two curves and there is little scatter in the experimental results. The small differences between the two curves may be attributed to small differences in material behavior from one piece of fused silica to another.

This experiment served two purposes. The first was to determine the thermal expansion of the reference grating which was needed in order to make the necessary correction when determining the thermal expansion of a specimen. Secondly, it served as a validation of the moiré technique for determining the thermal expansion of materials. The results indicate that this is an accurate and reliable method.

6.2 Apparent Strain for Strain Gages Subjected to Thermal Loading

Apparent strain versus temperature curves were generated for repeated thermal cycling of both gage lengths employed in this study. The gages of different length were designated Type I (6.35 mm (0.25 in.)) and Type II (3.175 mm (0.125 in.)). The gages were bonded to ULE for

these tests. Each thermal cycle consisted of heating from 297 K (75°F) to 422 K (300°F) and then cooling to 297 K (75°F). Data were obtained from four thermal cycles for each gage type. The variation of results between cycles was random for both gage types. There was also some difference in the output obtained from back to back gages. This difference was approximately constant from cycle to cycle indicating that its origin was the result of differences in the gages or differences in bonding.

For all data at a particular temperature, the mean and standard deviation were computed for each gage type. This information, along with a least-squares fit of a third order polynomial through the mean values and the manufacturer's apparent strain curve are shown in Fig. 15. Coefficients of the polynomial are listed in Table 2. Data was presented in this manner so as to provide a representation of the thermal response of the strain gage as well as the variation that might be expected from cycle to cycle and from gage to gage.

Note the much larger standard deviation obtained for the Type I than for the Type II gage. The standard deviation for the Type I gage at 422 K (300°F) was approximately 24 $\mu\epsilon$ compared to only 12 $\mu\epsilon$ for the Type II gage. The reason for this large discrepancy is not known. However, it was necessary to make several attempts before a satisfactory bond between the Type I gage and the ULE was obtained. The quality of this bond was determined by observation under a microscope, which was the only method available. It should also be noted that the manufacturer's curve falls well below the experimental

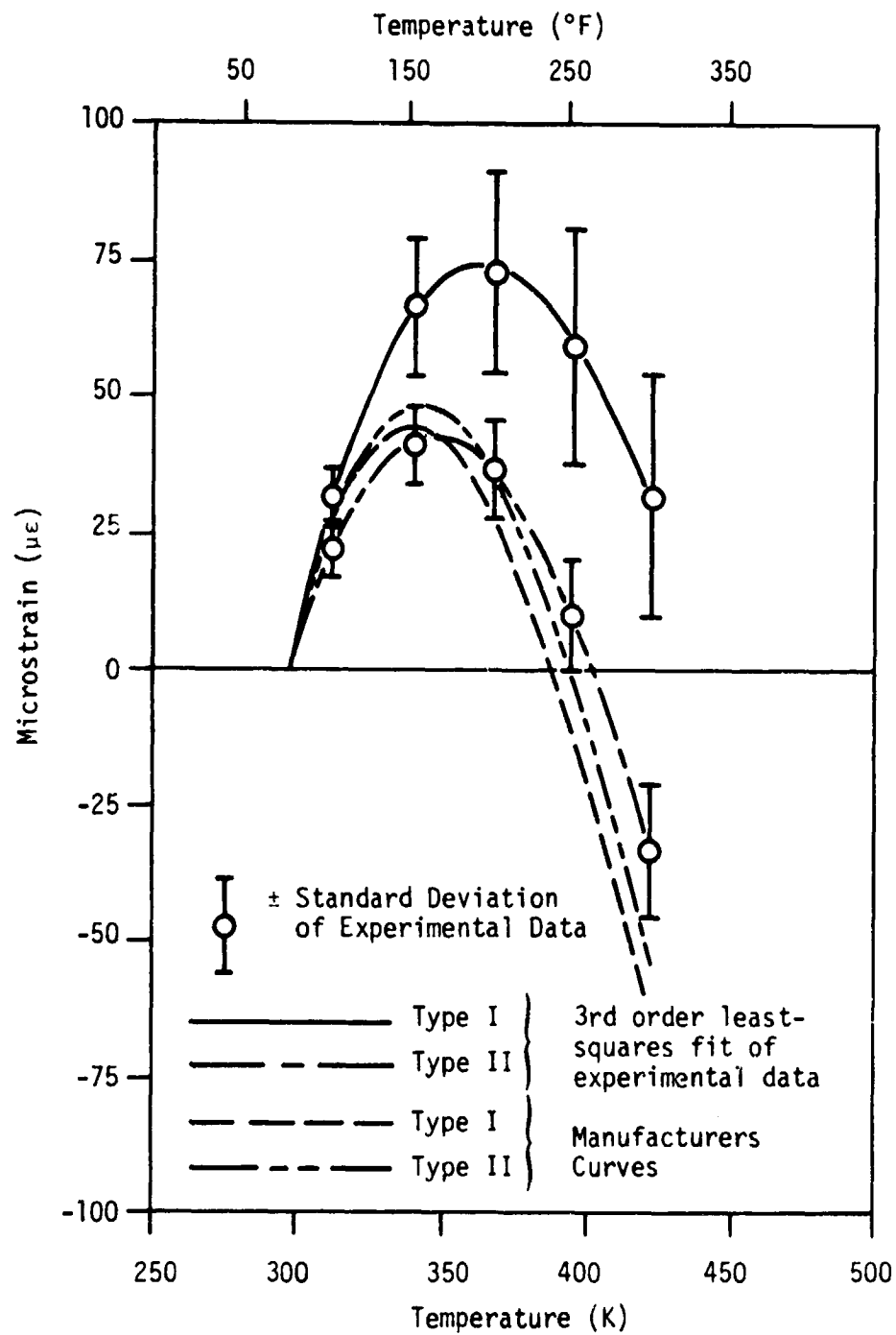


FIGURE 15. APPARENT STRAIN CURVES FOR STRAIN GAGES ON ULE

curve for this gage.

For the Type II gage, a satisfactory bond was obtained on the first attempt. As can be seen in Fig. 15, the manufacturer's curve falls very close to the bounds given by the standard deviations of the experimental curve.

Results of this work compare reasonably well with those obtained by Hyer and Hagaman [33], in which gages bonded to ULE were subjected to 15 thermal cycles between 297 K (75°F) and 422 K (300°F). They also obtained a random variation of strain response from cycle to cycle, and a scatter of less than 80 $\mu\epsilon$ at the maximum temperature. A direct comparison between results cannot be made, since they used gages that had different thermal properties of the backing material, resulting in a strain difference of different magnitude.

From the results obtained above, it is clear that strain gages are only marginally useful in determining the thermal response of low expansion materials. This suggests caution in the case of composite materials with very small CTE's.

When the thermal strain of a composite specimen was determined, the apparent strain obtained from gages on the ULE was used to make corrections as described in Section 5.4.3. These corrections were based on the assumption of an identical gage and bond on both the ULE and the composite specimen. The obtained results show that this assumption is not always valid. Strain readings can vary as much as 50 $\mu\epsilon$ for supposedly identical gages with identical bonds. In many instances, 50 $\mu\epsilon$ is greater than the total strain being measured.

6.3 Thermal Expansion of Composites

Discussion of results for the composite specimens examined in this investigation will be grouped according to laminate type. Comparison between strain gage and moiré interferometry measurements, between experimental results and theoretical predictions, and between the results of this research and that of other researchers (when applicable) will be presented for each laminate type.

6.3.1 Unidirectional Laminates

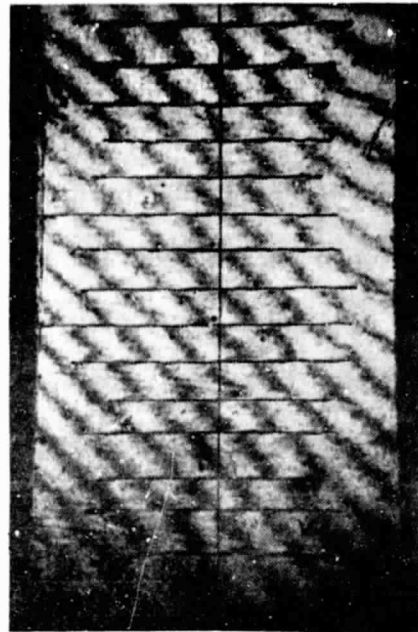
6.3.1.1 [0] Laminate

A large fringe rotation was observed when the [0] laminate (Spec. I.D. 38-15A, Table 1) was heated from room temperature to 422 K (300°F). A large number of fringes of rotation make fringe interpretation difficult. This problem was reduced by beginning with initial fringes of rotation at room temperature. This initial rotation was in the opposite direction to that during heating, and therefore, the number of fringes of rotation at the maximum temperature was reduced. However, rotation was still severe enough to prohibit data from being taken past 394 K (250°F). Fringe patterns of the [0] laminate at 297 K (75°F), 360 K (200°F) and 394 K (250°F) are shown in Figs. 16 a, b, and c.

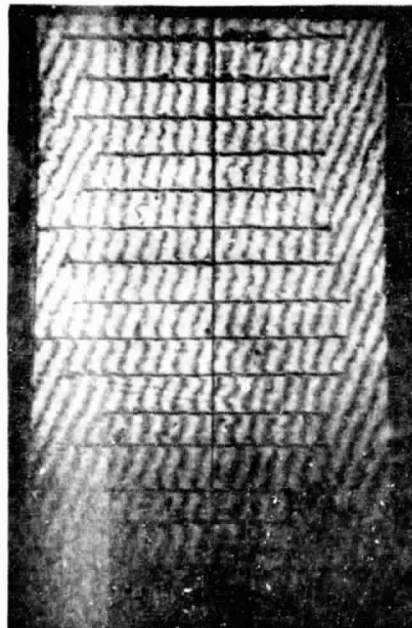
If the change in fringe order, N , is measured along a line perpendicular to the grating rulings, these fringes of rotation do not introduce any significant errors. The apparent extensional strain is given by



(a) 297 K (75°F)



(b) 366 K (200°F)



(c) 394 K (250°F)

FIGURE 16. MOIRÉ FRINGE PATTERN FOR [0] LAMINATE

ORIGINAL PAGE IS
OF POOR QUALITY

$$\epsilon_{\text{app/rot}} = \frac{1}{2} N_r^2 g_r^2 \quad (6.1)$$

where N_r is the number of fringes of rotation per unit length. For this particular laminate, $\epsilon_{\text{app/rot}}$ was less than $0.5 \mu\epsilon$, and was therefore disregarded. However, if N is measured along a line that is not perpendicular to the grating rulings, fringes of rotation will cause an apparent strain given by

$$\hat{\epsilon}_{\text{app/rot}} = \phi N_r g_r \quad (6.2)$$

where ϕ is the misalignment angle (i.e. deviation from a line perpendicular to the grating rulings). This can result in apparent strains on the order of $5 \mu\epsilon$, which for the [0] laminate is a large percentage of the total strain. The sign of $\hat{\epsilon}_{\text{app/rot}}$ is determined from the direction of fringe rotation with respect to ϕ , and the sign of the initial fringe pattern.

In this investigation, ϕ was measured as 0.2° by viewing the photoplate used to replicate the grating onto the specimen with a microscope at 600 X magnification. The photoplate was scribed with the line along which data was taken, and thus the angle between this line and grating rulings could be measured. (This angle was measured as 89.8° .) By counting N_r at each temperature, the strain as given by Equ. (5.4) could be corrected to account for the apparent strain described above. Results based on the above procedure are given in Fig. 17. A first order least-squares line was fit to the data, and yields a CTE of $-0.088 \mu\epsilon K^{-1}$ ($-0.049 \mu\epsilon F^{-1}$). Based on the error

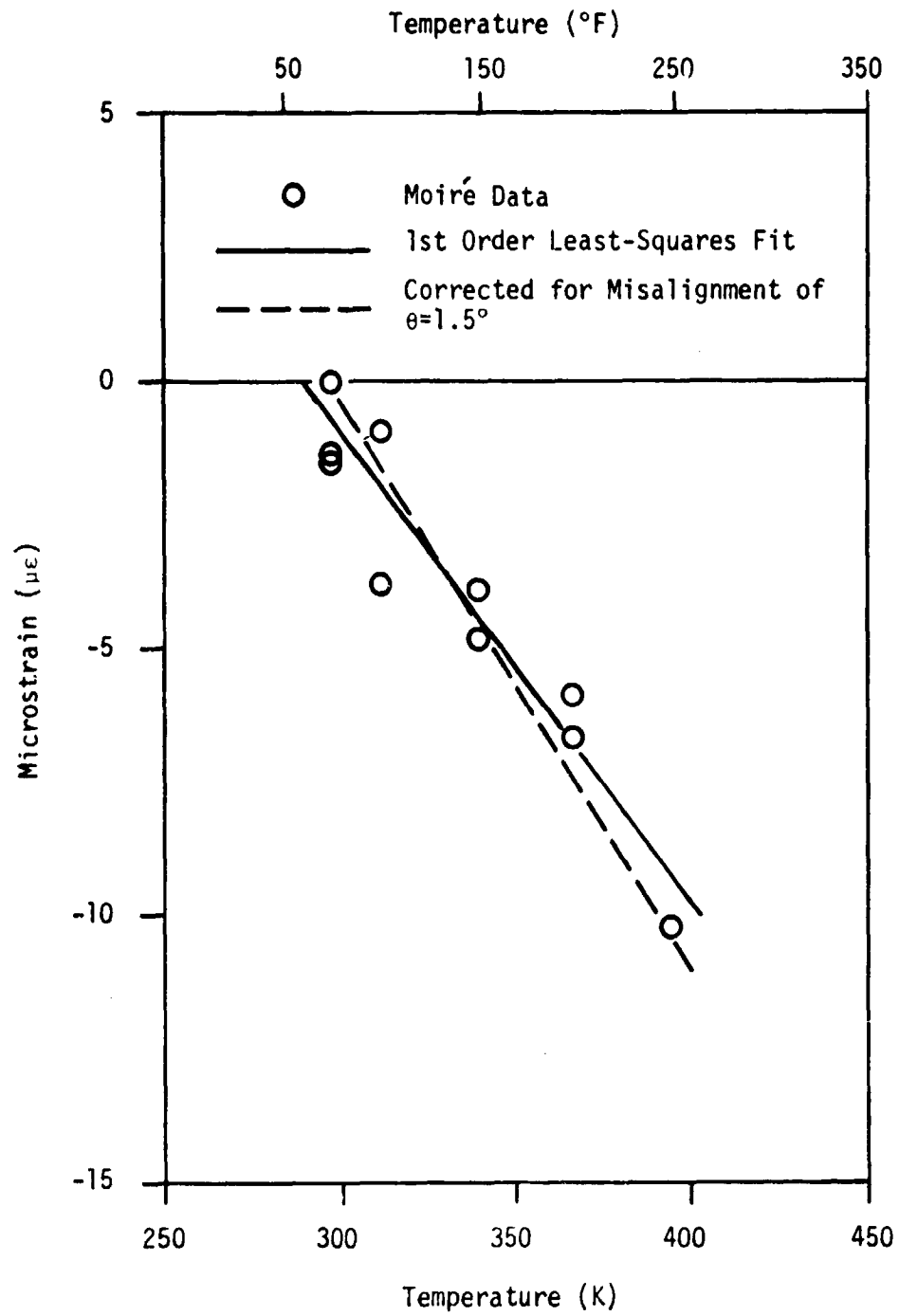


FIGURE 17. MOIRÉ THERMAL EXPANSION OF [0] LAMINATE

analysis of Appendix A, the deviation on the CTE is $\pm 0.046 \mu\text{eK}^{-1}$ ($0.026 \mu\text{e}^\circ\text{F}^{-1}$).

There are two possible causes for this fringe rotation. The first is an in-plane rigid body rotation of the specimen, which causes a rotation between the rulings of the specimen and reference grating. The second cause is unique for anisotropic materials, which for certain orientations and laminate configurations, possess a shearing CTE, α_{xy} , as well as the normal CTE's α_x and α_y . This shearing CTE results in a rotation of the specimen grating rulings when exposed to a uniform change in temperature. Rotation of the fringes may be caused by either of these effects or by a combination of the two, and it is impossible to distinguish between them.

In this investigation, this shearing CTE was only possible for certain orientations of the unidirectional specimens. For directions parallel and transverse to the fibers, there existed two CTE's, α_1 and α_2 , respectively (Fig. 1). However, if measurements are inadvertently taken in two orthogonal directions that were slightly rotated from the material principal directions then three CTE's exist, α_x , α_y and α_{xy} . The relationship between α_1 , α_2 and α_x , α_y and α_{xy} is given by

$$\begin{aligned}\alpha_x &= m^2\alpha_1 + n^2\alpha_2 \\ \alpha_y &= n^2\alpha_1 + m^2\alpha_2 \\ \alpha_{xy} &= 2mn\alpha_1 - 2mn\alpha_2\end{aligned}\tag{6.3}$$

where $m = \cos\theta$ and $n = \sin\theta$ (Fig. 1).

The misalignment angle, θ , was measured for the [0] laminate as 1.5° . By using values of α_x as $-0.088 \mu\epsilon K^{-1}$ ($-0.049 \mu\epsilon^\circ F^{-1}$) and α_y as $27.24 \mu\epsilon K^{-1}$ ($15.1 \mu\epsilon^\circ F^{-1}$) at 360 K ($188^\circ F$), computed from the moiré data for the [0] and [90] laminates, respectively, values of α_1 and α_2 were computed from Equ. (6.3) as

$$\alpha_1 = -0.107 \mu\epsilon K^{-1} (-0.059 \mu\epsilon^\circ F^{-1})$$

$$\alpha_2 = 27.24 \mu\epsilon K^{-1} (15.1 \mu\epsilon^\circ F^{-1})$$

This misalignment caused approximately an 18% error in the measurement of α_1 , but had a negligible effect on the measurement of α_2 .

Strain gage results for the [0] laminate are presented and discussed separately in Appendix B because of problems that were unique to this particular laminate.

6.3.1.2 [90] Laminate

Thermal expansion results for the [90] lamainte (Spec. I.D. 39-11B, Table 1) obtained using moiré interferometry are shown in Fig. 18. These results were based on data obtained from tests on two successive days. The specimen was stored in dry nitrogen overnight. Strain values were computed using the methods described in Section 5.2, and both the experimental values and a 2nd order least-squares curve which was fit through the date are shown in Fig. 18. Photographs of the fringe pattern at 297 K ($75^\circ F$), 366 K ($200^\circ F$), and 422 K ($300^\circ F$) are shown in Fig. 19 a, b, and c.

The maximum strain upon heating to 422 K ($300^\circ F$) was approximately 3300 $\mu\epsilon$. As stated previously, the sensitivity of this method was

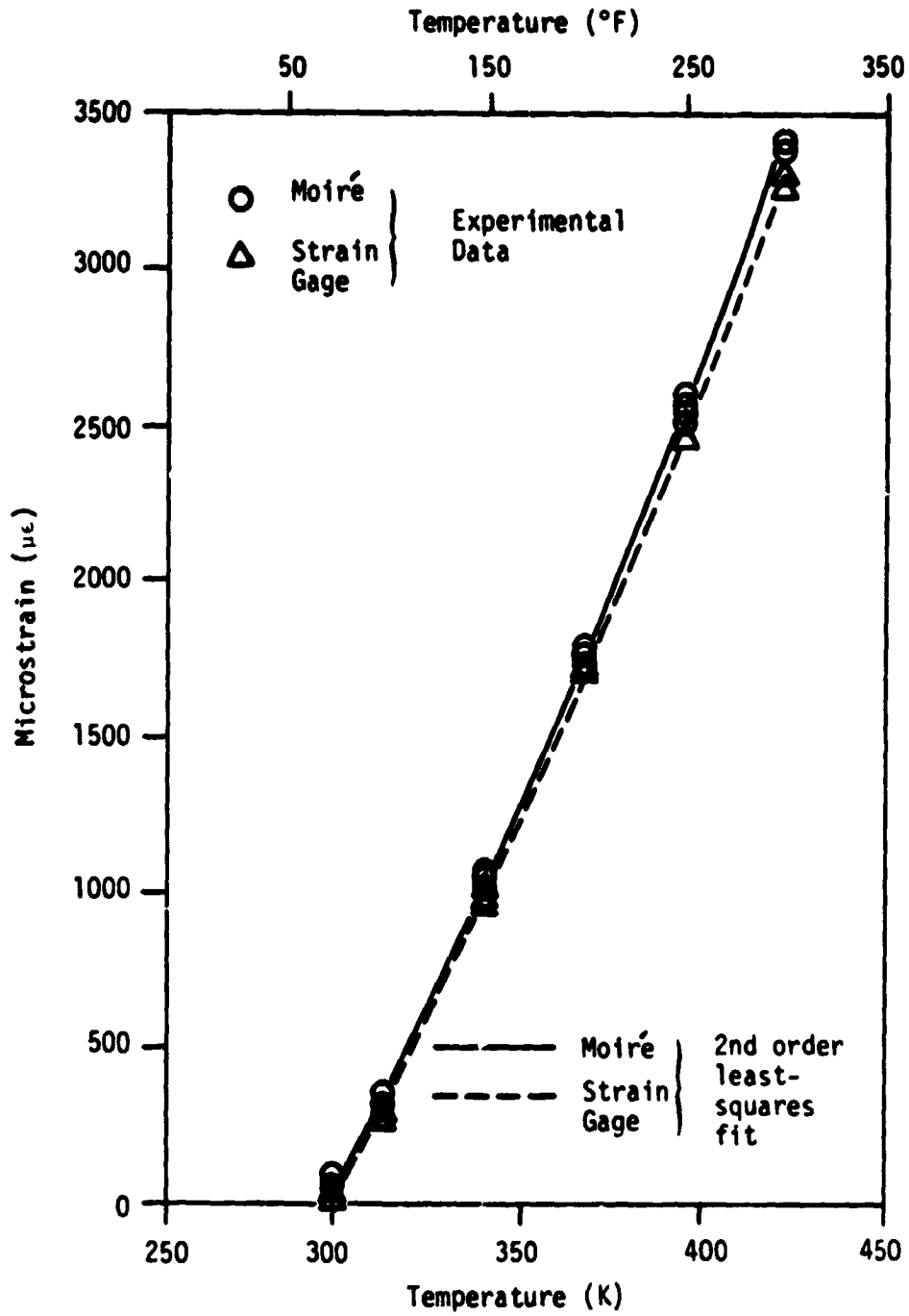


FIGURE 18. THERMAL EXPANSION OF [90] LAMINATE



(a) 297 K (75°F)



(b) 366 K (200°F)



(c) 422 K (300°F)

FIGURE 19. MOIRÉ FRINGE PATTERN FOR [90] LAMINATE

ORIGINAL PAGE IS
OF POOR QUALITY

833 nm (32.8 μ in.) per fringe, yielding a corresponding fringe density of approximately 4 fringes per mm (101 fringes per in.). For the 33 mm (1.3 in.) gage length used in this research, this would result in 132 fringes at the maximum temperature. Because this was an inconveniently high number of fringes to count, an alternate approach was sought to reduce the number of fringes.

For this particular specimen the number of fringes at room temperature was large, and was caused by drying of the specimen after replication of the grating and prior to testing. Because the [90] laminate had a very large coefficient of moisture expansion, a large contraction took place when moisture desorbed from the specimen. This gave the condition

$$g_s < \beta_g g_r$$

and resulted in the large number of initial fringes.

As described in Section 5.2.4, the fringe density for the above condition decreases upon heating if the specimen expands more than the reference grating. This was the case for the [90] laminate. As the specimen was heated to 422 K (300°F), the fringe density decreased, reached a null field, and then increased (Fig. 19 a, b, and c). Therefore, the total number of fringes at 422 K (300°F) was 132 - initial number of fringes, or in this case, 132 - 80.

Because a large number of fringes still remained to be counted at both room temperature and 422 K (300°F), a gage length of 15 mm (0.6 in.) was used, which reduced the number of fringes to be counted approxi-

mately in half. This reduced the sensitivity to $10 \mu\epsilon$, but was still less than 0.5% of the maximum strain.

Also shown in Fig. 18 are results obtained from strain gage output. Although back to back gages were placed on the specimen, data was collected from only one gage. The other gage was defective. The [90] laminate was equipped with a Type I gage, and strains were computed using the mean values of the apparent strain given in Section 6.2, according to the procedures outlined in Section 5.4.3. A second order polynomial was fit to the data using a least-squares procedure.

The correction factor for the transverse sensitivity as defined by Equ. (5.10) was negligible for the [90] laminate. The ratio of the transverse to axial strain, ϵ_t/ϵ_a , arising from a uniform temperature change was on the order of 10^{-2} . By substituting into Equ. (5.10), the resulting correction was less than 1%.

Listed in Table 3 are the CTE's, for both moiré and strain gage data, for the [90] laminate at three different temperatures (297 K (75°F), 360 K (188°F), and 422 K (300°F)). This gives the maximum, minimum, and mean values of the CTE in this temperature range. These values were obtained by differentiating the polynomial expression for the thermal strain, obtained by the least-square analysis, with respect to temperature. Since the relationship between strain and temperature was a second order polynomial, the temperature dependence of α was linear. As shown, the results obtained using moiré interferometry agreed very closely with those obtained from the strain gage output. The maximum difference was only 6% at 422 K (300°F).

TABLE 3
 COEFFICIENTS OF THERMAL EXPANSION FOR
 T300/5208 LAMINATES

Laminate	CTE Values μK^{-1} ($\mu\text{E}^{\circ}\text{F}^{-1}$) Moiré/Strain Gage % Difference		
	297 K (75°F)	360 K (188°F)	422 K (300°F)
[0]	-0.107 (-0.059)	-0.107 (-0.059)	-0.107 (-0.059)
[90]	22.23 / 22.62 (12.35) / (12.57) 1.75%	27.24 / 26.45 (15.13) / (14.69) -2.91%	32.18 / 30.22 (17.88) / (16.79) -6.08%
[0/±45/90] _s (Dry)	1.89 / 2.41 (1.05) / (1.34) 28%	2.38 / 2.83 (1.32) / (1.57) 19%	2.87 / 3.25 (1.59) / (1.81) 13%
[0/90/±45] _s (Dry)	2.05 / 2.50 (1.14) / (1.39) 22%	2.40 / 2.88 (1.33) / (1.60) 20%	2.73 / 3.26 (1.52) / (1.81) 19%

The scatter in the apparent strain curve obtained for the Type I gage did not have a significant effect on the strain gage results for the [90] laminate. The maximum value of this scatter was approximately $50 \mu\epsilon$, which was less than 2% of the total strain in this specimen.

These results compare reasonably well with data obtained from Lockheed (data obtained by C. T. Herakovich through personal communication with Lockheed-California Company) for T300/5208 graphite epoxy. They obtained a linear variation of strain with temperature, which gave a constant value of α equal to $25.74 \mu\epsilon$ ($14.3 \mu\epsilon^{\circ}\text{F}^{-1}$). This was in close agreement with the mean value obtained at 360 K (188°F) of $27.24 \mu\epsilon \text{ K}^{-1}$ ($15.1 \mu\epsilon^{\circ}\text{F}^{-1}$) in this research. Limits on the CTE were computed as $\alpha \pm 0.64 \mu\epsilon \text{ K}^{-1}$ ($0.36 \mu\epsilon^{\circ}\text{F}^{-1}$), based on an error analysis of the moiré data, as described in Appendix A.

6.3.2 Quasi-Isotropic Laminates

6.3.2.1 $[0/\pm 45/90]_S$ and $[0/90/\pm 45]_S$ Laminates (Dry)

The $[0/\pm 45/90]_S$ and $[0/90/\pm 45]_S$ laminates (Specimen I.D. 43-1A and 44-1B, respectively) were each equipped with Type II back to back strain gages, as well as with moiré gratings.

The thermal strain versus temperature responses for tests on two successive days, as determined by the moiré technique, are presented in Figs. 20 and 21. The response for each laminate was nonlinear, and a second order polynomial was found to fit the data well. There were only small variations between the responses obtained on heating and cooling for each cycle, and between the response obtained from the first and

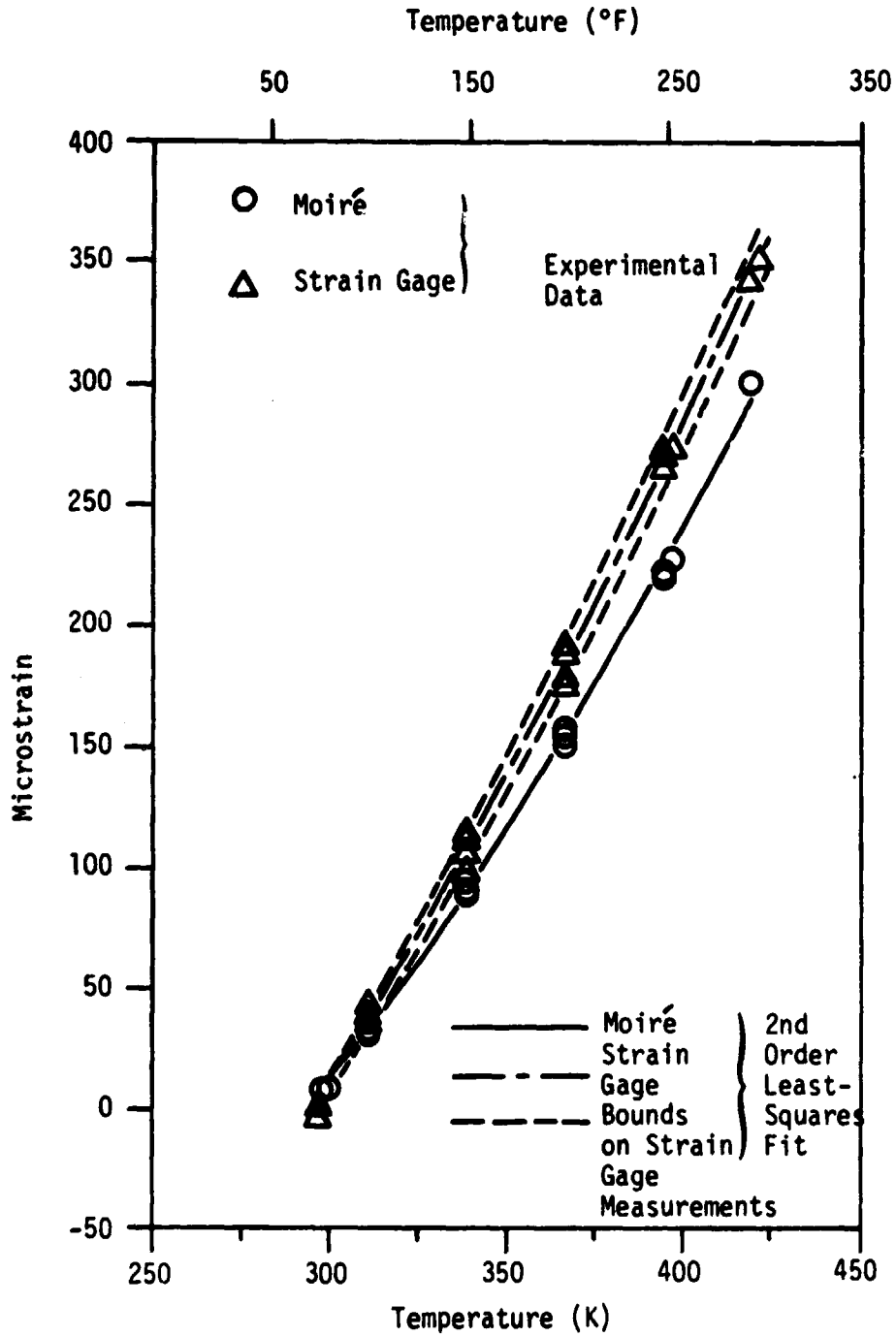


FIGURE 20. THERMAL EXPANSION OF $[0/\pm 45/90]_S$ LAMINATE

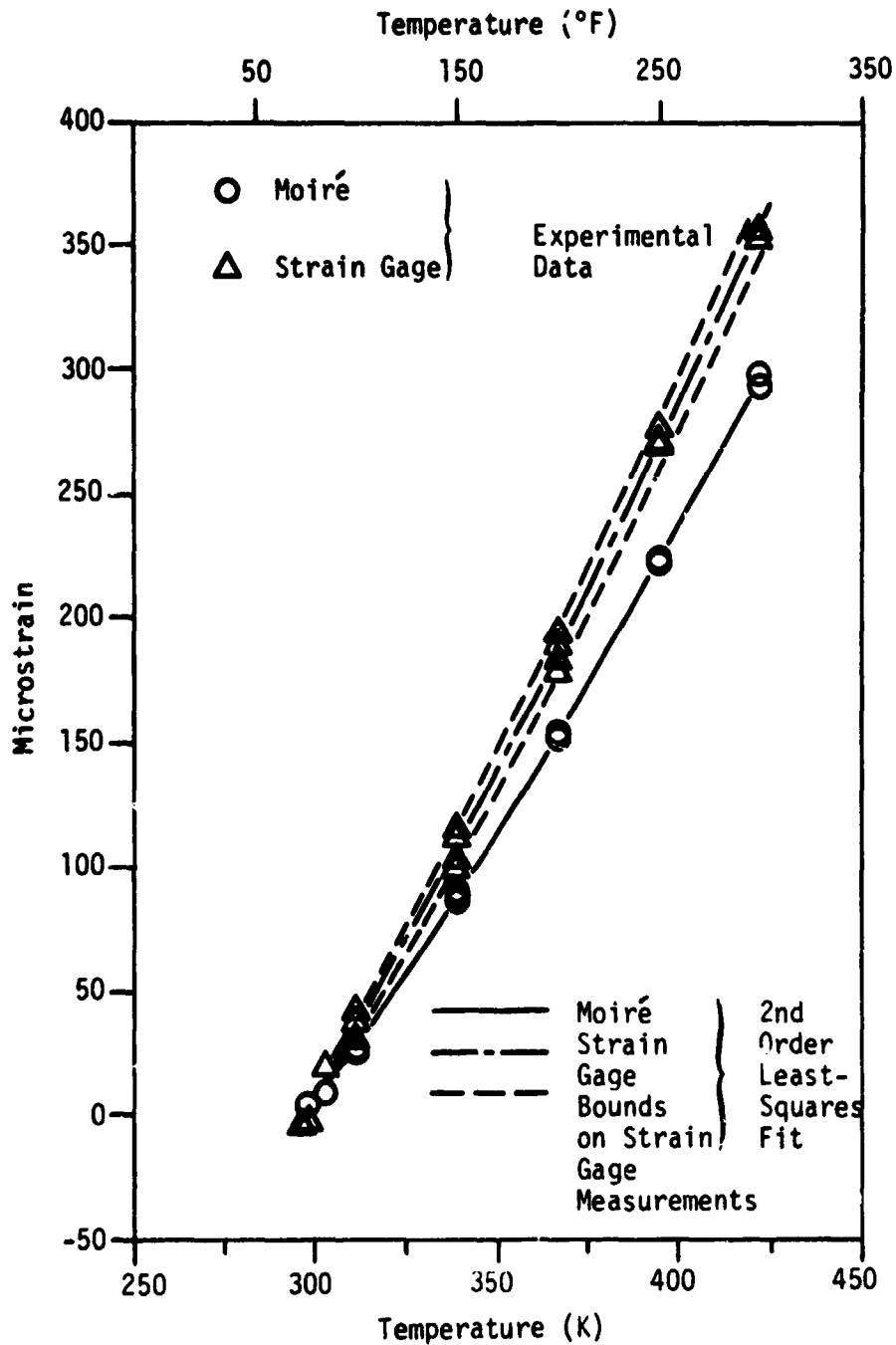


FIGURE 21. THERMAL EXPANSION OF $[0/90/+45]_s$ LAMINATE

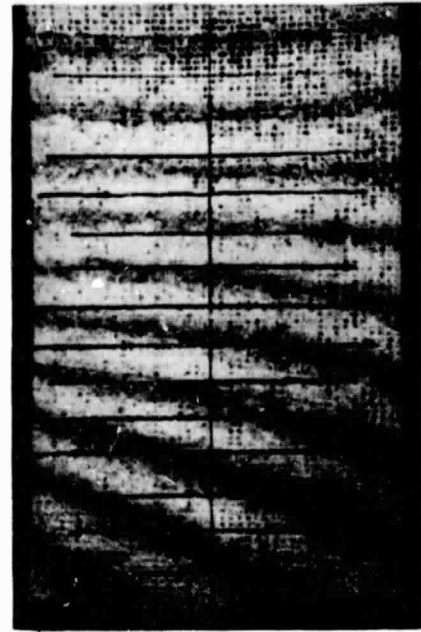
second cycles for each laminate. These variations were below the sensitivity limit of the technique ($5 \mu\epsilon$ for the 33 mm (1.3 in.) gage length used), and therefore, cannot be attributed to variations in material behavior. Photographs of a typical fringe pattern at 297 K (75°F), 366 K (200°F), and 422 K (300°F) for a quasi-isotropic laminate are given in Fig. 22.

Some small fringe rotations were observed upon heating for both of the specimens, but they were not severe enough to cause any problems in fringe interpretations, as was the case for the [0] laminate. The source of this rotation is believed to be a rigid body rotation of the specimen and not from the existence of a shearing coefficient of expansion. According to lamination theory, misalignments of the type described in Section 6.3.1.1 do not produce a shearing CTE for quasi-isotropic laminates. Also, these misalignments do not introduce any errors into the measurement of α_x and α_y of the laminate, because $\alpha_x = \alpha_y$ for a quasi-isotropic laminate, and is invariant for any set of orthogonal axes in the plane of the laminate. This assumes that the laminate configuration is truly isotropic (i.e. there is no misalignment of individual plies and all layers are of equal thickness), which may or may not be the case depending upon the quality control in the manufacturing process.

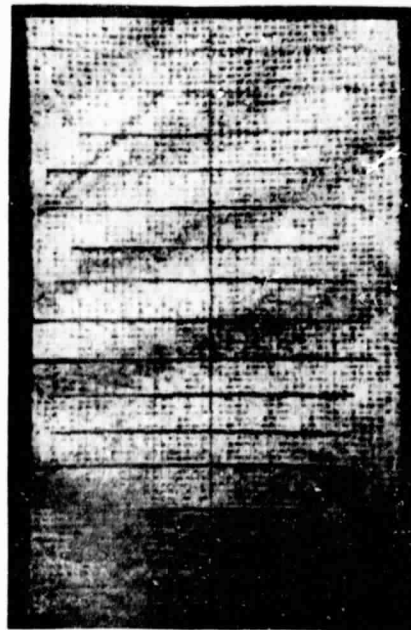
Strain gage results for these two quasi-isotropic laminates are also presented in Figs. 20 and 21. For each laminate, output from the back to back gages were nearly identical (less than $5 \mu\epsilon$), indicating that no bending took place during heating. This implies that the



(a) 297 K (75°F)



(b) 366 K (200°F)



(c) 422 K (300°F)

FIGURE 22. MOIRÉ FRINGE PATTERN FOR QUASI-ISOTROPIC LAMINATE

specimens were truly symmetric, and therefore exhibited no coupling between extension and bending. The results in Figs. 20 and 21 were based on the average of these two gages.

As indicated in the figures, variations in strain gage responses between heating and cooling and from test to test were slightly larger in magnitude than those observed in the moiré data. These variations were attributed to random scatter in strain gage response. A second order polynomial was fit to the strain gage versus temperature response for each laminate. Also shown in Figs. 20 and 21 are the results obtained by using the upper and lower bounds of the apparent strain response (Fig. 15) for the Type II gage. This gives an indication of the possible bounds on the strain gage results. All of the strain gage results included the correction for transverse sensitivity. The correction was small (approximately 3%), and was based on the assumption that $\epsilon_t/\epsilon_a = 1$ as predicted from lamination theory.

Listed in Table 3 are CTE values for the two laminates at three different temperatures for both moiré and strain gage measurements. These values were obtained by differentiating the polynomial expressions for strain as a function of temperature. This resulted in a linear variation of CTE with temperature. Values range from $1.89 \mu\epsilon K^{-1}$ ($1.05 \mu\epsilon^\circ F^{-1}$) to $2.87 \mu\epsilon K^{-1}$ ($1.59 \mu\epsilon^\circ F^{-1}$) for the $[0/\pm 45/90]_s$ laminate, and from $2.05 \mu\epsilon K^{-1}$ ($1.14 \mu\epsilon^\circ F^{-1}$) to $2.73 \mu\epsilon K^{-1}$ ($1.52 \mu\epsilon^\circ F^{-1}$) for the $[0/90/\pm 45]_s$ laminate, in the temperature range of 297 K (75°F) to 422 K (300°F). Limits on the CTE values from the moiré data were computed as $\alpha \pm 0.07 \mu\epsilon K^{-1}$ ($0.04 \mu\epsilon^\circ F$) and α

$\pm 0.03 \mu\epsilon K^{-1}$ ($0.02 \mu\epsilon^{\circ}F^{-1}$) for the $[0/\pm 45/90]_S$ and $[0/90/\pm 45]_S$ laminates, respectively. These values are based on the error analysis described in Appendix A. The $[0/\pm 45/90]_S$ laminate had a larger random error, thus causing the larger limits on the CTE. The reason for this is not completely understood, but is thought to be from a larger random variation in material behavior rather than in test technique.

As shown in Table 3, the comparison of results obtained using moiré interferometry and strain gages was not particularly good, with values obtained from strain gages being 13 to 28% higher. However, both moiré and strain gage results gave excellent support to the laminate theory prediction that changes in stacking sequence do not affect the in-plane behavior of the laminate. This is evident from comparison of the results.

6.3.2.2 Comparison with Lamination Theory

Using the equations from lamination theory, as outlined in Section 4.2, the thermal response of these laminates may be predicted. Because lamination theory predicts that the thermal response of quasi-isotropic laminates is independent of stacking sequence, the analytical predictions that follow will apply to both quasi-isotropic laminates studied in this investigation.

Predictions based on lamination theory require that the material properties of the individual lamina be known. Ideally, to compare experimental and predicted values of the thermal response of a composite material, its elastic properties as well as its thermal properties should be determined experimentally. However, it was beyond

the scope of this research to generate elastic property data. This data was therefore obtained from the literature. Kriz et al [39] generated lamina elastic properties for T300/5208 by the use of a micromechanics analysis which modeled the change in experimental data due to moisture absorption as a reduction of matrix elastic properties. They obtained properties for both the dry (totally free of moisture) and wet (saturated with moisture) states, but they did not include any temperature effects. The values for the dry state were used in this analysis. They are listed in Table 4.

Using the above temperature independent elastic properties, a linear analysis with α independent of temperature was performed as described in Section 4.2. Three different sets of thermal properties were used in the analysis. The first two were the temperature independent properties obtained from Lockheed, and from Hahn and Kim [40]. The third set of thermal properties were those determined experimentally for the [0] and [90] laminates of this investigation. Because moiré results for the [90] laminate showed a linear variation of CTE with temperature, the mean value was used as the temperature independent value of α_2 in this linear analysis. Results from these analyses predicted CTE values of 2.5 (1.39), 2.16 (1.20) and 2.3 (1.28) $\mu\epsilon K^{-1}$ ($\mu\epsilon^\circ F^{-1}$) using the thermal properties from Lockheed, Hahn and Kim [40], and the moiré data, respectively. These values agreed to within 10% of the mean values obtained from the moiré technique for the $[0/\pm 45/90]_s$ and $[0/90/\pm 45]_s$ laminates. The agreement with strain gage results ranged from 13-25%.

TABLE 4
ELASTIC PROPERTIES FOR T300/5208

Elastic Property	Lamina Value GPa (MSI)
E_1	130.3 (18.9)
E_2	9.72 (1.41)
G_{12}	5.39 (.782)
ν_{12}	0.308

A sensitivity analysis was performed to determine the effects of small changes in the elastic properties on the thermal response of the laminate. Each elastic property listed in Table 4 was independently raised 10% to determine the laminate's sensitivity to each particular property. The Lockheed thermal properties were used, giving a baseline CTE of $2.5 \mu\epsilon K^{-1}$ ($1.39 \mu\epsilon^{\circ}F^{-1}$). The results are presented in Table 5. For the given laminate configuration and material properties, E_1 and E_2 had a significant effect on the CTE, but act in an opposite sense. However, G_{12} and ν_{12} have a negligible effect on the CTE.

A second analysis was performed to determine the effect of temperature dependent material properties. Two cases were examined. First, the thermal properties were allowed to vary with temperature, but the elastic constants were assumed to be temperature independent (Case I). Secondly, both the thermal and elastic properties were allowed to vary with temperature (Case II). The computation of the laminates' variation of strain with temperature followed the procedure described by Eqs. (4.5) through (4.12). However, the laminates CTE values were not determined from Equ. (4.13), but rather, by obtaining a polynomial expression for the strain as a function of temperature by a least-squares procedure, and then differentiating this expression to obtain the CTE.

Values of α_1 and α_2 , determined experimentally from the [0] and [90] laminates were used for the temperature dependent thermal properties. Elastic properties used for Case I are given in Table 4. Elastic properties for use in Case II were more difficult to determine.

TABLE 5
 SENSITIVITY ANALYSIS FOR QUASI-ISOTROPIC LAMINATE

Elastic Property	New CTE $\mu\epsilon K^{-1}$ ($\mu\epsilon^{\circ}F^{-1}$)	% Change ¹
E_1	2.32 (1.29)	-7%
E_2	2.70 (1.50)	8%
ν_{12}	2.52 (1.40)	1%
G_{12}	2.50 (1.39)	0%

¹% change from baseline CTE of $2.5 \mu\epsilon K^{-1}$
 ($1.39 \mu\epsilon^{\circ}F^{-1}$)

Information regarding the temperature dependence of those properties was very limited, and therefore, only rough estimations for this dependence were made for the purpose of this analysis. It was assumed that E_1 did not vary with temperature, and that E_2 was reduced to 80% of its original value at 450 K (350°F) with the reduction occurring in the following manner: reduced to 97% at 349 K (169°F), 93% at 400 K (260°F), 87% at 425 K (305°F) and 80% at 450 K (350°F). Although G_{12} and ν_{12} undoubtedly vary with temperature, their effect on the CTE is very small (as shown in the sensitivity analysis discussed earlier). They were therefore treated as constants for this analysis.

Fig. 23 shows the nonlinear variation of strain with temperature obtained from fitting second order polynomials through the strain versus temperature data obtained from the above analysis. Also shown are the experimentally determined responses for the $[0/\pm 45/90]_S$ and $[0/90/\pm 45]_S$ laminates. As can be seen, Case I compared well with the experimental results. For Case II, the analysis predicted a response with curvature in the opposite direction from that of the experimental results and from Case I.

6.3.2.3 $[0/\pm 45/90]_S$ Laminate (Moist)

This laminate (Spec. I.D. 43-4B) was the first specimen tested. It was not dried nor was any effort made to determine the moisture content prior to testing. Type I back to back gages were placed on this specimen in addition to the moiré grating. The specimen was then subjected to repeated thermal cycling between 297 K (75°F) and 422 K (300°F). The manner in which thermal cycling was to be conducted had

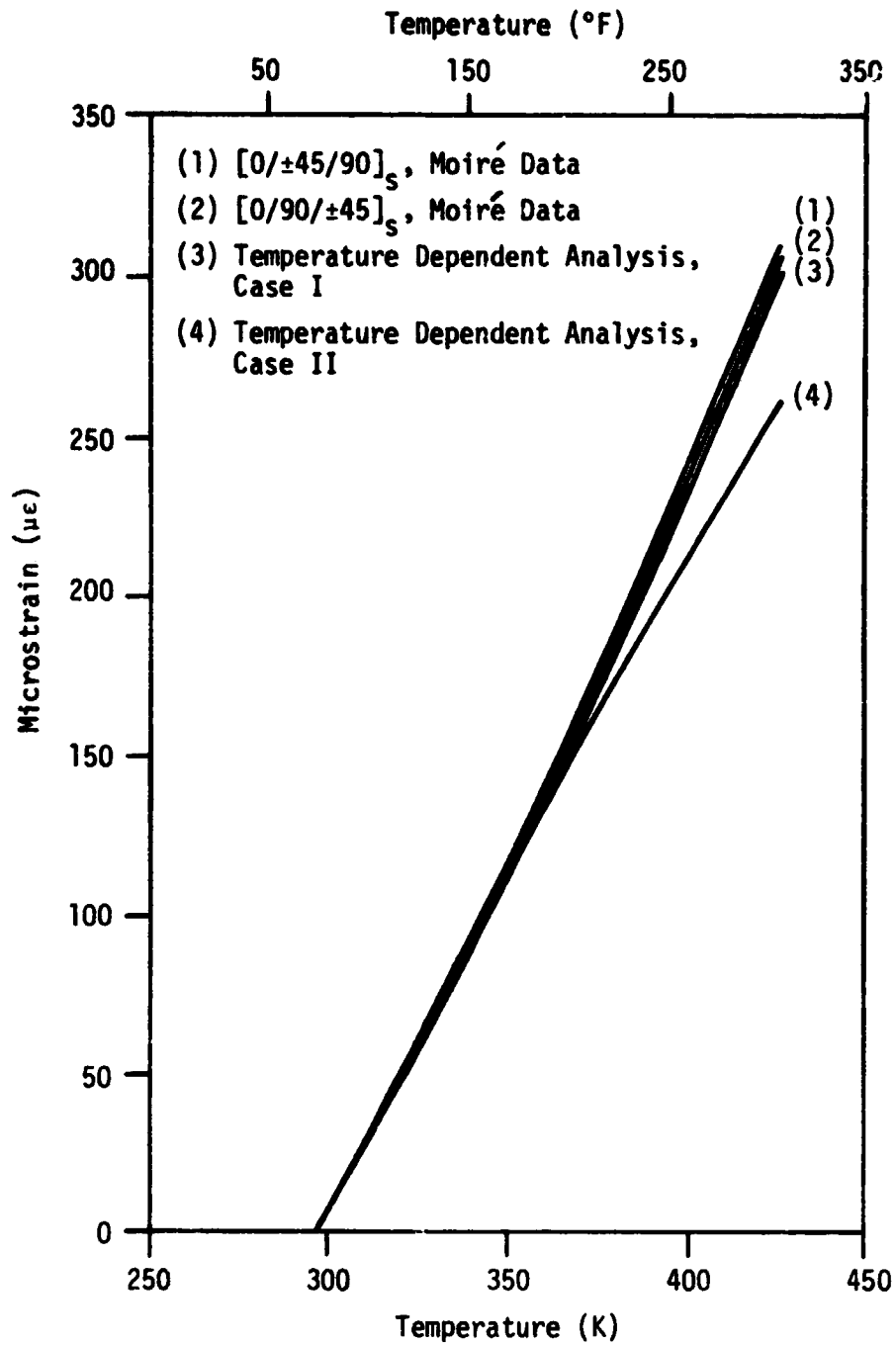


FIGURE 23. COMPARISON OF TEMPERATURE DEPENDENT ANALYSIS WITH EXPERIMENTAL RESULTS FOR QUASI-ISOTROPIC LAMINATES

not been firmly established and, therefore, was somewhat irregular. The specimen was subjected to the thermal cycles listed in Table 6. As can be seen, data were taken for eight cycles, however, cooling data were collected on only four of these cycles (2, 6, 7, and 8). Data will be referred to by cycle number for discussion of the results.

Fig. 24 shows the results obtained from moiré data for cycles 1, 3, 4, and 5, and the heating portion of cycles 2 and 6. Fig. 25 shows both the heating and cooling data for cycles 2 and 6. To avoid confusion, individual data points are not shown, but rather, only the least-squares curves. A first order fit was used for cycles 1 and 3 because of the limited amount of data taken on these cycles. A second order fit was used on the remaining cycles. CTE values computed from these curves are given in Table 7. The room temperature values ranged from a low of $1.75 \mu\epsilon K^{-1}$ ($0.97 \mu\epsilon^{\circ}F^{-1}$) to a high of $2.72 \mu\epsilon K^{-1}$ ($1.51 \mu\epsilon^{\circ}F^{-1}$).

Moisture desorption and resulting contraction of the specimen occurred during each successive cycle, as evidenced by the residual compressive strain after cooling (Fig. 24). The specimen contracted approximately $160 \mu\epsilon$ from the 1st to the 6th cycle because of this moisture desorption. The change in residual strain after each cycle was not constant. As can be seen in Fig. 24, there is a large increase in residual strain between cycles 2 and 3, and between cycles 5 and 6. However, there is only a small increase in residual strain between cycles 3, 4, and 5. Cycle 2 was the first thermal cycle to attain

TABLE 6
THERMAL CYCLES FOR THE QUASI-ISOTROPIC
LAMINATE WITH MOISTURE

Cycle No.	Temperature Range K (°F)
1	297(75) to 366(200)
2	297(75) to 422(300) to 297(75)
3	297(75) to 366(200)
4	297(75) to 422(300)
5	297(75) to 422(300)
6 ¹	297(75) to 422(300) to 297(75)
7	297(75) to 422(300) to 297(75)
8	297(75) to 422(300) to 297(75)

¹Specimen was removed after the 6th cycle and placed in a drying oven for one week.

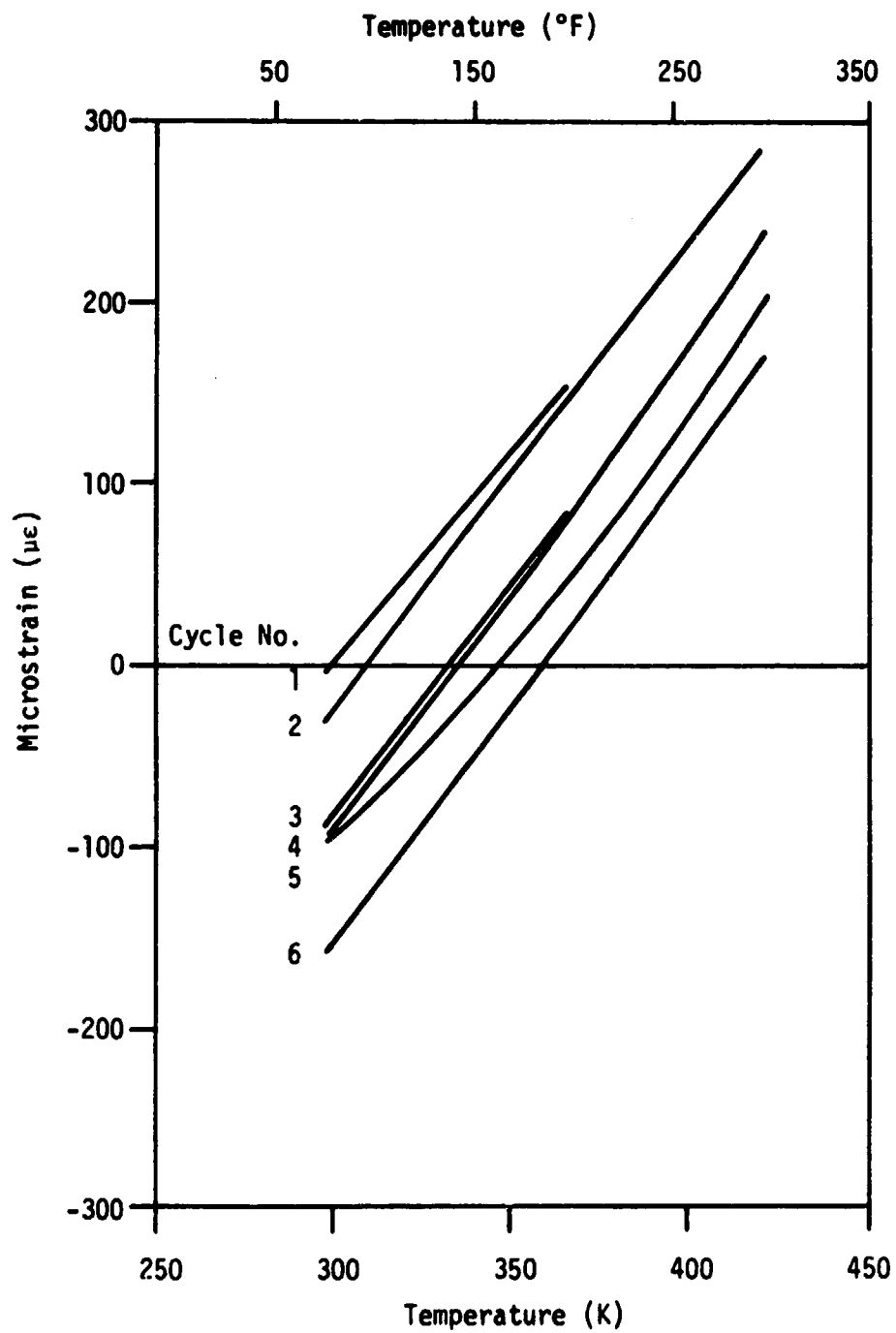


FIGURE 24. MOIRÉ THERMAL EXPANSION FOR HEATING OF $[0/\pm 45/90]_s$ LAMINATE WITH MOISTURE

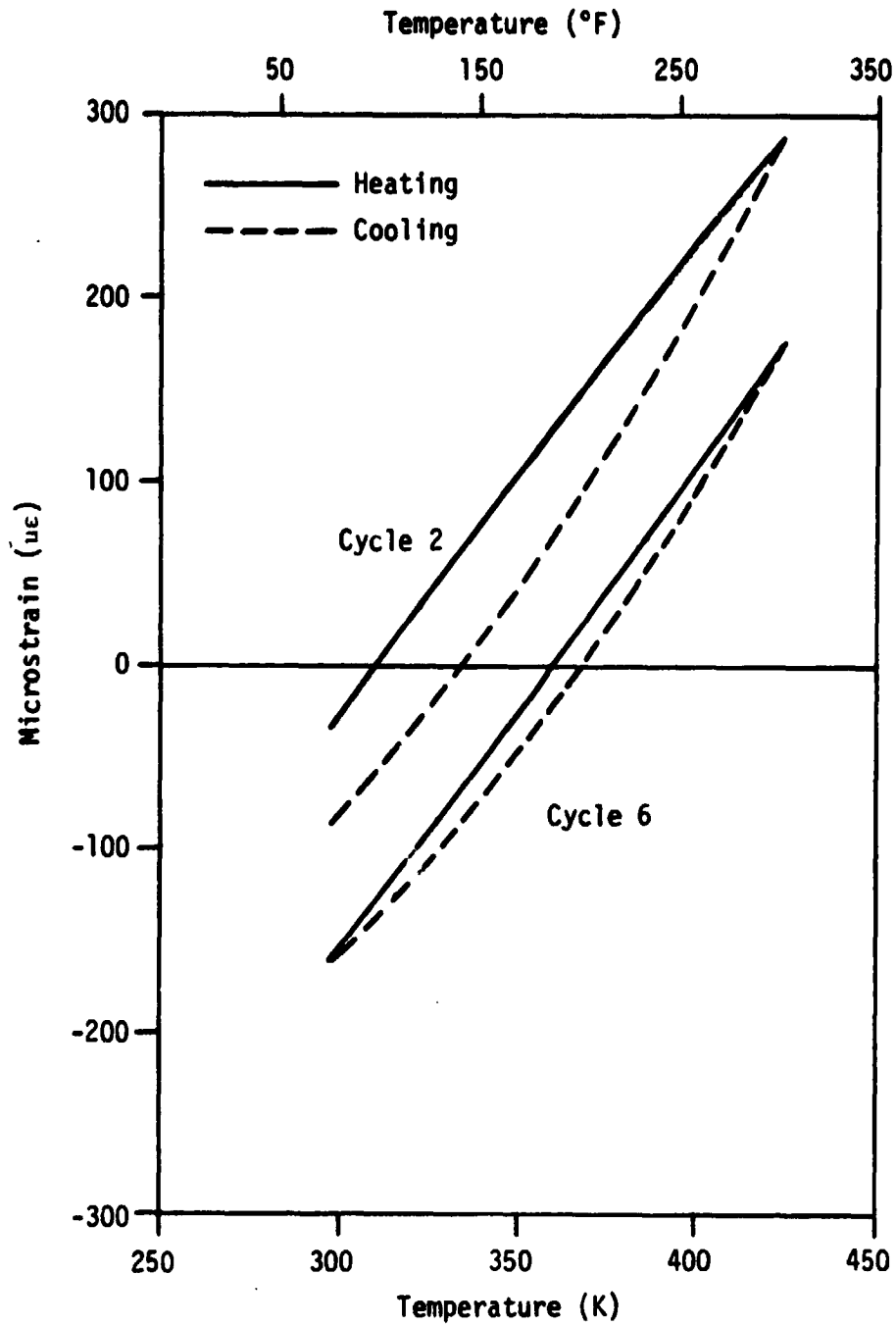


FIGURE 25. MOIRÉ THERMAL EXPANSION FOR HEATING AND COOLING OF $[0/\pm 45/90]_s$ LAMINATE WITH MOISTURE

TABLE 7
 CTE VALUES FOR THERMAL CYCLING OF A
 QUASI-ISOTROPIC LAMINATE WITH MOISTURE

Cycle	CTE $\mu\epsilon \text{ K}^{-1} (\mu\epsilon^{\circ}\text{F}^{-1})$		
	297 K (75°F)	360 K (188°F)	422 K (300°F)
1	2.34 (1.30)	2.34 (1.30)	2.34 (1.30)
2, Heating	2.72 (1.51)	2.58 (1.43)	2.44 (1.36)
2, Cooling	2.12 (1.18)	3.00 (1.67)	3.88 (2.16)
3	2.54 (1.41)	2.54 (1.41)	2.54 (1.41)
4	2.48 (1.38)	2.72 (1.51)	2.95 (1.64)
5	1.75 (0.97)	2.46 (1.37)	3.16 (1.76)
6, Heating	2.52 (1.40)	2.69 (1.49)	2.85 (1.58)
6, Cooling	1.90 (1.06)	2.71 (1.51)	3.51 (1.95)
7 and 8 combined	2.17 (1.21)	2.60 (1.44)	3.02 (1.68)

422 K (300°F) and therefore, a significant amount of moisture desorption took place causing the large residual strain after this cycle. The large residual strain between cycles 5 and 6 is, however, unexplained. Also, as can be seen in Fig. 24, the thermal response for cycles 2, 4, and 6 was nearly linear while cycle 5 was quite nonlinear (as discussed previously cycles 1 and 3 were fit with linear curves). Cycle 5 appears to be an anomaly, with no explanation for the erratic behavior. CTE values (Table 7), at a given temperature, differed by as much as 20% between heating cycles 2, 4, and 6.

The response during cooling was much more nonlinear than that for heating, as shown for cycles 2 and 6 in Fig. 25. The hysteresis in these two cycles was undoubtedly associated with the presence of moisture. The difference in slope of the heating and cooling curves may be explained qualitatively by a change in the rate of moisture desorption with temperature. DeIasi and Whiteside [41] have shown that the moisture diffusivity (area per unit time) increases with temperature for graphite-epoxy composites. For heating, from 297 K (75°F) to 422 K (300°F), moisture desorption produced a contraction while the increase in temperature produced an expansion. However, the rate of moisture desorption increased with temperature, thus producing the decreasing slope with temperature for the heating curve of cycle 2. For cooling, from 422 K (300°F) back to 297 K (75°F), moisture desorption continued to result in contraction, but the decrease in temperature also produced contraction. Thus the two effects were additive during cooling whereas they had opposite influence during heating. The ratio of moisture

desorption decreased as the specimen was cooled, thus explaining the decreasing slope with decreasing temperature for the cooling curve of cycle 2. For cycle 6 the majority of the moisture had been removed and thus the above effects were not as prominent. As seen in Fig. 25 there was very little residual strain from the beginning to the end of cycle 6 indicating that little additional moisture desorption was taking place.

After the 6th cycle, the specimen was removed and placed in a drying oven with a dry nitrogen purge at 340 K (152°F) for one week, after which the specimen was retested (cycles 7 and 8). The results obtained from the moiré data for these last two cycles are shown in Fig. 26. This data was referenced to zero strain at the start of cycle 7. Data points are shown for heating and cooling of both cycles, and as can be seen, all of this data fell along the same curve, with a minimal amount of scatter. A second order least-squares curve was computed for this data, and is shown in the figure. CTE values computed from this curve are listed in Table 7, and compared reasonably well with those of the heating portion of cycles 2, 4, and 6.

The data obtained for these last two cycles showed none of the hysteresis that was evident in the first six cycles. The total shrinkage due to moisture loss was computed by comparing the fringe pattern at the beginning of cycle 1 with that of the beginning of cycle 7. This value was computed as 170 $\mu\epsilon$, which is very close to the 160 $\mu\epsilon$ observed after cycle 6. This indicated that only a very small amount of moisture was desorbed during the one week drying

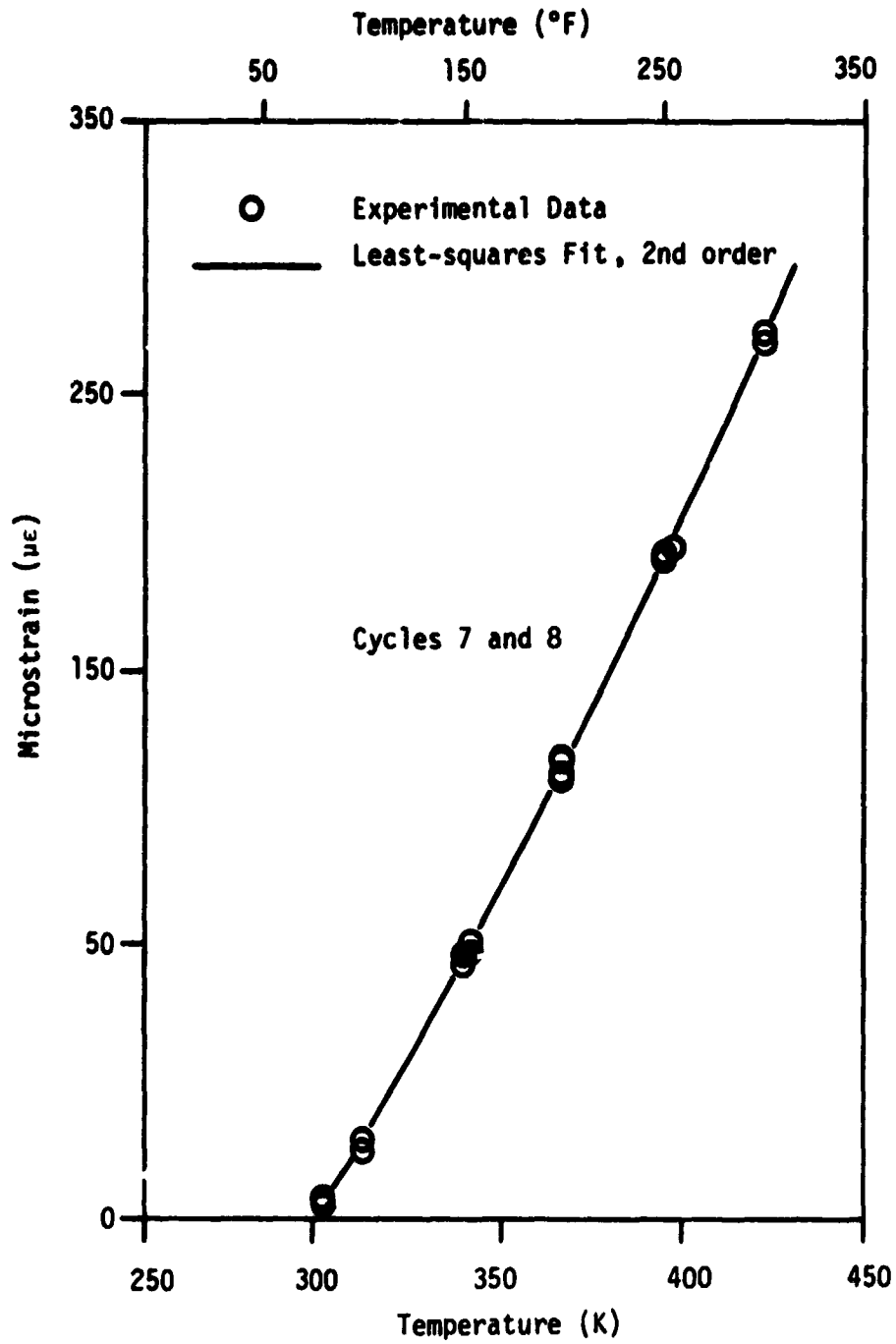


FIGURE 26. MOIRÉ THERMAL EXPANSION AFTER DRYING OF $[0/\pm 45/90]_S$ LAMINATE

period between cycles 6 and 7. This was supported by the fact that the initial and final value of the strain for cycle 6 (see Fig. 25) were almost identical. Therefore, it was concluded that hysteresis is associated with the presence of moisture.

An estimate of the total moisture desorbed during all cycles was made using lamination theory (Section 4.2.2). The lamina coefficients of moisture expansion (CME) reported by Hahn and Kim [40],

$$\beta_1 = 0 \text{ and } \beta_2 = 5900 \text{ } \mu\epsilon/\% \text{ H}_2\text{O}$$

were used in conjunction with the elastic properties in Table 5. The laminate CME for a quasi-isotropic configuration was computed as $\bar{\beta} = 513.8 \text{ } \mu\epsilon/\% \text{ H}_2\text{O}$. Using this value, a strain of $170 \text{ } \mu\epsilon$ corresponds to a change in moisture content of 0.33%. However, it was found that in drying other quasi-isotropic specimens for one month, the total moisture desorbed was approximately 0.7%. This would imply that all of the moisture had not been removed from the specimen by the end of cycle 8, as was previously thought, and that additional drying for an extended period of time would have been needed to remove the remaining moisture. It is possible that the rate at which moisture was lost was reduced by the silicone rubber grating on the surface of the specimen. However, definite conclusions cannot be made from this limited amount of data.

A general comment based on data from this specimen is that CTE values are affected by moisture. A change in moisture content during heating or cooling changes the strain versus temperature response,

causing changes in CTE values. An error analysis was not performed for this laminate due to the large scatter in material response caused by moisture desorption.

A comparison between the results obtained from cycles 7 and 8 of the moist specimen and the other two quasi-isotropic specimens which were dried, is shown in Fig. 27. The agreement between the three responses is reasonably good with a maximum difference of approximately 20 $\mu\epsilon$ at the maximum temperature. The two specimens that were dried gave essentially identical results with the moist specimen, which had been cycled previously a number of times, giving slightly different results. CTE values for the moist specimen agreed to within 15% of the values obtained from the two dry quasi-isotropic specimens.

The slightly greater CTE values for cycles 7 and 8 of the moist specimen may be explained by its surface preparation. As described in Section 5.4.2, this specimen was inadvertently sanded more than the other two quasi-isotropic laminates studied, resulting in a 50% decrease in the thickness of the outer ply. A linear analysis was performed using the elastic properties listed in Table 4 and the thermal properties obtained from Lockheed, to determine the effect a decrease in the thickness of the 0° ply of $[0/\pm 45/90]_5$ laminate could have on the CTE. This analysis showed that a 50% decrease in the thickness of the 0° ply would cause significant bending with an increase of 200 $\mu\epsilon$ at the surface, and a 65% increase in the CTE. The change observed experimentally was not as severe. One reason for this difference may be that the decrease in the "effective" thickness of the 0° ply was

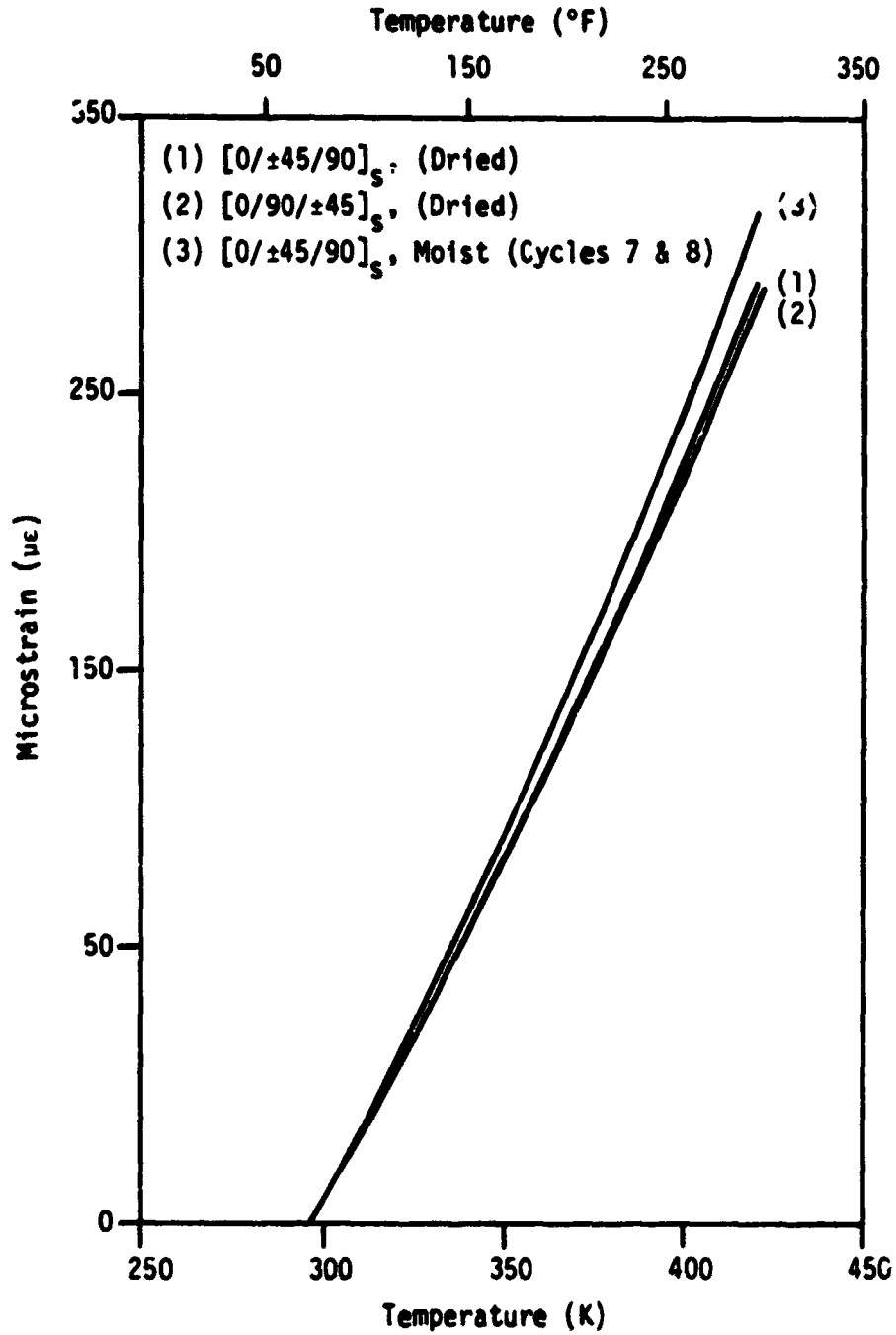


FIGURE 27. THERMAL RESPONSE OF QUASI-ISOTROPIC LAMINATES WITH AND WITHOUT MOISTURE

probably less than 50% because a majority of the decrease in thickness was associated with surface roughness and a reduction in resin content.

Strain gage data was also obtained for the moist specimen. The comparison between strain gage and moiré results showed basically the same trends as the comparisons for the other quasi-isotropic laminates (Figs. 20 and 21). The primary reason for obtaining strain gage data was to compare strain gage data with moiré data, and it was felt that sufficient data was obtained from the other specimens discussed previously to make this comparison. Therefore, because strain gage data from this specimen provided no new information, results are not presented.

Chapter 7

CONCLUSIONS

The primary purpose of this investigation was to develop an experimental technique which would provide accurate and reliable data on the thermal response of fiber-reinforced composites with a minimum complexity and cost. Moiré interferometry, using fringe multiplication to enhance the sensitivity, was selected for this investigation. Measurements from this method were compared with those obtained from electrical resistance strain gages. In order to assess the validity of the method, the thermal responses of four graphite-epoxy laminates were studied. A secondary aim of the investigation was to compare the experimentally determined thermal response of the composites with that predicted by lamination theory. Results from this investigation led to the following main conclusions:

1. Moiré interferometry has been shown to be an effective and precise technique for the experimental determination of the temperature dependent coefficients of thermal expansion. The method has been successively applied to both isotropic materials and laminated composites subjected to cyclic thermal loading in the temperature range of 297 K (75°F) to 422 K (300°F).
2. Using moiré interferometry the CTE's of four T300/5208 graphite-epoxy laminates have been determined as follows:
[0] laminate has a temperature independent CTE of

$-0.107 \mu\text{eK}^{-1}$ ($-0.059 \mu\text{e}^\circ\text{F}$). [90] laminate has a linear temperature dependent CTE ranging from $22.23 \mu\text{eK}^{-1}$ ($12.35 \mu\text{e}^\circ\text{F}^{-1}$) at 297 K (75°F) to $32.18 \mu\text{eK}^{-1}$ ($17.88 \mu\text{e}^\circ\text{F}^{-1}$) at 422 K (300°F), $[0/\pm 45/90]_s$ and $[0/90/\pm 45]_s$ laminates have almost identical linear temperature dependent CTE's ranging from $1.97 \mu\text{eK}^{-1}$ ($1.09 \mu\text{e}^\circ\text{F}^{-1}$) at 297 K (75°F) to $2.80 \mu\text{eK}^{-1}$ ($1.56 \mu\text{e}^\circ\text{F}^{-1}$) at 422 K (300°F).

3. Comparisons between moiré and strain gage measurements were inconclusive with both techniques giving consistent but systematically different results. For the two quasi-isotropic laminates, strain gage measurements gave CTE values of approximately 29% higher than those obtained using the moiré technique. For the [90] laminate agreement was within 6%. Comparisons for the [0] laminate were inconclusive due to uncertainties in the correction for transverse sensitivity of the strain gage (the transverse sensitivity correction has a dominant effect on the results for this particular laminate).
4. Results predicted from lamination theory compare reasonably well with experimental results. However, the analysis was seen to be sensitive to elastic property data which was not directly determined for this investigation.
5. Moisture effects were very apparent in the thermal response of a quasi-isotropic laminate that was not dried prior to testing. A change in moisture content gave rise to hysteresis

and residual compressive strains for a complete thermal cycle. These effects were not observed in laminates that were dried prior to testing.

Modifications to the present moiré technique which would further enhance the precision include:

1. an improved specimen fixture to reduce possible rigid body rotations during testing;
2. an improved procedure to align the grating on the specimen surface, and to align the gage line on the grating.

An area in which the present measurement technique might prove useful is to the study of long term environmental effects on composites. This is because measurements using the moiré technique are geometrical in nature, and therefore are not subject to signal conditioning problems that arise in this type of test.

REFERENCES

1. Wolff, E. G., "Measurement Techniques for Low Expansion Materials," Materials and Processes -- In Service Performance, Vol. 9, National SAMPE Technical Conference, Oct. 1977.
2. Dally, J. W. and Riley, W. F., Experimental Stress Analysis, McGraw-Hill, New York, 1965, pp. 337-421.
3. Micro-Measurements Tech Note, "Temperature-Induced Apparent Strain and Gage Factor Variation in Strain Gages," TN-128-2.
4. ASTM Standard Test Method for "Linear Thermal Expansion of Rigid Solids with a Vitreous Silica Dilatometer," Designation E228-71, 1977 Annual Book of ASTM Standards, Part 44.
5. Freeman, W. T. and Campbell, M. D., "Thermal Expansion Characteristics of Graphite Reinforced Composite Materials," Composite Materials; Testing and Design (Second Conference), ASTM STP 497, American Society for Testing and Materials, 1972, pp. 121-142.
6. ASTM Standard Test Method for "Linear Thermal Expansion of Rigid Solids with Interferometry," Designation E289-70, 1977 Annual Book of ASTM Standards, Part 44.
7. Wolff, E. G., Eselun, S. A., "Double Michelson Interferometer for Crackless Thermal Expansion Measurements," Proceedings of the Society of Photo-Optical Instrumentation Engineers, Vol. 192, Aug. 1979.
8. Chiang, Fu-Pen, "Moiré Methods of Strain Analysis," Chapter 6, Manual on Experimental Stress Analysis, Third Edition, Society for Experimental Stress Analysis.
9. Pipes, R. B. and Daniel, I. B., "Moiré Analysis of the Interlaminar Shear Edge Effect in Laminated Composites," J. Comp. Mat'ls., Vol. 5, (1971), pp. 255-259.
10. Daniel, I. M. and Rowlands, R. E., "Determination of Strain Concentration in Composites by Moiré Techniques," J. Comp. Mat'ls., Vol. 5, (1971), pp. 250-254.
11. Chians, Fu-Pen, "Crack Measurements in Composite Materials," J. Comp. Mat'ls., Vol. 7, (1973), pp. 134-137.
12. Oplinger, D. W., Parker, B. S., and Chiang, Fu-Pen, "Edge-Effect Studies in Fiber-reinforced Laminates," Experimental Mechanics, Vol. 14, (1974), pp. 347-354.

13. Marchant, M. and Bishop, S. M., "An Interference Technique for the Measurement of In-plane Displacements of Opaque Surfaces," J. Strain Analysis, Vol. 9, No. 1, (1974), pp. 36-43.
14. Daniel, I. M., Rowlands, R. E., and Post, D., "Strain Analysis of Composites by Moiré Methods," Experimental Mechanics, Vol. 13, (1973), pp. 246-252.
15. Post, D., "Analysis of Moiré Fringe Multiplication Phenomena," Applied Optics, Vol. 6, No. 11, Nov. 1967, pp. 1938-142.
16. Post, D., "New Optical Methods of Moiré Fringe Multiplication," Experimental Mechanics, 8(2), Feb. 1968, pp. 63-68.
17. Post, D., "Moiré Fringe Multiplication with a Non-Symmetrical Doubly-blazed Reference Grating," Applied Optics, Vol. 11, No. 9, Sept. 1971, pp. 408-413.
18. Post, D. and MacLaughlin, T. F., "Strain Analysis by Moiré Fringe Multiplication," Experimental Mechanics, Vol. 11, No. 9, Sept. 1971, pp. 408-413.
19. Schapery, R. A., "Thermal Expansion Coefficients of Composite Materials Based on Energy Principles," J. Comp. Mat'ls., Vol. 2, No. 3,, (1968), pp. 380-404.
20. Greszczuk, L. B., "Thermoelastic Properties of Filamentary Composites," AIAA 6th Structures and Mat'ls. Conf., Palm Springs, Calif., 1965.
21. Schneider, W., Kunststoffe, Vol. 61, No. 4, (April 1971), pp. 273-277.
22. Chamberlain, N. J., "Derivation of Expansion Coefficients for a Fiber Reinforced Composite," BAC Report SON(P)33, (Nov. 1968).
23. Knibbs, R. H., Baker, D. J., Rhodes, G., "The Thermal and Electrical Properties of Carbon Fibre Unidirectional Reinforced Epoxy Composites," 26th Annual Tech. Conf., Reinforced Plastics/Composites Division, The Society of the Plastics Industry, (1971), Section 8-F, pp. 1-10.
24. Rogers, K. F., Phillips, L. N., Kingston-Lee, D. M., Yates, B., Overy, M. J., Sargent, J. P., McCella, B. A., "The Thermal Expansion of Carbon Fibre-Reinforced Plastics," J. Mat'l. Sci., Vol. 12, (1977), pp. 718-733.
25. Strife, J. R. and Prevo, K. M., "The Thermal Expansion Behavior of Unidirectional and Bidirectional Kevlar/Epoxy Composites," J. Comp. Mat'ls., Vol. 13, (Oct. 1979), pp. 264-277.

26. Kalnin, I. L., "Thermal Expansion of High Modulus Graphite Fiber/Epoxy Composites," Proceedings, The Society of the Plastics Industry, Vol. 29, (1974), Section 21-C, pp. 1-8.
27. Ishikawa, T., Koyama, K., Kobayashi, S., "Thermal Expansion Coefficients of Unidirectional Composites," J. Comp. Mat'ls., Vol. 12, (1978), pp. 153-166.
28. Wang, A. S. D., Pipes, R. B., Ahmadi, A., "Thermoelastic Expansion of Graphite-Epoxy Unidirectional and Angle-Ply Composites," Composites Reliability, ASTM STP 580, American Society for Testing and Materials, 1975.
29. Pirgon, O., Wostenholm, G. H., Yates, B., "Thermal Expansion at Elevated Temperature IV. Carbon-Fibre Composites," J. Phys. D: App. Phys., Vol. 6, (1973), pp. 309-321.
30. Fahmy, A. A. and Rajai, A. N., "Thermal Expansion of Graphite Epoxy Composites," J. App. Phys., Vol. 41, No. 13, (1970), pp. 5112-5115.
31. Goggin, W. R., "Thermomechanical Stability of Graphite-Epoxy Composites," Applied Optics, Vol. 13, No. 2, (1974), pp. 444-450.
32. Geiler, D. E., "Analysis, Test, and Comparison of Composite Material Laminates Configured for Isotropic Low Thermal Expansion," 28th Annual Tech. Conf., Reinforced Plastics/Composites Div., The Society of the Plastics Industry, (1973), Section 9-D, pp. 1-8.
33. Hyer, M. W., Hagaman, J. A., "Thermal Cycling of Graphite-Polyimide," Virginia Polytechnic Inst. and State University, VPI-E-79-15, April 1979.
34. Eselun, S. A., Neubert, H. D., Wolff, E. G., "Microcracking Effects on Dimensional Stability," 24th Nat. SAMPE Symposium and Exhibition, 1979.
35. Mackey, G. B., Kural, M. H., Johnson, R. R., "Thermal Expansion Properties of Composite Materials," LMSC/D667815, Feb. 1979.
36. Hashin, Z., Rosen, B. W., Pipes, R. B., "Nonlinear Effects on Composite Laminate Thermal Expansion," MSC/TFR/808/1015, July 1978.
37. Jones, R. M., Mechanics of Composite Materials, Scripta Book Company, 1975.
38. Hahn, H. T. and Pagano, N. J., "Curing Stresses in Composite Laminates," J. Comp. Mat'ls., Vol. 9 (1975), pp. 91-106.

39. Kriz, R. D., Stinchcomb, W. W., Tenney, D. R., "Effects of Moisture, Residual Thermal Curing Stresses and Mechanical Load on the Damage Development in Quasi-Isotropic Laminates," Virginia Polytechnic Institute and State University, VPI-E-80-5, 1980.
40. Hahn, H. T. and Kim, R. Y., "Swelling of Composite Laminates," Advanced Composite Materials - Environmental Effects, ASTM 658, American Society for Testing and Materials, 1978, pp. 98-120.
41. DeIasi, R., Whitside, J. B., "Effect of Moisture on Epoxy Resins and Composites," Advanced Composite Materials - Environmental Effects, ASTM STP 658, American Society for Testing and Materials, 1978, pp. 2-20.
42. Lipson, C. and Narenda, J. S., Statistical Design and Analysis of Engineering Experiments, McGraw-Hill Book Company, New York, 1973.

APPENDIX A
ERROR ANALYSIS OF MOIRÉ MEASUREMENTS

Appendix A

ERROR ANALYSIS OF MOIRÉ MEASUREMENTS

An attempt was made to identify the sources of error, and estimate their magnitude, for the moire method of measurement used in this investigation. Two types of error were identified, random error and systematic error.

The random error manifests itself as the scatter of the experimental data about the best fit line, as obtained by a least-squares analysis. This scatter may be caused by random variations in the specimen or its environment, by reading errors in the data points, or by a combination of these sources. Its magnitude may be characterized by the standard deviation from the least-squares line, given by

$$s_y = \sqrt{\frac{\sum_{i=1}^n (y_i - \hat{y}_i)^2}{n-1}}$$

where n is the number of data points, y_i are the actual values of the dependent variable, and \hat{y}_i are the values predicted from the least-squares line.

Systematic error is defined as altering the data in some regular or orderly manner. For this investigation, possible sources of this error included the following: an error in the assumed pitch of the reference grating, g_r ; an error in the gage length measurement; an error in the correction for the thermal expansion of the reference grating; an error caused by data not being taken along a line normal

to the specimen grating rulings, and an error associated with inexact orientation of the specimen grating relative to the fiber direction of the specimen.

The pitch of the reference grating was stated by the manufacturer to be accurate to within 0.001%. Considering the method of measurement, a conservative estimate of the error in the gage length is 0.01%. Both of these errors have a negligible influence on the results. A constant systematic error in temperature measurement (i.e. each temperature reading was in error by the same constant amount) would not cause any change in the slope of the strain versus curve, and therefore not effect the CTE value.

The thermal expansion of the reference grating is itself a systematic variable, and the appropriate correction to the data was made as described in Section 5.2.4. However, the correction itself has some error which must also be included in this analysis. An estimate of this error was made by considering the errors associated with the experimental determination of the thermal expansion of the ULE and reference grating, which are factors in the correction. The combined random error, as computed from the standard deviation, for these two experiments was 2.6 $\mu\epsilon$. The error in the correction was therefore assumed to vary linearly from 0 at 297 K (75°F) to 2.6 $\mu\epsilon$ at 422 K (300°F). Errors caused by data not being taken along a line normal to the specimen grating rulings, and by inexact orientation of the specimen grating relative to the fiber direction only had an effect

on the results of the [0] laminate, and are therefore discussed in the Section describing the [0] laminate (Section 6.3.1.1).

The random error and systematic error from the correction for the thermal expansion of the reference grating were used to compute a one standard deviation error band for the strain versus temperature response. Typical curves are shown in Fig. A.1. Limiting values of the CTE for this one standard deviation error band were determined from the maximum and minimum slopes of lines which fell within the error band, an example of which is shown in Fig. A.2. This procedure for expressing limiting bounds on CTE values is thought to be conservative. These limits are expressed as a \pm deviation from the CTE values, and are listed in Table A.1.

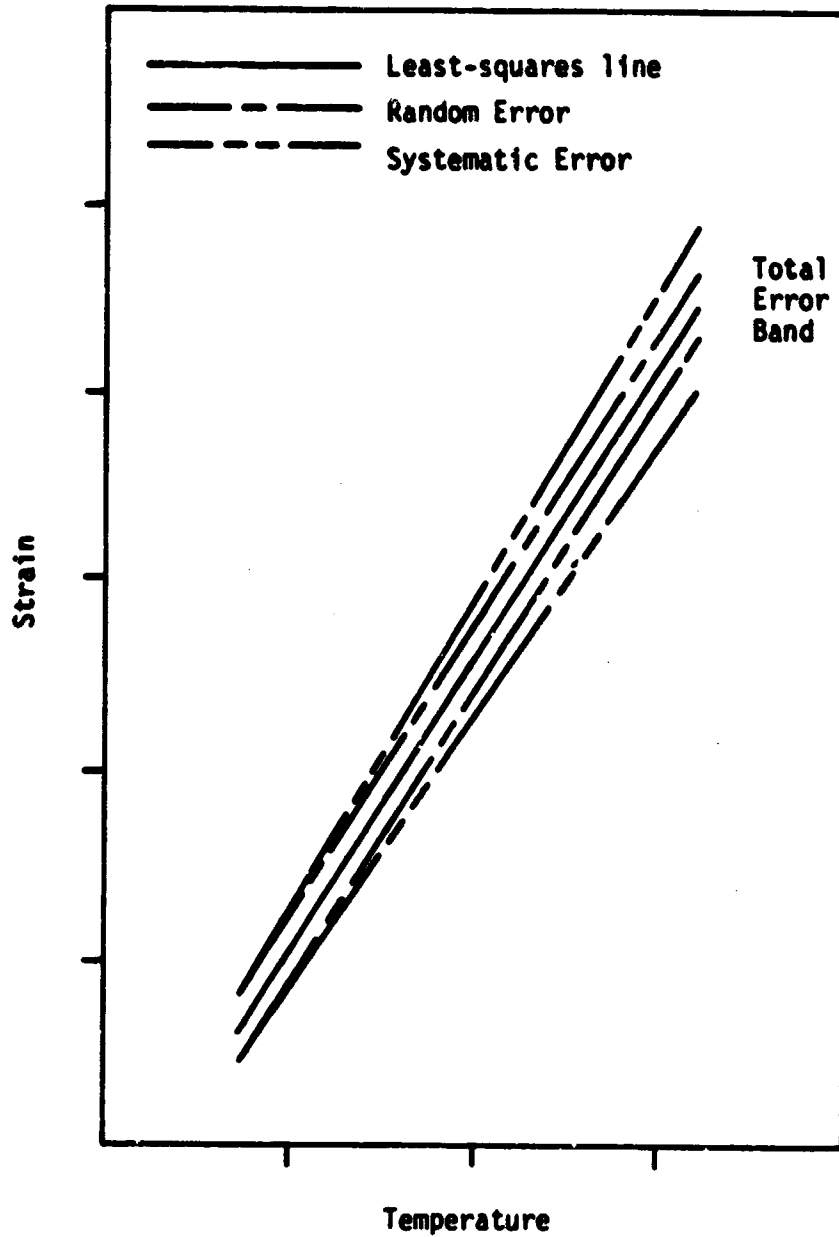


FIGURE A.1. TYPICAL ERROR BAND FOR STRAIN VERSUS TEMPERATURE RESPONSE

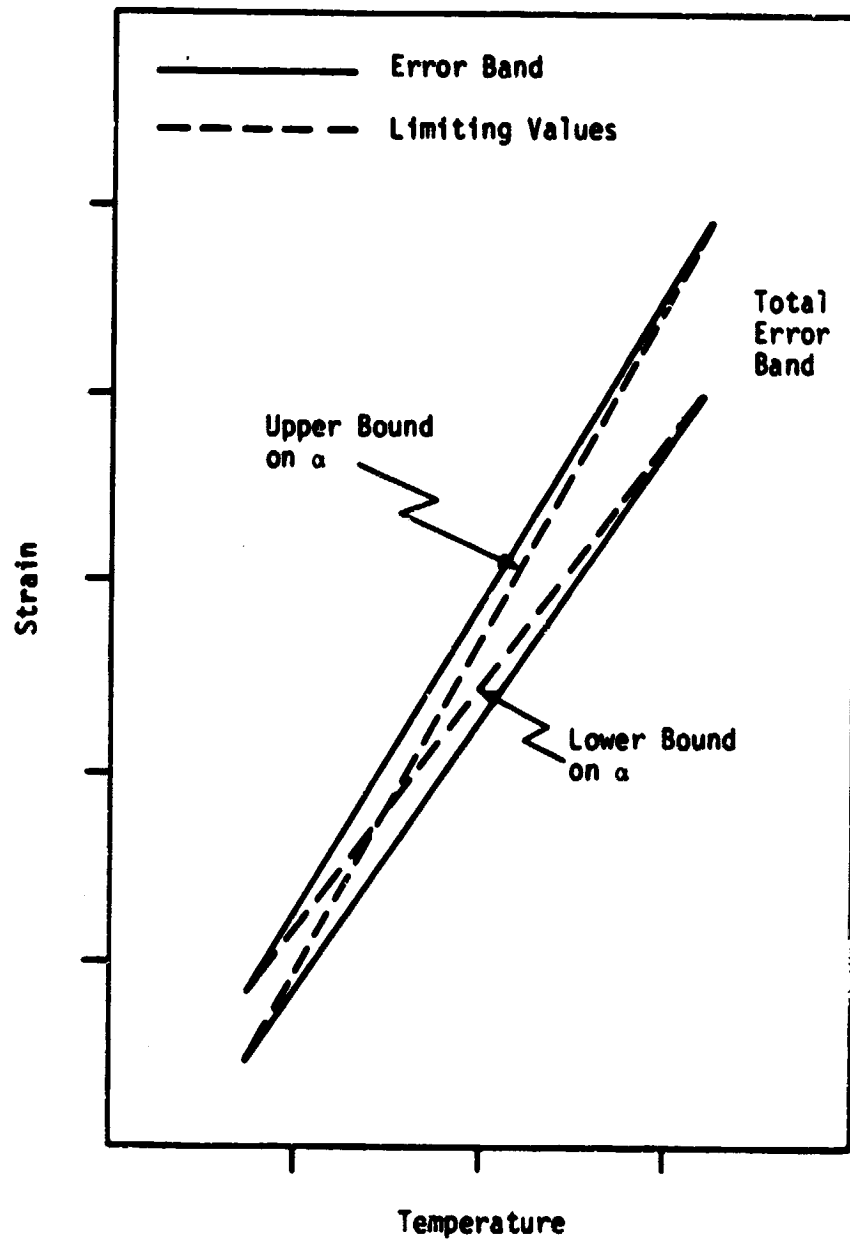


FIGURE A.2. TYPICAL ERROR BAND WITH LIMITING VALUES OF STRAIN VERSUS TEMPERATURE RESPONSE

TABLE A.1
LIMITS ON CTE VALUES FOR A ONE STANDARD
DEVIATION ERROR BAND

Laminate	Limits μeK^{-1} ($\mu\text{e}^{\circ}\text{F}^{-1}$)
[0]	$\alpha \pm 0.046$ (0.026)
[90]	$\alpha \pm 0.64$ (0.36)
$[0/\pm 45/90]_s$ (Dry)	$\alpha \pm 0.07$ (0.04)
$[0/90/\pm 45]_s$ (Dry)	$\alpha \pm 0.03$ (0.02)

APPENDIX B
STRAIN GAGE RESULTS FOR THE [0] LAMINATE

Appendix B

STRAIN GAGE RESULTS FOR THE [0] LAMINATE

Results obtained from strain gage output for the [0] laminate are shown in Fig. B.1. Type II gages were used on this laminate, and the results were obtained by averaging the output of the back to back gages for both heating and cooling of two thermal cycles. Outputs varied only slightly ($5 \mu\epsilon$) between heating and cooling and from cycle to cycle, but varied as much as $30 \mu\epsilon$ at the maximum temperature between back to back gages.

Corrections for the transverse sensitivity for the [0] laminate were very significant (approximately a 90% reduction in uncorrected strain readings). The ratio of the transverse to axial strain, ϵ_t/ϵ_a , was quite large in magnitude, causing the correction defined in Equ. (5.10) to be large. To make a precise correction, this ratio had to be accurately known. If a two element rosette is used (gages at right angles) then this ratio can be obtained directly from the strain gage output. Equations exist for determining the transverse sensitivity correction for these rosettes, and this is the recommended procedure for cases where this correction must be included. In this investigation, the specimen was equipped with single gages (it was not known that the transverse sensitivity was critical until after the specimen had been gaged) and therefore, the ratio ϵ_t/ϵ_a had to be determined in an alternate manner. It was decided to use the ratio of strains as computed from the moiré data obtained from the [0] and [90] laminates.

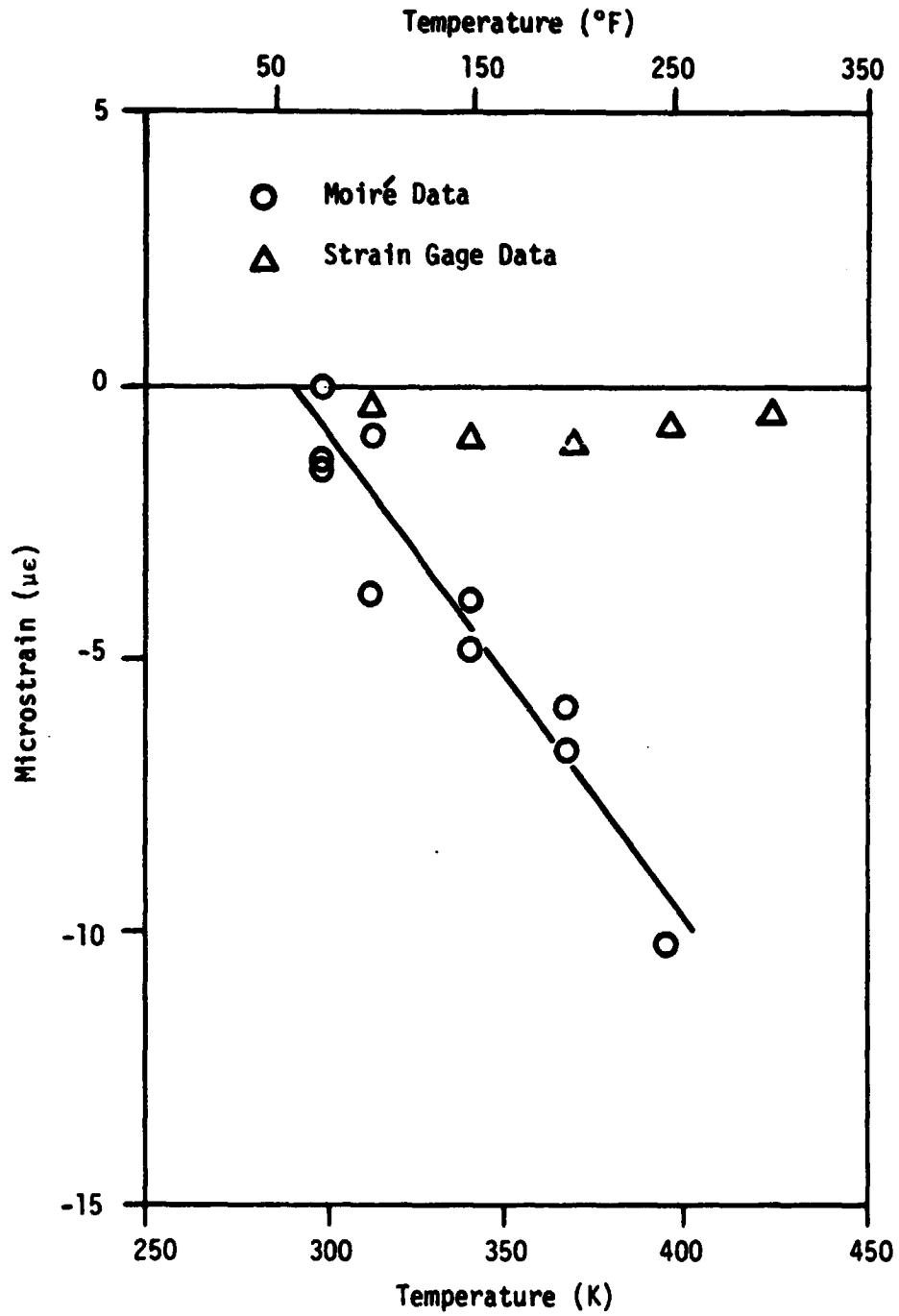


FIGURE B.1. COMPARISON OF MOIRÉ AND STRAIN GAGE DATA FOR [0] LAMINATE

Because this data came from two different specimens cut from two different panels, its validity was suspect. However, this was the only source of data available to make the correction.

As can be seen, the strain response obtained from strain gages and moiré data is of the same order of magnitude, but exhibit different trends (and therefore different CTE values). However, because of the large amount of scatter in the apparent strain curves associated with strain gage measurements, variations in back to back gages on this specimen of as much as $30 \mu\epsilon$, and the uncertainty of the transverse sensitivity correction, results obtained by strain gages are not considered reliable for this test. Therefore, no conclusions can be drawn regarding the applicability of strain gages for the [0] laminate.

Prof. Donald P. Adams
Dept. Of Mechanical Engineering
University Of Wyoming
Laramie, WY 82070

Dr. M. R. Adsit
General Dynamics Convair
P.O. Box 80837
San Diego, CA. 92138

Dr. Clifford J. Astill
Solid Mechanics Program
National Science Foundation
1800 G St. N.W.
Washington, D.C.

Dr. J. A. Bailie
D81-12 Bldg. 154
Lockheed Missiles & Space Co, Inc
1111 Lockheed Way
Sunnyvale, CA. 94088

Dr. Charles W. Bert, Director
School Of Aerospace, Mechanical
& Nuclear Engineering
The University Of Oklahoma
Norman, Oklahoma 73069

Mr. Richard Boitnott
Mail Stop 190
Nasa-Langley Research Center
Hampton, VA. 23665

Mr. David Bowles
Mail Stop 188B
NASA-Langley Research Center
Hampton, Va. 23665

Dr. R. P. Brinson
ESH Dept.
Virginia Tech
Blacksburg, VA. 24061

Mr. Ernie Brooks
ESH Dept.
Virginia Tech
Blacksburg, VA. 24061

Dr. Michael P. Card
Mail Stop 190
NASA-Langley Research Center
Hampton, VA 23665

Dr. C. Chamis
NASA-Lewis Research Center
2100 Brook Park Rd.
Cleveland, Ohio 44135

Dr. Paul A. Cooper
Mail Stop 190
NASA-Langley Research Center
Hampton, Va. 23665

Dr. Frank Crossman
Lockheed Research Lab
Org. 52-41, Bldg. 204
3251 Hanover Street
Palo Alto, CA. 94304

Dr. I. H. Daniel, Manager
IIT Research Institute
10 West 35 Street
Chicago, IL. 60616

Dr. John R. Davidson
Mail Code 188E
ND-Structural Integrity Branch
Langley Research Center
Hampton, VA. 23665

Dr. John G. Davis, Jr.
Mail Stop 188A
Langley Research Center
Hampton, VA. 23665

Mr. Jerry W. Deaton
Mail Stop 188A
NASA-Langley Research Center
Hampton, VA. 23665

Mr. H. Benson Dexter
Mail Stop 188A
NASA-Langley Research Center
Hampton, VA. 23665

Mr. O. Earl Dhanau
 Section 2-53400
 Vought Corp.
 P.O. Box 5907
 Dallas, TX. 75222

Dr. E. F. Duggan
 52-33/205/2
 Lockheed Palo Alto Lab.
 3251 Hanover St.
 Palo Alto, Ca. 94304

Prof. John C. Duke, Jr.
 ESM Dept.
 Virginia Tech
 Blacksburg, VA. 24061

Prof. George J. Dvorak
 Civil Engineering
 University of Utah
 Salt Lake City, UT. 84112

Dr. Wolf Elber
 Mail Stop 188E
 NASA-Langley Research Center
 Hampton, VA. 23665

Mr. Dave Erb
 Aero & Ocean Engr. Dept.
 Virginia Tech
 Blacksburg, VA. 24061

Mr. Gary L. Farley
 Mail Stop 188A
 NASA-Langley Research Center
 Hampton, VA. 23665

Mr. Larry Fogg
 Lockheed-California
 Dept. 7572, Bldg. 63, Plant A1
 P.O. Box 551
 Burbank, CA. 91520

Dr. R. L. Foye
 USAMRDL
 SAUDLAS (207-5)
 Moffet Field, CA. 94035

Dr. D. Frederick
 ESM Dept.
 Virginia Tech
 Blacksburg, VA. 24061

Mr. Samuel P. Garbo
 McDonnell Aircraft Co.
 Bldg. 34, Post 350
 St. Louis, MO. 63166

Mr. Ramon Garica
 Mail Stop 190
 NASA-Langley Research Center
 Hampton, VA. 23665

Prof. Jim Goree
 Dept. of Mechanical Engr.
 Clemson University
 Clemson, S.C. 29631

Dr. Login B. Greszczuk
 McDonnell Douglas Astr. Co.
 5301 Bolas Avenue
 Huntington Beach, CA. 92647

Dr. Hayden O. Griffin
 B. F. Goodrich
 500 South Main Street
 Akron, Ohio 44318

Mr. Glen C. Grimes, Engr. Spec.
 Structures R & T, Dept 3780/62
 Northrop Corp., Aircraft Div.
 3901 W. Broadway
 Hawthorne, CA. 90250

Dr. H. T. Hahn
 Washington University
 St. Louis, MO. 63130

Dr. J. C. Halpin
 Flight Dynamics Lab
 Wright-Patterson AFB
 Ohio 45433

Professor Z. Hashin
 School of Engineering
 Solid Mech. Materials & Struc.
 Tel Aviv University
 Tel Aviv, Israel

Dr. R. A. Heller
ESH Dept.
Virginia Tech
Blacksburg, VA. 24061

Dr. E. G. Henneke
ESH Dept.
Virginia Tech
Blacksburg, VA. 24061

Prof. Carl T. Herakovich
Laboratoire de Mecanique
des Solides
Ecole Polytechnique
91128 Palaiseau cedex, FRANCE

Professor Phil Hodge
107 Aeronautical Engr. Bldg.
University of Minnesota
Minneapolis, MN 55455

Dr. K. E. Hofer
IIT Research Institute
10 West 35 Street
Chicago, Illinois 60616

Dr. Peter W. Hsu
Hamilton Standard Division
U. Technology
Hartford, CT. 06141

Mr. Edward A. Humphreys
Materials Science Corporation
Blue Bell Office Campus
Blue Bell, PA. 19422

Dr. Michael W. Hyer
ESH Dept.
Virginia Tech
Blacksburg, VA. 24061

AVCO, Systems Division
Subsystems & Meth. Structures
201 Lowell Street
Wilmington, MA. 01887

Dr. Eric B. Johnson
ESH Dept.
Virginia Tech
Blacksburg, VA. 24061

Dr. M. J. Johnson
Mail Stop 226
NASA-Langley Research Center
Hampton, VA. 23665

Dr. M. P. Kanat
ESH Dept.
Virginia Tech
Blacksburg, VA. 24061

Dr. Keith T. Redward
1768 Granite Hills Dr.
El Cajon, CA. 92021

Mr. John H. Kennedy
Mail Stop 188E
NASA-Langley Research Center
Hampton, VA. 23665

Mr. Eric Klang
ESH Dept.
Virginia Tech
Blacksburg, VA. 24061

Mr. James P. Knauss
Northrop Corporation
3901 West Broadway
Dept. 3852/82
Hawthorne, CA. 90250

Dr. Ronald D. Kriz
Dept. Com. MBS Bldg. 2
Boulder, CO. 80302

Dr. S. V. Kulkarni
L342 Lawrence Livermore Lab
P. O. Box 808
Livermore, Ca. 94550

Dr. Trent B. Logan
Mgr. Structures, Design, Dev.
Boeing Commercial Airplane Co.
P.O. Box 3707 - M.S. 3M-23
Seattle, WA. 98124

Dr. H. R. Louthan
Materials Engineering
Virginia Tech
Blacksburg, VA. 24061

Mr. Vic Mazzio
General Electric Co.
P.O. Box 8555
Bldg. 100, Rm. H4018
Philadelphia, PA. 19101

Dr. Martin H. Mikulas
Mail Stop 190
NASA-Langley Research Center
Hampton, VA. 23665

Mr. J. Steve Mills
6100 Edinger Ave., Apt. 525
Huntington Beach
CA 92647

Dr. D. H. Morris
ESH Dept.
Virginia Tech
Blacksburg, VA. 24061

Mr. Anya Nagarkar
Material Sciences Corp.
Blue Bell Office Campus
Blue Bell, PA. 19422

NASA Scientific & Technical
Information Facility
P.O. Box 8757
Baltimore/Washington Inter. Air.
Baltimore, MD. 21240

Mr. Michael Meneth
ESH Dept.
Virginia Tech
Blacksburg, VA. 24061

Newman Library - Virginia Tech

Mr. David A. O'Brien
5902 Kingsford Pl.
Bethesda, MD 20034

Dr. Donald W. Oplinger
Army Materials & Mechanics
Research Center
Department of the Army
Watertown, MA. 02171

Dr. Nicholas J. Pagano
WPAFB/MBM
Wright Patterson AFB
Ohio 45433

Mr. Michael Parin
3M Co., 3M Center
Bldg. 230-1F
St. Paul, MN. 55101

Dr. Nicholas Perrone, Director
Structural Mechanics Program
Department of the Navy
Office of Naval Research
Arlington, VA. 22217

Prof. T. H. H. Pian
Mass. Inst. of Tech.
Dept. of Aero. & Astr.
Cambridge, MA. 02139

Mr. Marek-Jerzy Pindera
ESH Dept.
Virginia Tech
Blacksburg, VA. 24061

Dr. A. Byron Pipes
Dept. of Mech. & Aero. Engr.
107 Evans Hall
University of Delaware
Newark, DE. 19711

Prof. Robert Plunkett
Dept. Aero & Eng. Mech.
Aero 107
University of Minnesota
Minneapolis, MN. 55455

Dr. K. L. Reifsnider
ESH Dept.
Virginia Tech
Blacksburg, VA. 24061

Dr. Gary D. Renieri
McDonnell Douglas Astro. Co-East
P.O. Box 516
Bldg. 106, Level 4, Post C-5
St. Louis, MO. 63166

Dr. Michael W. Renieri
McDonnell Aircraft Co.
Bldg. 34, Post 350
St. Louis, MO. 63166

Dr. Larry Roderick
Mail Stop 188E
NASA-Langley Research Center
Hampton, VA. 23665

Dr. B. W. Rosen
Materials Science Corporation
Blue Bell Office Campus
Blue Bell, PA. 19422

Dr. R. E. Rowlands
Dept. of Engineering Mechanics
University of Wisconsin
Madison, WI. 53706

Dr. Edmund F. Rybicki
Mechanical Engineering Dept.
The Univ. of Tulsa
Tulsa, OK. 74104

Mr. Harbinder Saluja
Boeing Vertol Company
Structural Technology
P.O. Box 16858
Philadelphia, PA. 19142

Dr. J. Wayne Sawyer
Mail Stop 190
NASA-Langley Research Center
Hampton, VA. 23665

Dr. George P. Sendeckyj
Structures Division
Air Force Flight Dynamics Lab.
Wright-Patterson AFB
Ohio 45433

Mr. Steven M. Serabian
28 Berkeley Drive
Chelmsford, MA. 01824

Mr. John S. Short, Jr.
ESH Dept.
Virginia Tech
Blacksburg, VA. 24061

Mr. Mark J. Shuart
Mail Stop 188
NASA-Langley Research Center
Hampton, VA. 23665

Dr. James H. Starnes, Jr.
Mail Stop 190
NASA-Langley Research Center
Hampton, VA. 23665

Prof. Yehuda Stavsky
Gerard Swope Prof. of Mech.
Technion-Israel Inst. of Tech.
Technion City, Haifa, Israel

Dr. W. W. Stinchcomb
ESH Dept.
Virginia Tech
Blacksburg, VA. 24061

Dr. Darrel R. Tenney
Mail Code 188B
ND-Materials Research Branch
Langley Research Center
Hampton, VA. 23665

Dr. S. W. Tsai
Nonmetallic Materials Division
Air Force Materials Laboratory
Wright-Patterson AFB
Ohio 45433

Dr. J. R. Vinson
Dept. of Mech. & Aero. Engr.
107 Evans Hall
University of Delaware
Newark, DE. 19711

Mr. H. E. Waddoups
General Dynamic Corp.
Fort Worth, TX 76101

Prof. A. S. Wang
Mechanical Engineering
Drexel University
Philadelphia, PA. 19104

Prof. S. S. Wang
Dept. Theoretical & Applied
Mechanics
University of Illinois
Urbana, IL. 61801

Dr. T. A. Weisshaar
School of Aero. & Astro.
331 Grisson Hall
Purdue Univ.
West Lafayette, IN. 47907

Dr. J. M. Whitney
Nonmetallic Materials Division
Air Force Materials Laboratory
Wright-Patterson AFB
Ohio 45433

Dr. Ernest G. Wolff
The Aerospace Corp.
P.O. Box 92957
Los Angeles, CA. 90009

Dr. Edward Wu
Lawrence Livermore Lab.
University of California
Box 808, L-338
Livermore, CA. 94550

Mr. Thomas A. Zeiler
School of Aero. & Astro.
c/o Dr. T. A. Weisshaar
Purdue Univ.
West Lafayette, IN. 47907

Dr. Carl H. Zweben
General Electric Co.
Space Division
P.O. Box 8555
Philadelphia, PA. 19101